

LDEF M&D SIG SUPPORT

NAS9-17900, SC-02N0165768  
Project No. 960-12-171

Final Report

THE MAGNITUDE OF IMPACT DAMAGE ON LDEF MATERIALS

ORIGINAL CONTAINS  
COLOR ILLUSTRATIONS

Prepared by

Martha Allbrooks and Dale Atkinson  
POD Associates, Inc.  
2309 Renard Place, S.E.  
Suite 201  
Albuquerque, New Mexico 87106

Prepared for

NASA JSC and Lockheed ESC  
2400 NASA Road 1  
Houston, TX 77058

July 11, 1992

N94-10666

Unclas

G3/18 0182638

(NASA-CR-188258) THE MAGNITUDE OF  
IMPACT DAMAGE ON LDEF MATERIALS  
Final Report (POD Associates)

89 p



# TABLE OF CONTENTS

LIST OF TABLES.....	ii
LIST OF FIGURES.....	iii
1.0 INTRODUCTION.....	1
1.1 LDEF BACKGROUND.....	2
1.2 INTRODUCTION TO THE IMPACT ENVIRONMENT.....	4
2.0 IMPACT EFFECTS ON MATERIALS.....	8
2.1 IMPACT EFFECTS ON STRUCTURAL MATERIALS.....	14
2.1.1 IMPACT EFFECTS ON METALS.....	14
2.1.2 IMPACT EFFECTS ON COMPOSITE MATERIALS.....	23
2.2 IMPACT EFFECTS ON THERMAL CONTROL MATERIALS.....	23
2.2.1 IMPACT EFFECTS ON THERMAL BLANKETS.....	25
2.2.2 IMPACT EFFECTS ON THERMAL CONTROL PAINTED MATERIALS.....	41
2.3 IMPACT EFFECTS ON OPTICS AND POWER SYSTEM COMPONENTS.....	54
2.4 IMPACT EFFECTS ON OTHER TYPES OF MATERIALS.....	63
2.5 IMPACT-CAUSED CONTAMINATION VIA EJECTA BLOW-OFF.....	65
3.0 CONCLUSIONS AND RECOMMENDATIONS.....	74
REFERENCES.....	76
APPENDIX.....	A-1
A.1 CTH CODE VALIDATION.....	A-1
A.2 ILLUSTRATION OF CTH RESULTS.....	A-2

## LIST OF TABLES

TABLE	DESCRIPTION	PAGE
Table A-1	Data comparison from CTH run and Hörz laboratory data.	A-1
Table A-2	Variables used in CTH calculations.	A-2
Table A-3	Yield and tensile strengths used in CTH calculations.	A-2

## LIST OF FIGURES

FIGURE	DESCRIPTION	PAGE
Figure S1-1	Schematic of the LDEF structural grid layout.	2
Figure S1-2	Schematic of LDEF 's on-orbit orientation.	3
Figure S2-1a	Schematic of damage morphology and diameter measurements for impacts into metals.	9
Figure S2-1b	Schematic of damage morphology and diameter measurements for highly-oblique impacts into metals.	9
Figure S2-1c	Schematic of damage morphology and diameter measurements for multi-cratering impacts into metals.	10
Figure S2-1d	Schematic of damage morphology and diameter measurements for impacts into composites.	10
Figure S2-1e	Schematic of damage morphology and diameter measurements for impacts into thermal control blankets and laminated materials.	11
Figure S2-1f	Schematic of damage morphology and diameter measurements for impacts into thermal control paints.	11
Figure S2-1g	Schematic of damage morphology and diameter measurements for impacts into optics and brittle materials.	12
Figure S2-1h	Schematic of damage morphology and diameter measurements for penetrations through separated layers of materials.	12
Figure P2-1a	Photograph of a typical hypervelocity impact feature in aluminum.	15
Figure P2-1b	Photograph of a spallation feature on the back surface of the experiment tray located at Bay D02.	15
Figure P2-2	Photograph of a penetration through a painted aluminum panel on LDEF.	16
Figure P2-3	Photograph of an impact feature into the edge of an aluminum plate.	18
Figure P2-4	Photograph of an elliptical crater in aluminum resulting from an impact at a highly-oblique angle.	18
Figure P2-5	Photograph of a multi-cratering impact feature in an aluminum surface.	19
Figure P2-6	Photograph of a multi-cratering impact feature in an aluminum surface.	19
Figure P2-7	Photograph of the largest impact feature on LDEF.	21
Figure P2-8	Photograph of the largest impact feature on LDEF.	21

<b>FIGURE</b>	<b>DESCRIPTION</b>	<b>PAGE</b>
Figure P2-9	Photograph of the largest impact feature on LDEF.	22
Figure P2-10	Photograph of an impact feature in graphite-epoxy.	24
Figure P2-11a	Photograph of a multi-layer insulation thermal control blanket.	26
Figure P2-11b	Photograph of an impact feature in a Lexan surface.	26
Figure P2-12	Photograph of a multi-layer insulation thermal control blanket.	27
Figure P2-13	Photograph of an impact feature in a multi-layer insulation thermal control blanket.	27
Figure P2-14	Photograph of an impact feature in a multi-layer insulation thermal control blanket.	29
Figure P2-15a	Photograph of a multi-layer insulation thermal control blanket.	29
Figure P2-15b	Photograph of post-deintegration view of the entire B04 experiment tray.	30
Figure P2-15c	Photograph of post-deintegration view of the entire D10 experiment tray.	32
Figure P2-16	Photograph of the front surface of an impact penetration through an aluminized-Mylar foil.	32
Figure P2-17	Photograph of the back surface of an impact penetration through an aluminized-Mylar foil.	33
Figure P2-18	Photograph of an impact penetration through a silvered-Teflon thermal control blanket adhesively bonded to a heat pipe.	33
Figure P2-19	Photograph of post-deintegration view of an entire A0178 experiment tray (Scheldahl thermal control blanket).	34
Figure P2-20	Photograph of the back surface of a Scheldahl G411500 silvered-Teflon thermal control blanket.	36
Figure P2-21	Photograph of a large impact penetration through a Scheldahl G411500 silvered-Teflon thermal control blanket.	36
Figure P2-22	Photograph of two impact penetrations through a Scheldahl G411500 silvered-Teflon thermal control blanket.	37
Figure P2-23	Digitized image of an impact penetration through a Scheldahl G411500 silvered-Teflon thermal control blanket on tray A10.	39
Figure P2-24	Digitized image of an impact penetration through a Scheldahl G411500 silvered-Teflon thermal control blanket on tray A02.	39
Figure P2-25	Photograph of an impact feature in a Scheldahl G411500 silvered-Teflon thermal control blanket.	40
Figure P2-26	Photograph of several impacts in a Scheldahl G411500 silvered-Teflon thermal control blanket.	40

<b>FIGURE</b>	<b>DESCRIPTION</b>	<b>PAGE</b>
Figure P2-27	Photograph of post-deintegration view of the entire F08 experiment tray taken at an oblique angle.	42
Figure P2-28	Photograph of multiple craters in the white painted surface on experiment M0004.	42
Figure P2-29	Photograph of an impact feature in the white painted surface on experiment M0004.	43
Figure P2-30	Photograph of an impact feature in a white painted surface showing ring features.	43
Figure P2-31a	Photograph of an impact feature in a white painted surface showing ring features.	45
Figure P2-31b	Photograph of the same impact as Figure P2-31a at a higher magnification showing ring features.	45
Figure P2-32	Photograph of an impact feature in a white painted surface showing ring features.	46
Figure P2-33	Photograph of an impact feature in a white painted surface showing ring features.	46
Figure P2-34	Photograph of an impact feature in a white painted surface showing ring features.	47
Figure P2-35	Photograph of an impact feature in the painted aluminum surface from the Grapple plate on tray C10.	49
Figure P2-36	Photograph of an impact feature in the painted surface from the Grapple plate on tray C10 showing ring features.	49
Figure P2-37	Photograph of an impact feature in the painted surface from the Grapple plate on tray C01.	50
Figure P2-38	Photograph of an impact penetration through a white painted aluminum surface from the trailing edge.	50
Figure P2-39a	Photograph of an impact feature in a yellow painted aluminum scuff plate from the trailing edge.	52
Figure P2-39b	Photograph of an impact feature in a yellow painted aluminum scuff plate from the trailing edge.	52
Figure P2-39c	Photograph of an impact feature in a yellow painted aluminum scuff plate from the trailing edge.	53
Figure P2-40a	Photograph of an impact feature in a metal-oxide silicon (MOS) detector sample.	55
Figure P2-40b	Photograph of a higher magnification view of Figure P2-40a.	57
Figure P2-40c	Photograph of a higher magnification view of Figure P2-40b.	57
Figure P2-41	Photograph of an impact feature in an infrared (IR) multi-layer filter material on top of a germanium substrate.	58

<b>FIGURE</b>	<b>DESCRIPTION</b>	<b>PAGE</b>
Figure P2-42	Photograph of an impact feature in a germanium substrate from experiment A0187-2.	58
Figure P2-43	Photograph of an impact feature in a germanium substrate from experiment A0187-2.	59
Figure P2-44	Photograph of an impact feature in a germanium substrate from experiment A0187-2.	59
Figure P2-45	Photograph of an impact feature in a brittle substrate (glass sample).	61
Figure P2-46	Photograph of a portion of a solar panel from the A0171 experiment from Bay A08.	61
Figure P2-47	Photograph of an impact feature in a solar cell cover glass.	62
Figure P2-48	Photograph of damage caused by breaking a silver interconnect of a solar cell.	62
Figure P2-49	Photograph of an impact feature in a fiber optic bundle.	64
Figure P2-50	Photograph of an impact feature in a composite material.	64
Figure P2-51	Photograph of an impact feature in beta cloth.	66
Figure P2-52	Photograph of an impact penetration through a fiberglass material.	66
Figure P2-53	Photograph of a urine spot contamination feature.	68
Figure P2-54	Photograph of ejecta spray onto a germanium substrate on experiment A0187-2.	68
Figure P2-55	Photograph of an impact feature in the side of a structure with ejecta spray across the surface adjacent to it.	69
Figure P2-56	Photograph of an impact feature in the edge of an experiment tray holder with its associated ejecta spray.	69
Figure P2-57	Photograph of ejecta spray across an optical surface.	70
Figure P2-58	Photograph of ejecta spray from an impact feature onto a tray lip.	72
Figure P2-59	Photograph of ejecta spray from an impact into a solar cell holder.	72
Figure P2-60	Photograph of the largest impact feature on LDEF with its associated ejecta spray.	73
Figure A-1	Example of an alumina projectile impacting a 2-layer target.	A-4
Figure A-2	Example of an aluminum projectile impacting a 3-layer target.	A-5

## 1.0 INTRODUCTION

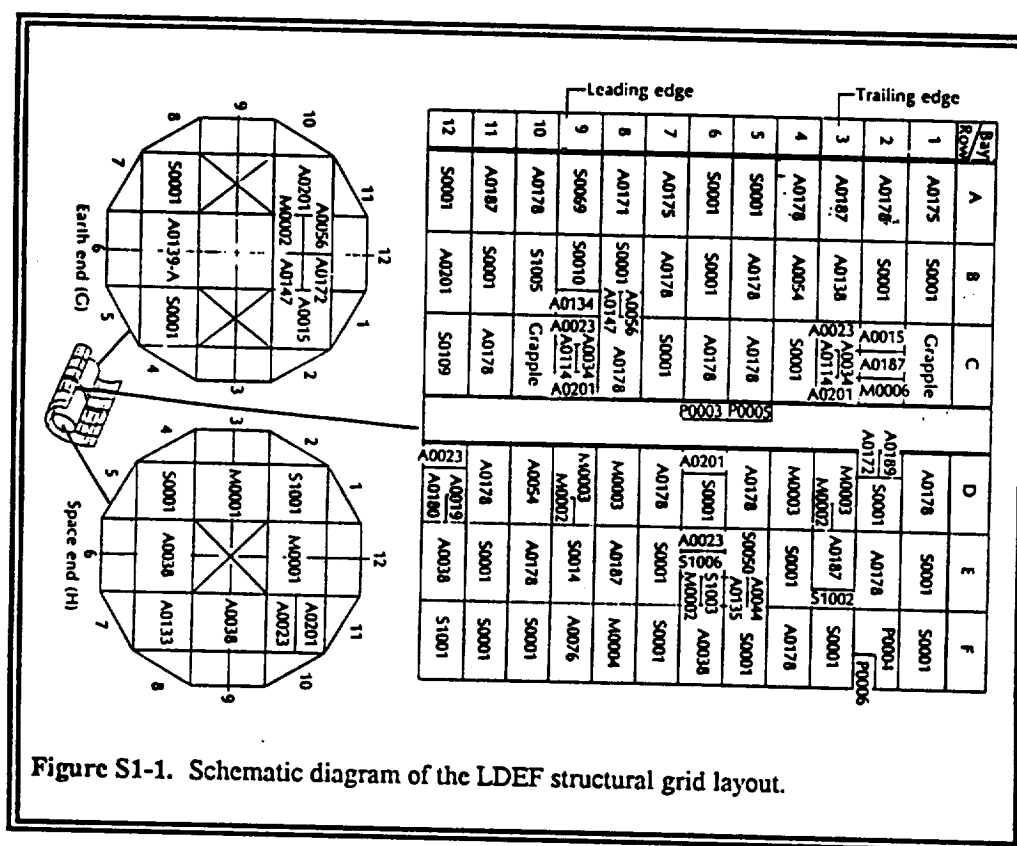
After the recovery of the Long Duration Exposure Facility (LDEF) the NASA Meteoroid and Debris Special Investigation Group (M&D SIG) decided that there is a need for a higher level of awareness of the extent of damage caused by meteoroid and debris impacts into the various types of spacecraft materials. This is especially important due to the number of new satellites, and due to the number of companies and younger individuals becoming involved with the space program who have minimal knowledge of the threats and the effects of these impacts. As a result, this report was requested by the M&D SIG and the LDEF Project Office in order to increase the awareness among scientists and engineers of the effects of the meteoroid and debris environment on the different types of materials and systems which were flown on LDEF and which may be flown on future spacecraft.

The purpose of this report is to document the magnitude and types of impact damage to materials and systems on the LDEF spacecraft. This report will provide insights which permit NASA and industry space-systems designers to more rapidly identify potential problems and hazards in placing a spacecraft in low-Earth orbit (LEO). This report is structured to provide (1) a background on LDEF, (2) an introduction to the LEO meteoroid and debris environments, and (3) descriptions of the types of damage caused by impacts into structural materials (*e.g.*, metals and composites), thermal control materials (*e.g.*, blankets, paints, and coatings), power and optical systems (*e.g.*, solar cells, cover glasses, optical surfaces, and coatings), and contamination caused by spallation and ejecta from impact events.

This report was sponsored by the M&D SIG and the LDEF Project Office and was prepared for NASA Johnson Space Center Solar System Exploration Division under subcontract SC-02N0165768 to Lockheed Engineering and Science Company prime contract NAS9-17900.

## 1.1 LDEF Background

Following is a brief review of the LDEF mission and its relevance to this report and current studies. LDEF was designed as a low-cost, reusable platform to transport various experiments into low-Earth orbit. The 6061-T6 aluminum satellite structure was a 12-sided open grid, 14 feet in diameter and 30 feet long, which weighed 8,000 pounds. The spacecraft carried 57 separate investigations ranging from power and propulsion, materials, coatings and thermal systems to exobiology and cosmic physics. The experiments flown on LDEF were self contained trays mounted on the exterior of the structure. The specific LDEF arrangement of 72 peripheral trays and 14 end trays of smaller dimensions provided a total of 130 m<sup>2</sup> of space exposed area, contained over 10,000 material samples, and weighed a total of ~21,000 pounds (Figure S1-1); (Ref. 1).



Initially intended for a nine month survey of low Earth orbit at 257 nautical miles altitude, LDEF was deployed from Space Shuttle STS 41-C on April 7, 1984. Unfortunate circumstances and

subsequent scheduling delays prevented LDEF from being retrieved until January 12, 1990, 5.75 years later, at an altitude of 179 nautical miles (Ref. 2). LDEF was placed in a gravity gradient stabilized orbit (Figure S1-2) at an inclination of  $28.4^\circ$ . As LDEF was gravity gradient stabilized

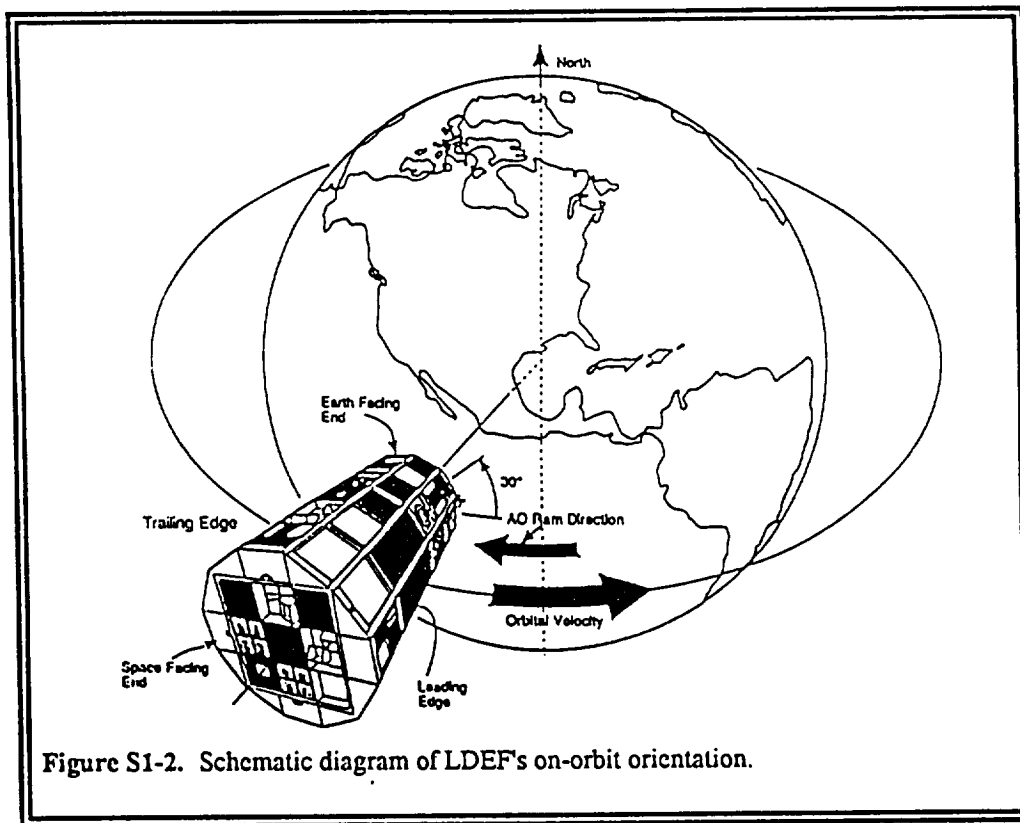


Figure S1-2. Schematic diagram of LDEF's on-orbit orientation.

in its orbit, a constant orientation was maintained with respect to the vertical and the velocity vector with one end always facing the Earth and the other facing space. Row 9 faced toward RAM (or the velocity direction) and Row 3 faced the wake as the trailing edge.

The residual oscillations in attitude upon deployment were corrected by a device utilizing the terrestrial magnetic field and energy absorption by viscous damping. In actuality, LDEF was rotated approximately  $8^\circ$  off nominal RAM (Row 9) for its lifetime in space (Ref. 3). The constant orientation of LDEF has allowed for separate aspects of the near-Earth space environment to be analyzed. Specifically, atomic oxygen (AO) was known to strongly affect only the RAM facing direction, thus good controls for the AO experiments were available on LDEF's trailing edge. The leading edge of LDEF was exposed to atomic oxygen, meteoroids and debris (mostly debris), ultraviolet light and thermal cycling, whereas the trailing edge was only exposed to meteoroids and debris (mostly meteoroids), ultraviolet light and thermal cycling.

## 1.2 Introduction to the Impact Environment

The near-Earth meteoroid and debris environment has been studied for the past 30 years. The meteoroid environment comes from natural sources such as comets, asteroids, the moon, or other planets, and has been measured (via surface impacts and/or penetrations) using numerous satellites at various distances from the Earth, as well as interplanetary craft. The current models of the meteoroid environment treat the meteoroids as an isotropic source, with elliptical orbits associated with their parent bodies but crossing the plane of the Earth. This gives them relative velocities with respect to the Earth ranging from ~12 km/s all the way up to 72 km/s. After taking into account the velocity of a satellite in orbit around Earth, the relative impact velocities of meteoroids on the satellite ranges from ~4.0 km/s to ~79 km/s. However, the distribution is heavily weighted towards the lower (10-30 km/s) velocities, giving an average relative impact velocity of ~19 km/s.

The cometary meteoroids are made primarily of a conglomeration of ice particles with small amounts of higher density minerals mixed with the ice. This gives them a relative density of ~0.5 g/cm<sup>3</sup>. The asteroidal particles are primarily of higher density minerals with densities that can go as high as ~8 g/cm<sup>3</sup>. Meteoroids have been detected with sizes as small as 0.4 microns and as large as several meters in diameter. However, the primary threat of meteoroids in the near-Earth space environment is from particles ranging from 50  $\mu$ m to 1 mm in diameter. The very small meteoritic particles (less than 1  $\mu$ m in diameter) are primarily from beta meteoroids. These are meteoroids which are accelerated by radiation pressure outward from the sun. Beta meteoroids were discovered in the 1970's by interplanetary spacecraft, and LDEF became the first orbital satellite to detect beta meteoroids using its Interplanetary Dust Experiment (IDE-A0201) (Ref. 4).

Cour-Palais *et al.* (Ref. 5) provides a good general model of the near-Earth meteoroid environment. Eberhard Grün's 1985 model (Ref. 6) provides a good update to the Cour-Palais model by including the beta meteoroid environment, which had been discovered after the development of the Cour-Palais model.

One of the main disagreements within the models, which is still being defined today using the LDEF data and analysis, is the percentage of the environment which is cometary as compared to asteroidal. This affects both the velocity distribution and the expected impact phenomena (*i.e.*, cratering depth or penetration diameter) for the meteoroids (Ref. 7). Another discrepancy within the models is their assumption of the meteoroid environment's isotropic distribution. The LDEF IDE experiment was the first experiment to show that the total environment is non-isotropic and highly dynamic.

Orbital debris refers to man-made particles orbiting the Earth. These particles are a result of standard launch and spacecraft operations as well as rocket and satellite breakups. Launch and spacecraft operations place both large particles (*i.e.*, greater than 1 cm diameter such as satellite shrouds, lens covers, and dropped tools) and small particles (*i.e.*,  $\sim 10 \mu\text{m}$  diameter solid rocket exhaust) in orbit. Exposure of satellites and spent rocket bodies to the space environments (*i.e.*, UV, AO, thermal cycling, radiation, and impact) also creates small particles, less than 1 mm diameter, due to materials' degradation and erosion. After shutdown, spent spacecraft and rocket bodies are allowed to remain in orbit as very large (*i.e.*, greater than 1 m diameter) pieces of orbital debris. In addition, both operational and spent spacecraft and rocket bodies are susceptible to intentional and accidental breakups, either due to explosions or hypervelocity impacts. These breakups create orbital debris of all sizes.

The orbital debris environment began to be measured in the 1960's. However, the focus was on tracking very large particles using ground-based radar systems in order to provide safety and collision avoidance for the manned spacecraft systems. This was an offshoot of the need to monitor space for incoming ballistic missiles. Therefore, this role was maintained by the North American Air Defense Command (NORAD) and was ultimately taken over by the United States Space Command (USSPACECOM) in Colorado. Since the man-made debris particles are in orbit around the Earth, their relative impact velocities (with respect to the satellite) vary with the differences in inclination between the satellite and the particles and with the eccentricity of the orbits.

The first attempts to model or monitor the debris environment for the smaller, radar non-trackable particles (*i.e.*, those less than  $\sim 10$  cm in diameter) occurred in the middle and late 1970's (Ref. 9). It had been discovered that particles larger than  $\sim 1$  cm in diameter, impacting at typical orbital velocities, could cause catastrophic damage to satellites and that particles larger than 1 mm could also cause system failure. If a 1 mm particle struck the wrong component or subsystem, it could also cause catastrophic damage to the entire system. NASA had the first data on the actual environment for small impactors ( $<100$   $\mu\text{m}$  in diameter) due to the return of the Solar Maximum Mission (SMM) satellite materials. Using extrapolations of the radar data from USSPACECOM, combined with ground-based optical measurements and the on-orbit data from the returned SMM materials, Don Kessler of NASA Johnson Space Center (JSC) published a debris environment model in 1987 (Ref. 10). This model, which forms the basis for numerous other models of the debris environment, has been widely adopted and used by the U.S. Department of Defense, NASA, and the European Space Agency (ESA).

In general, the LEO debris environment flux surpasses the LEO meteoroid environment flux for particles larger than  $\sim 1$  mm in diameter. In this size regime the debris is composed primarily of particles from orbiting spacecraft which have broken apart. These particles are irregular in shape. They may also be of much higher densities (*e.g.*, stainless steel and tantalum) but the average density is that of aluminum. The LEO debris environment also contains more particles in the size regime less than  $\sim 50$   $\mu\text{m}$  in diameter than does the meteoroid environment. In this population regime, the particles which are  $\sim 10$   $\mu\text{m}$  in diameter are primarily aluminum oxide from solid rocket motors, whereas the other particles in this range are primarily paint pigments, both averaging  $\sim 4$   $\text{g/cm}^3$  density.

For a circular orbit at 500 km altitude and  $28.5^\circ$  inclination (the inclination and altitude of the proposed Space Station), the average relative impact velocity of orbital debris is about 10 km/s. However, this relative velocity can range from almost 0 to  $\sim 19$  km/s for particles in highly elliptical orbits. Since the majority of impacts occur at oblique angles, the relative normal incidence impact velocity averages  $\sim 8$  to 10 km/s (Ref. 8).

The meteoroid environment impinging on a spacecraft in orbit around the Earth shows a tendency to impact about twice as much on the satellite's leading edge (which is moving in the velocity, or RAM, direction) as on the trailing, or wake, edge. Orbital debris, on the other hand, is much more focused towards the leading sides of the spacecraft, with the exception that particles in elliptical orbits have higher fluences at  $\sim 45^\circ$  either side of the RAM direction (Ref. 11). With orbital debris, approximately 1/10th to 1/20th of the number of particles hit the trailing edge compared to the leading edge surfaces. Generally, the meteoroid environment is modeled as unchanging over both time and spacecraft inclination whereas the orbital debris environment is highly changed both over time and with spacecraft inclination. The higher inclinations possess a much higher population of debris particles.

The debris environment is considered to be increasing with time, with the small particle population increasing faster (at a compound rate of  $\sim 2\%$  per year) than the population of the much larger trackable particle (which increase at a linear rate of  $\sim 5\%$  per year); (Ref. 10). Both the meteoroid and debris environments increase with altitude, although the current models of the debris environment show the flux decreasing at altitudes above  $\sim 1000$  km. This latter may change as the elliptical orbits of the debris are included in future models.

The environment models continue to be updated with the addition of LDEF data and data from other returned satellite materials (such as the Palapa satellite). With these updates, predictions made using the most recent version of the Kessler debris model (NASA TM-100471, 1990) come to within a factor of two to three of the actual data from LDEF. However, the Kessler model has several major downfalls: (1) it does not currently account for particles in elliptical orbits, which may total 20-30 times the amount currently trackable by USSPACECOM, and which pose a substantial threat to satellites at much higher altitudes than 1000 km (Ref. 11); and (2) it cannot account for the highly dynamic nature of the debris environment which was detected by the IDE experiment on LDEF. An alternate model which will handle both the dynamics of the environment as well as the elliptical orbits is in development at the Jet Propulsion Laboratory by Dr. Neal Divine (Ref. 12).

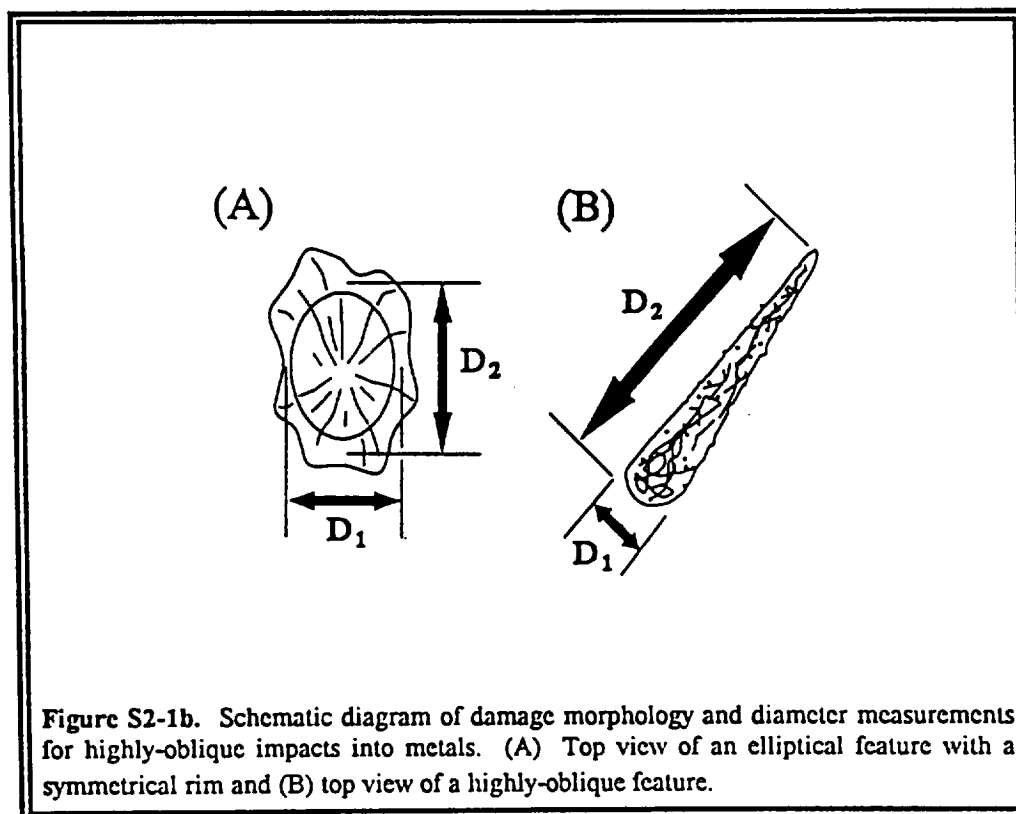
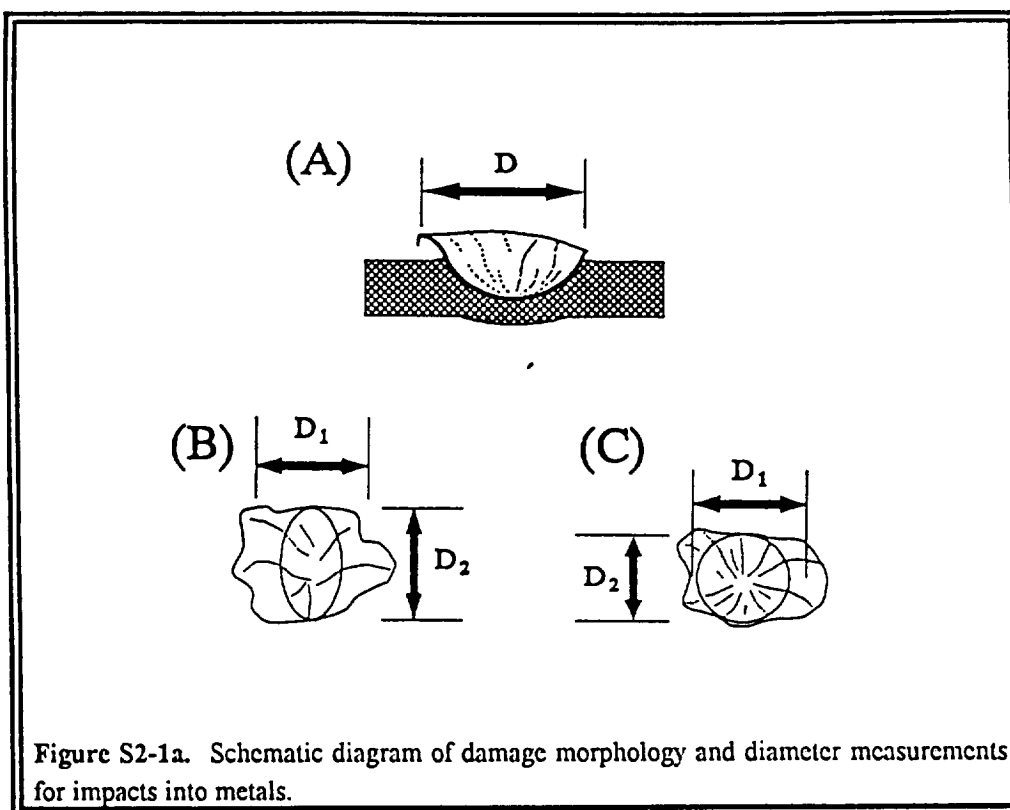
## 2.0 IMPACT EFFECTS ON MATERIALS

Impact damage can degrade the performance of exposed spacecraft materials and, in some cases, destroy a satellite's ability to perform or complete its mission. Large particles can penetrate through protective wall surfaces. With a relative impact velocity of 10 km/s, a piece of aluminum debris which is ~0.7 mm in diameter can penetrate through a typical 2.5 mm (100 mil) thick aluminum satellite wall. During its 5.75 year exposure, LDEF saw 1 impact of this size per 7 m<sup>2</sup> of area exposed in the RAM direction. In addition to this, LDEF experienced ~1 impact/m<sup>2</sup>, on the RAM-exposed surfaces, which could have penetrated a typical 1.5 mm (60 mil) thick aluminum electronics box wall (Ref. 8). While these impacts can be extremely damaging to internal components, electronics, batteries, motors and mechanisms, they are relatively rare.

Smaller impacts which can degrade mission performance or cause mission denial are extremely common. Tens of thousands to even millions of these impacts may occur per square meter of typical surfaces which are exposed throughout the mission lifetime of the satellite. The effects of these smaller impacts are the primary focus of this report. This chapter first addresses impact effects in structural materials, followed by thermal control materials, then solar power and optical systems, and ends with contamination caused by impact spallation and ejecta.

Damage caused by impacts is typically described in terms of crater or perforation diameters, with only an occasional reference to spallation areas. This is primarily due to the fact that other damage mechanisms are not well understood, nor are they currently included in analytical equations.

This report does not address the damage mechanisms in detail, but rather shows pictures of typical examples of various types of impact damage which may occur. Figures S2-1a through S2-1h are schematics identifying the damage morphologies which will be described in the text and shown in the damage photographs. These schematics provide a reference to help the reader understand the descriptions of damage in materials and damage effects on space system performance. An introduction to damage mechanisms is provided by See, et al. (Ref. 13).



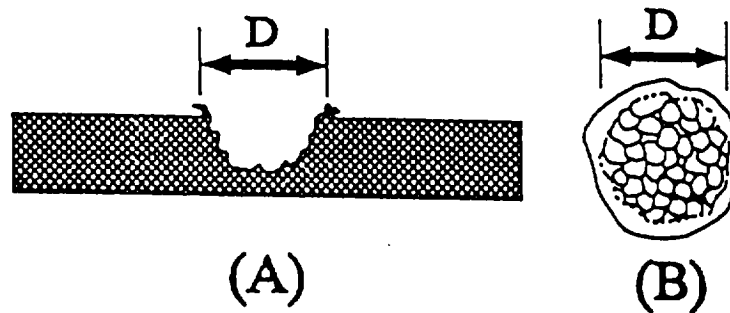


Figure S2-1c. Schematic diagram of damage morphology and diameter measurements for multi-cratering impacts into metals. (A) Cross-sectional view and (B) top view.

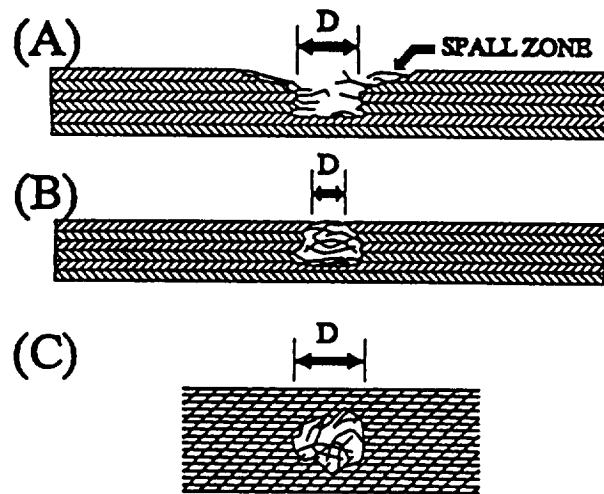


Figure S2-1d. Schematic diagram of damage morphology and diameter measurements for impacts into composites. (A) Cross-sectional view of feature with surrounding spall zone, (B) feature with a larger damage zone, beneath the composite surface, than is visually seen at the original material surface, and (C) top view of a feature in a composite surface. Note the overlapping of the entrance hole by fibers of the composite material.

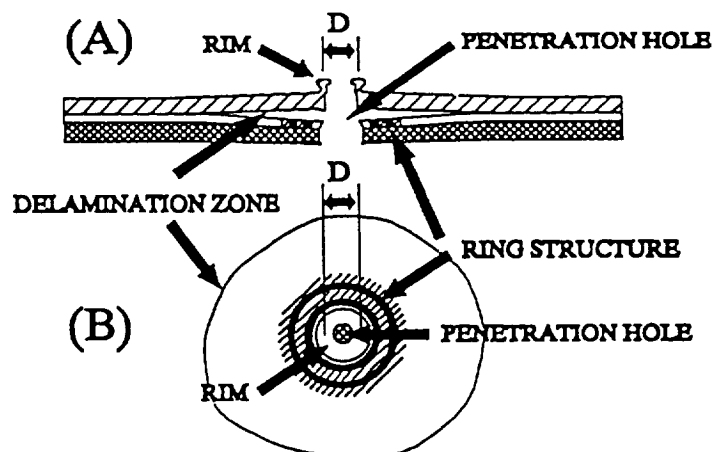


Figure S2-1e. Schematic diagram of damage morphology and diameter measurements for impacts into thermal control blankets and laminated materials. (A) Cross-sectional view depicting the delamination of the Teflon layer from the underlying silver/inconel/paint surface and (B) top view showing the extent of the delamination zone and the presence of the "rings" generally found in association with these features.

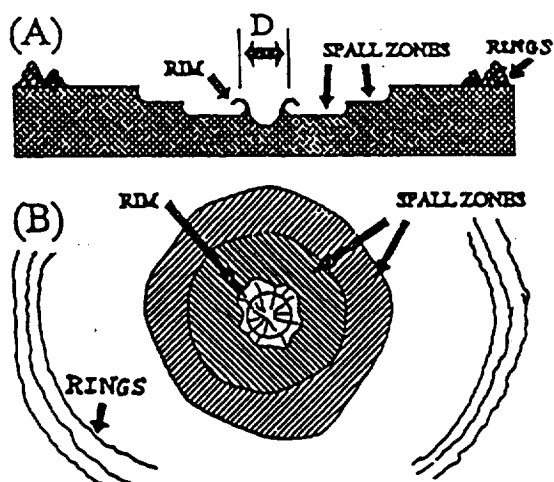


Figure S2-1f. Schematic diagram of damage morphology and diameter measurements for impacts into thermal control paints. (A) Cross-sectional view and (B) top view.

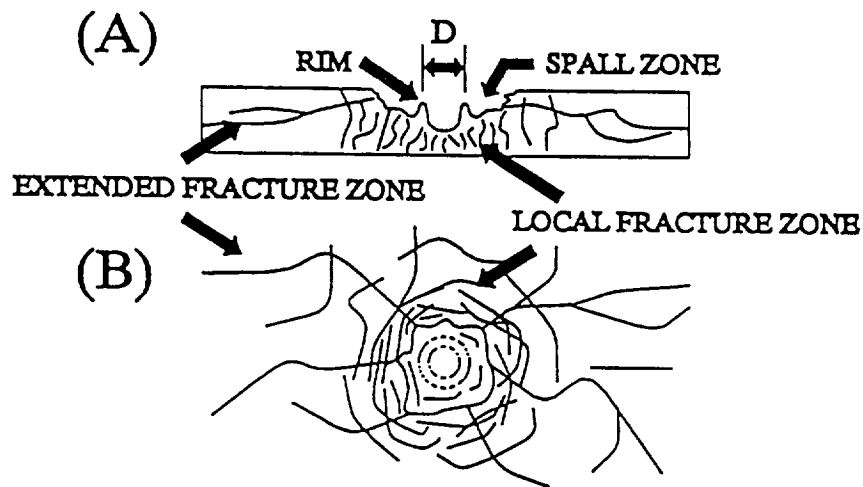


Figure S2-1g. Schematic diagram of damage morphology and diameter measurements for impacts into optics and brittle materials. (A) Cross-sectional view and (B) top view.

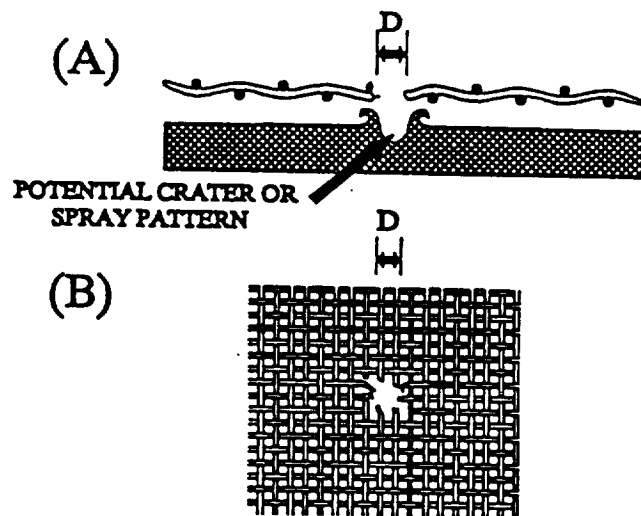


Figure S2-1h. Schematic diagram of damage morphology and diameter measurements for penetrations through separated layers of materials. (A) Cross-sectional view with potential crater or spray pattern underneath the separated layer and (B) top view.

In addition, detailed analyses of damage mechanisms are in progress for optics (Ref. 14) and thermal control paints (Ref. 15). Numerous other sources provide detailed analyses of impacts into metals (*e.g.*, Ref. 16).

The pictorial approach taken in this report is intended to provide the engineer or spacecraft designer with a better idea of the magnitude of damage caused by small impactors, particularly for materials wherein the crater perforation is only a small percentage of the total damage. In addition, this report should help designers to better define the types of analyses and tests which need to be performed in order to validate and improve the performance of a satellite's components, subsystems and system. Unless otherwise stated, all of the impact craters and penetrations shown are between 0.5 and 1.0 mm in diameter.

For the reader's reference, the NASA or POD photo numbers of the examples discussed in the following text are given in parentheses following the figure number. Copies of the NASA photo numbers can be ordered from the following address:

Commercial Desk  
Mail Code AP3  
NASA Johnson Space Center  
Houston, TX 77058

Please cite the full NASA stock number of each image when ordering. Examples of such stock numbers are: 108-KSC-383C-4418/4, KSC-390C-3385.09, S32-89-029, and S90-44980. POD photographs can be ordered from the following address:

POD Associates, Inc.  
2309 Renard Place S.E., Suite 201  
Albuquerque, NM 87106

Please cite the full POD stock number of each image when ordering. Examples of such stock numbers are: POD-91-S-020 and POD-9201-135.

## **2.1 Impact Effects on Structural Materials**

Currently, most satellite structures are metal, with the majority being aluminum. A few satellites are using composite materials such as graphite-epoxy and carbon-carbon, with more expected to do so in the future. Since LDEF was designed to withstand multiple launches, along with multiple retrieval and landing loads, its structure was made from atypically heavy (for satellites) aluminum I-beams. A few experiment structures (*e.g.*, electronics boxes) which were carried by LDEF had aluminum wall thicknesses (*i.e.*, 2-2.5 mm [80-100 mils]). Other experiments carried samples of graphite epoxy composites. Thus, LDEF-flown materials provide examples of typical impact cratering and penetration in the various structural materials. Below are examples of the types of damage caused by these impacts.

### **2.1.1 Impact Effects on Metals**

**Figures P2-1a and P2-1b (S90-44982 and KSC-390C-2038.4)** are typical of hypervelocity impacts into aluminum surfaces. Figure P2-1a shows an impact which has a symmetrical hemispherical crater characteristic of all impacts into aluminum surfaces. Here the typical symmetrical lips stand above the surface of the aluminum. Figure P2-1b is a picture of the back surface of the S0001/A0189/A0172 experiment tray, located at LDEF Bay D02, showing the spallation (removal) of black paint caused by a front surface impact. Spalled material can cause additional internal damage to satellite components or become a contamination source, as described later in Section 2.5.

**Figure P2-2 (S90-44980)** is a picture of a penetration through an aluminum panel on LDEF, and is typical of penetrations at hypervelocity speeds. It is a symmetrical penetration hole with lips which are also symmetrical. This feature is the back surface exit hole made by the impactor through the aluminum. The front surface (opposite side of this plate) of this feature is a penetration through a painted aluminum plate. A picture and discussion of the front surface of this feature is included in Section 2.2.2 under Figure P2-38. These types of penetrations provide

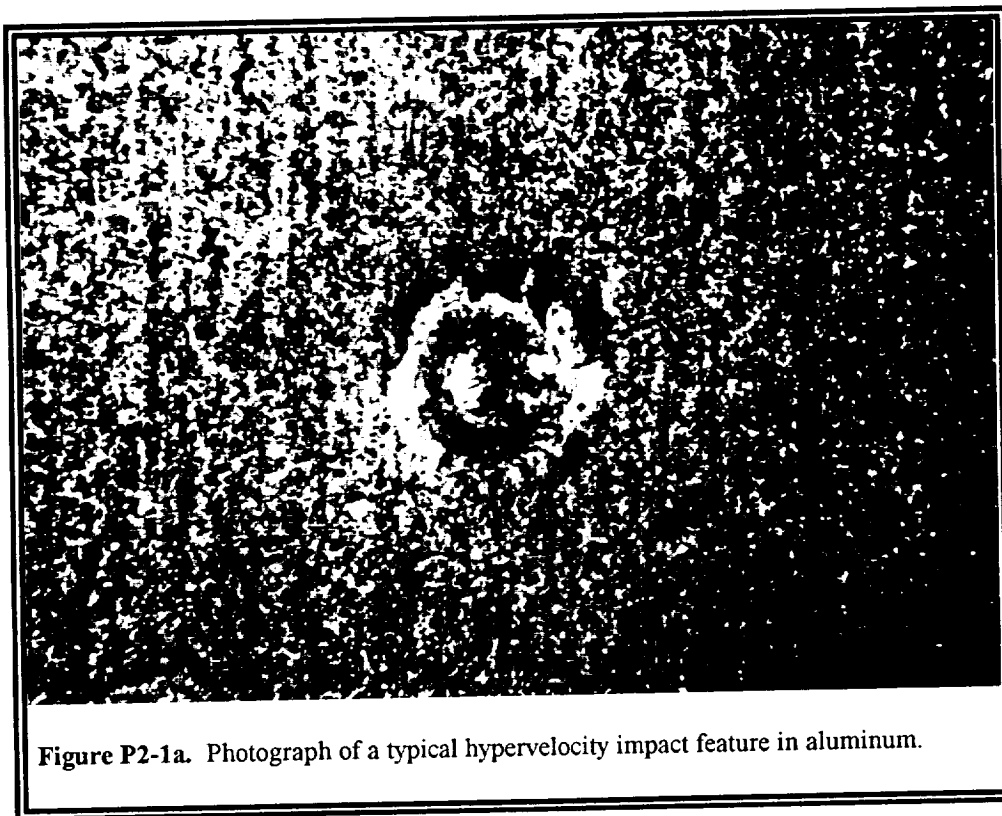


**Figure P2-1a.** Photograph of a typical hypervelocity impact feature in aluminum.

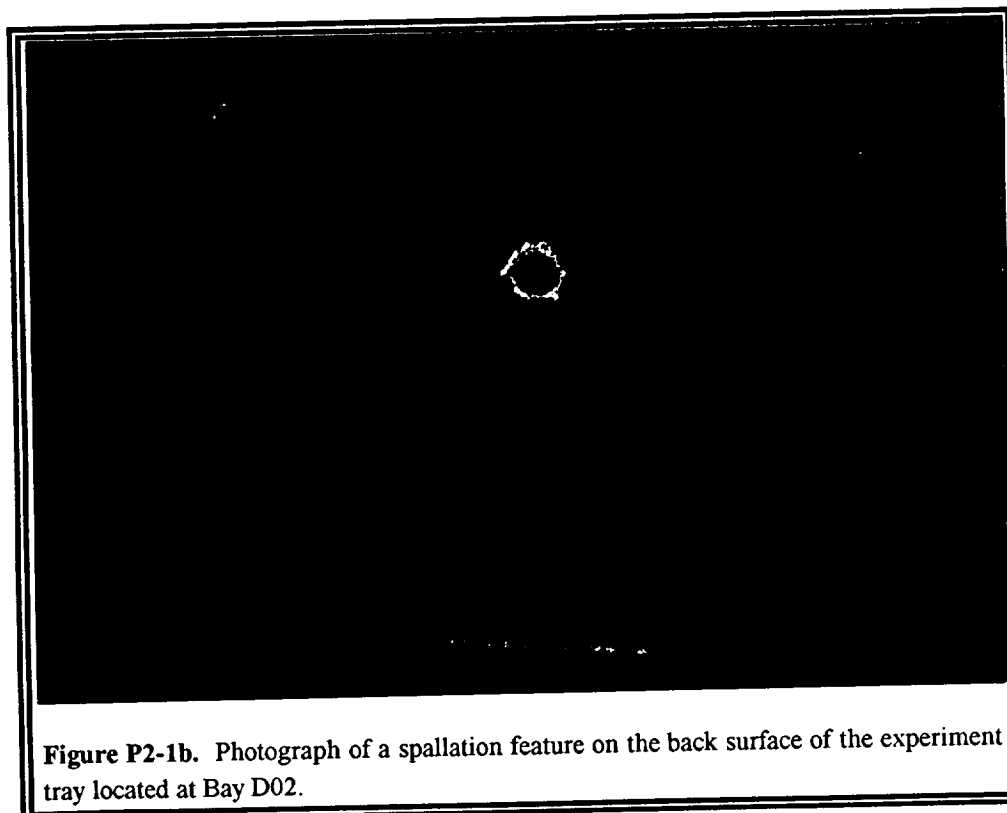


**Figure P2-1b.** Photograph of a spallation feature on the back surface of the experiment tray located at Bay D02.



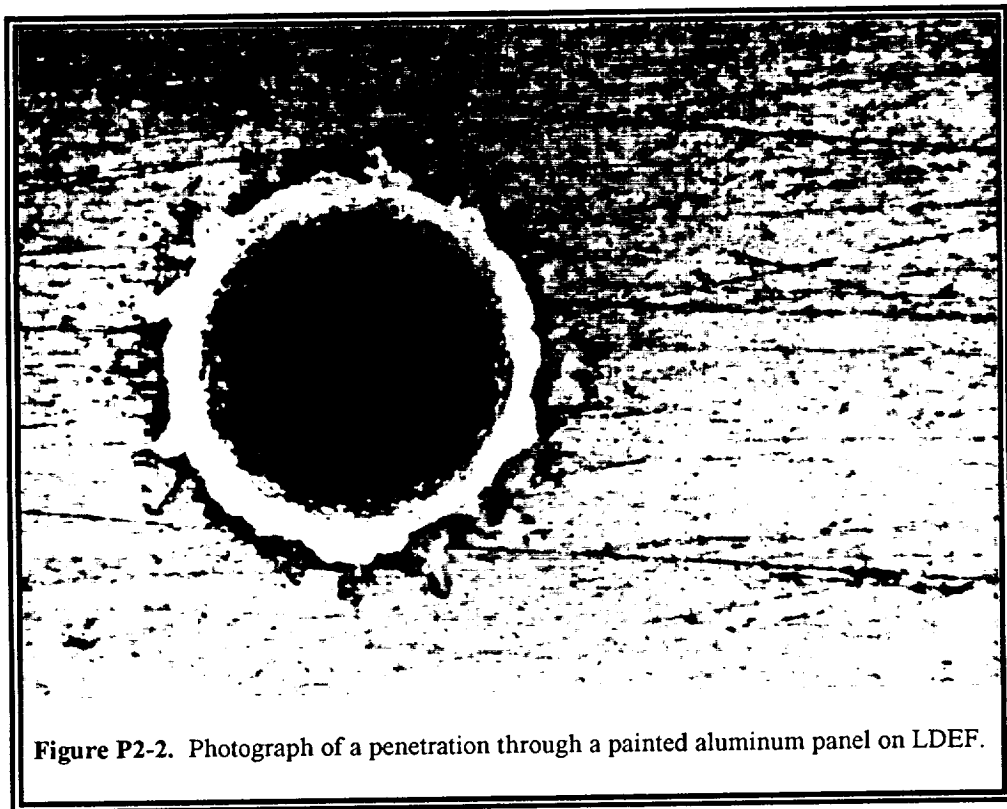


**Figure P2-2.** Photograph of a penetration through a painted aluminum panel on LDEF.



a substantial amount of secondary ejecta and an expanding debris cloud of solid, liquid, or gaseous particulates which can cause damage to other materials located immediately behind the surface. Loading pressures on internal components located approximately an inch away from the penetration could approach as much as 50 kilobars.

**Figure P2-3 (S90-44914)** shows an impact into the edge of an aluminum plate. The crater is very typical of a hypervelocity impact into aluminum but also shows the resultant effect on the edge of the surface, both from the raised crater lips and from the deformation of the aluminum edge, which can dramatically affect space systems. These types of impacts on deployment mechanisms, for example, could prevent them from operating and could prevent the retraction or the initial deployment of things such as solar panels or communications antennae.

**Figures P2-4, P2-5, and P2-6 (S90-44924, S90-44915, and R-9-13)** show craters which are typical of hypervelocity impacts into aluminum at highly-oblique angles (*e.g.*, greater than 60° from the surface normal). Figure P2-4 is a highly-oblique impact by a solid particle creating one crater which is elliptical. For angles closer to the normal the craters are more nearly hemispherical. Most impacts into LDEF occurred at oblique, but not highly-oblique, angles. The total view in this picture measures ~1.5 cm across. Figure P2-5 is another highly-oblique impact. This impactor appears to have been a conglomerate material (loosely held together) which, upon impact, broke into pieces and created two adjoining but distinct craters. Figure P2-6 is another example of a highly-oblique multi-cratering event, but with many separate craters located within the main crater.

Highly-oblique impacts were found in large numbers on LDEF, particularly on the Earth- and space-facing ends of the spacecraft, but were also found on all other surfaces of LDEF. Very oblique impact surface damage areas are much larger (but shallower) than those caused by normal incidence impacts. These highly-oblique impact craters are often accompanied, as in Figure P2-6, by a large amount of ejecta, which causes various spray patterns and contamination to nearby surfaces. These multiple cratering events cannot currently be duplicated in ground-based experiments nor can they be predicted using the current models.



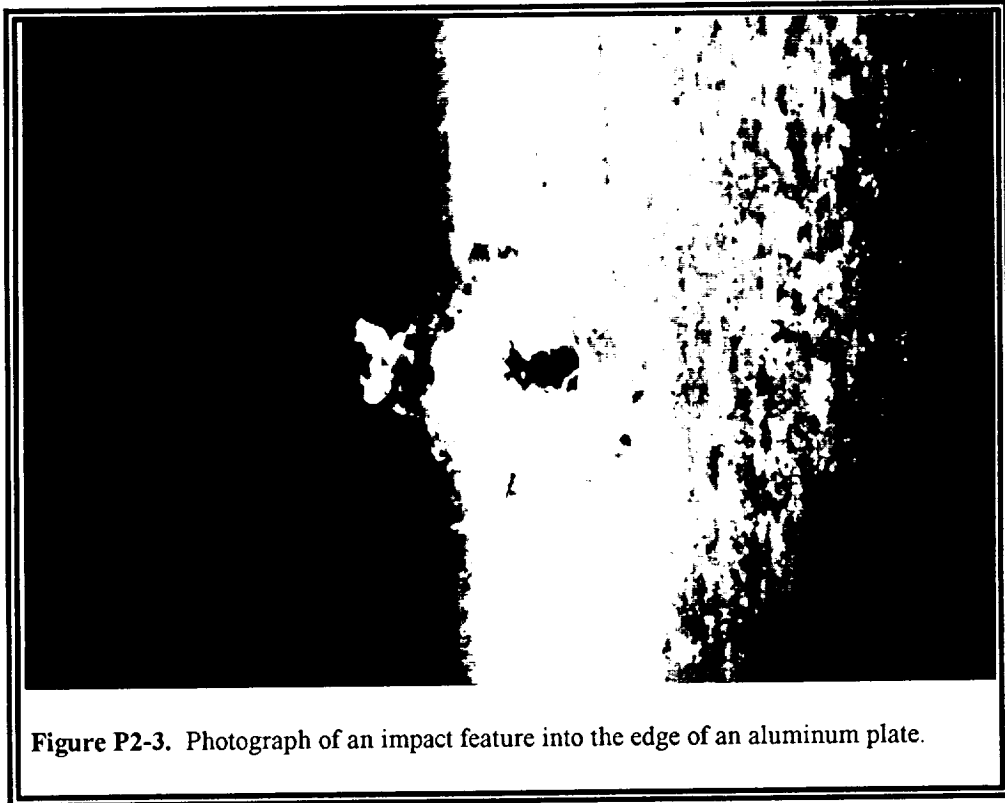


**Figure P2-3.** Photograph of an impact feature into the edge of an aluminum plate.

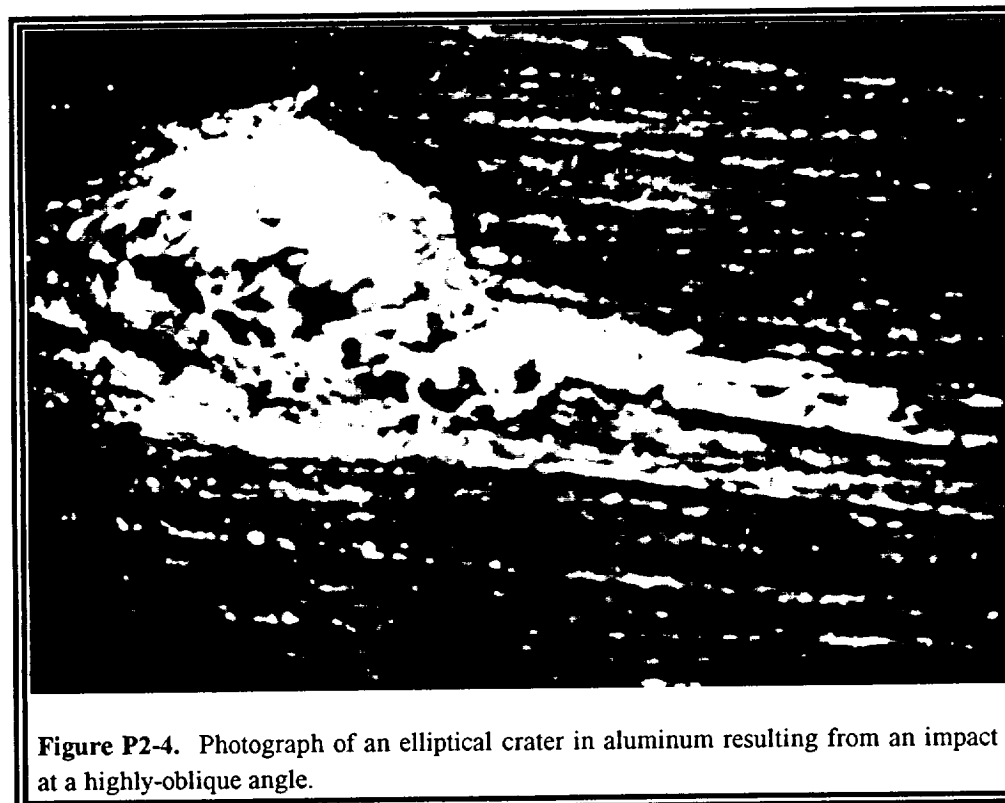


**Figure P2-4.** Photograph of an elliptical crater in aluminum resulting from an impact at a highly-oblique angle.





**Figure P2-5.** Photograph of a multi-cratering impact feature in an aluminum surface.



**Figure P2-6.** Photograph of a multi-cratering impact feature in an aluminum surface.



**Figures P2-7, P2-8, and P2-9 (KSC-390C-2033.10, S90-44921, and KSC-390C-1013.05)** are pictures of the largest impact on LDEF. This crater is 5.25 mm in diameter with a damage area which is over 5 cm in diameter. This crater is located on LDEF Bay H03 in the side of a structural aluminum "Z-frame" in the valley between two experiments. The surface of the Z-frame was aluminum which had been covered with a silvered-Teflon, adhesively-bonded thermal control tape. The entire Z-frame was backed with a solid block of aluminum which held the main experiment. This Z-frame side faced the RAM direction, but was located on the space-facing end of LDEF. In order to impact within this geometry, the particle would have to have been in an elliptical orbit. Figure P2-7 shows a very large delamination area caused by the crater. This is a delamination in the silvered-Teflon. Here, the Teflon delaminated from the silver and the silver delaminated from the aluminum substrate. There are large melted Teflon crater lips, shown in Figure P2-8, where the Teflon was melted and blown out like a volcano from the underlying surface. The large (5.25 mm) crater caused a large bulge in the back surface of the Z-frame and, had it not been for the backing block of aluminum, would have penetrated all the way through the Z-frame. If it was a piece of debris, as suspected, the impacting particle was approximately 0.9 mm in diameter (Ref. 8). Figure P2-9 shows the geometry of this impact feature, the height of the Teflon crater lips, and the extent of the ejecta spray which came from the Teflon, the underlying aluminum, and the impactor. The ejecta sprayed over a 20 cm wide swath across the adjacent surfaces. In typical satellite structural materials with wall thicknesses of less than 2.5 mm, this would have been a penetration with subsequent damage to internal components, possibly causing component failure.

In general, impacts into metals form craters which have diameters averaging about 5 times the impactor diameter. If the crater lips are included, the damage region across the highest point is ~7 times the impactor diameter, while the total region out to the extremes of the crater lips can be ~10 times the impactor diameter. The exact size of the crater is a function of impactor diameter, impact speed, and relative ratio of impactor density to target density. These craters are of concern because they can prevent impacted mechanisms from operating and can cause failure in highly stressed materials.



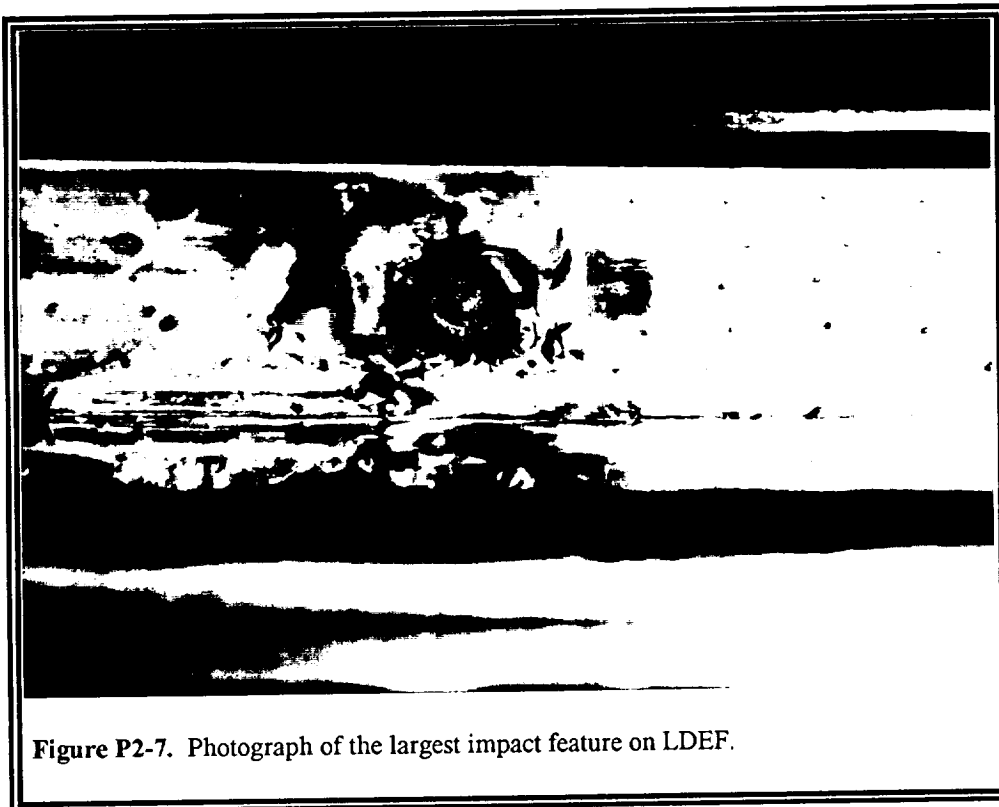


Figure P2-7. Photograph of the largest impact feature on LDEF.

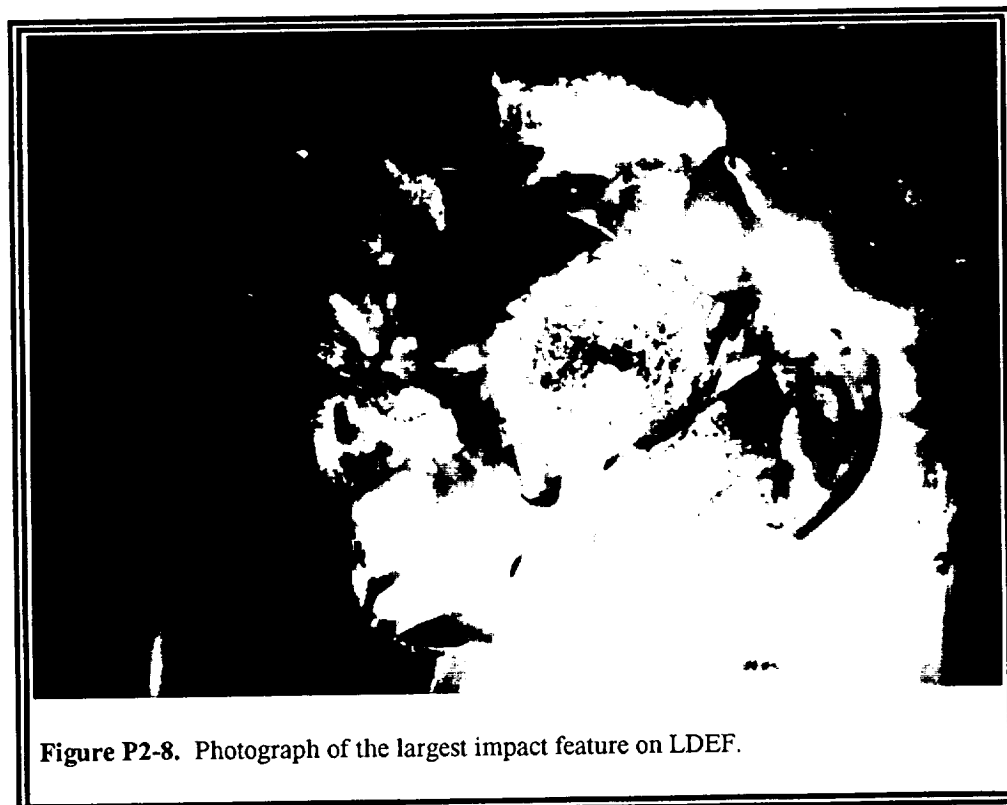
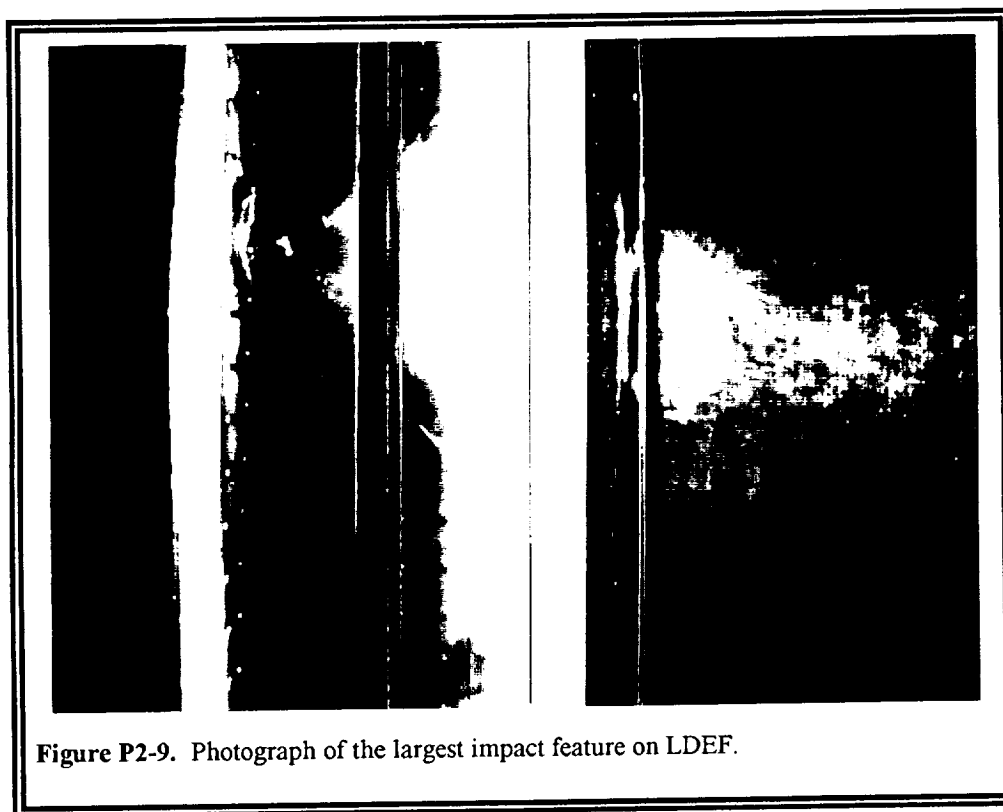


Figure P2-8. Photograph of the largest impact feature on LDEF.





**Figure P2-9.** Photograph of the largest impact feature on LDEF.



### **2.1.2 Impacts Effects on Composite Materials**

While not large in number, LDEF had composite structural material samples on board and was able to show some of the effects of impacts and penetrations through these materials. **Figure P2-10 (KSC-390C-1916.5)** shows several impacts into a graphite-epoxy material which was located at LDEF Bay B09. The view shown in the picture measures ~4 cm across. The largest hole (upper right hand corner) was an ~500  $\mu\text{m}$  diameter penetration through the surface. This type of impact is typical of penetrations seen in composite materials. These penetrations typically have jagged edges and contain broken fibers. When analyzed by the experiment's Principal Investigator, the penetration was determined to have an exit hole ~1 mm in diameter, along with a spallation area which extends out several millimeters and cracks which run along the matrix for several centimeters.

For the more brittle composite structural materials, the damage is rarely a simple crater. Rather, significant in-depth damage can occur and may be anisotropic, following the structure of fibers, etc. For complete penetrations the rear surface damage area is frequently larger than the entry hole area. This impact damage is of concern because the breaking of the fibers, cracking of the matrix, and removal of part of the matrix via the spallation process could cause failure in highly stressed components. This could also lead to further breakdown of the composite material during subsequent exposure to other space environments such as atomic oxygen or ultraviolet light.

### **2.2 Impact Effects on Thermal Control Materials**

Impacts into thermal control materials often display a different type of damage, typically with a greater damage area, than impacts into metals. Since these materials are often coatings or thin laminated layers, the impacts cause delamination of layers to many times the diameter of the crater or penetration (Ref. 15). In addition, the thermal control materials on LDEF demonstrated the greatest synergisms with other environments (*i.e.*, AO and UV). These synergisms further expanded the damage areas caused by impacts.



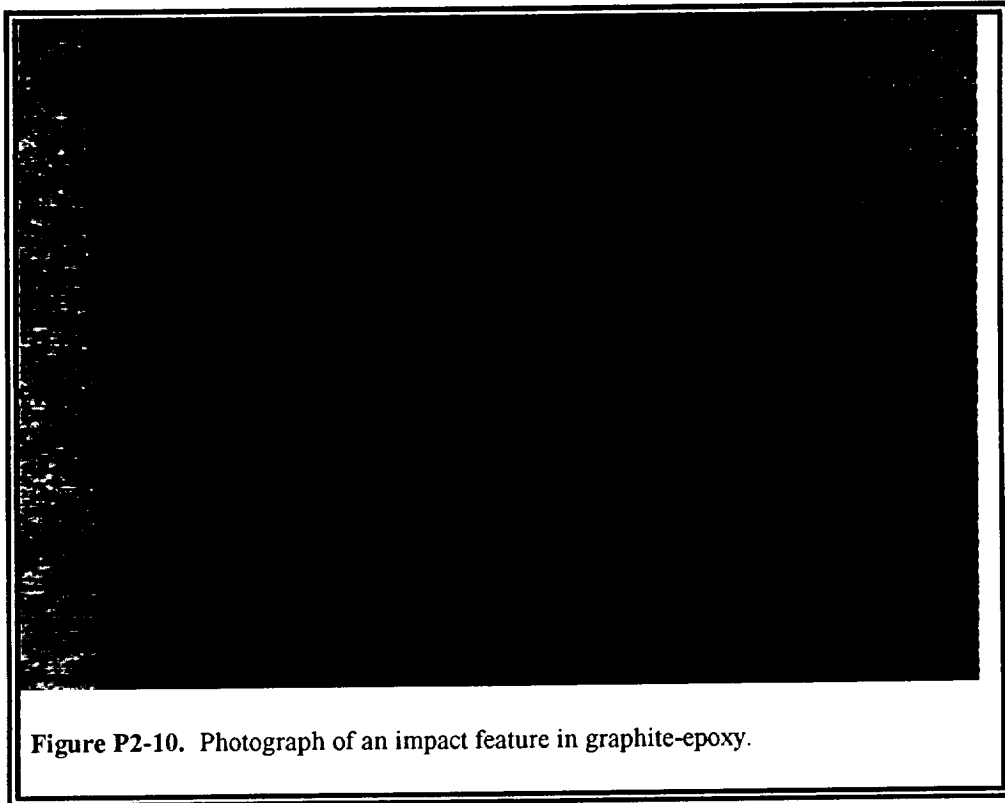


**Figure P2-10.** Photograph of an impact feature in graphite-epoxy.



While the damage mechanisms are related, the impact damage areas in thermal control blankets showed different total damage effects than the thermal control paints. These total damage effect differences were caused by different synergistic responses in the materials. For this reason, this report addresses the thermal control blankets and paints separately.

### **2.2.1 Impact Effects on Thermal Blankets**

**Figure P2-11a (KSC-390C-828.06)** shows the multi-layer insulation (MLI) thermal control blankets which were located on the space end of LDEF at LDEF Bays H03 and H12. The top-most layer of these blankets was painted with a white thermal control paint (Chemglaze A276). After being subjected to the UV light in space, the binder in the paint turned brown. The blankets were attached to the experiment trays by Kapton tape and this tape became embrittled by the UV. Thermal cycling and subsequent cracking of the tape allowed the blankets to lift and curl back, subjecting parts of the blanket to AO from the RAM direction and creating the white stripes in the photograph. These white stripes are where the binder was eroded by the AO, leaving behind only the white pigment particles. **Figure P2-11b (KSC-390C-1013.01)** shows an impact into the underlying exposed Lexan which had turned dark brown and become brittle from the UV light. This view measures ~8 cm across. Note the extremely long cracks propagating from the impact crater.

**Figure P2-12 (KSC-390C-828.05)** shows a more extensive version of the damage to the MLI shown in Figure P2-11a. The entire surface has been eroded by AO leaving almost none of the UV discolored binder. It is also interesting to note that these thermal control blankets were composed of very thin layers (approximately 22) of aluminum separated by layers of Dacron mesh. This photograph clearly shows the aluminum and Dacron mesh layers and how they began to come apart in the space environment.

**Figure P2-13 (S90-44950)** is a picture of an impact into the MLI thermal control blanket, described previously for Figures P2-11 & 12, located at LDEF Bay H12. This close-up photograph shows a total view measuring ~2 cm. In this area, the paint has changed colors due to





**Figure P2-11a.** Photograph of a multi-layer insulation thermal control blanket.



**Figure P2-11b.** Photograph of an impact feature in a Lexan surface.



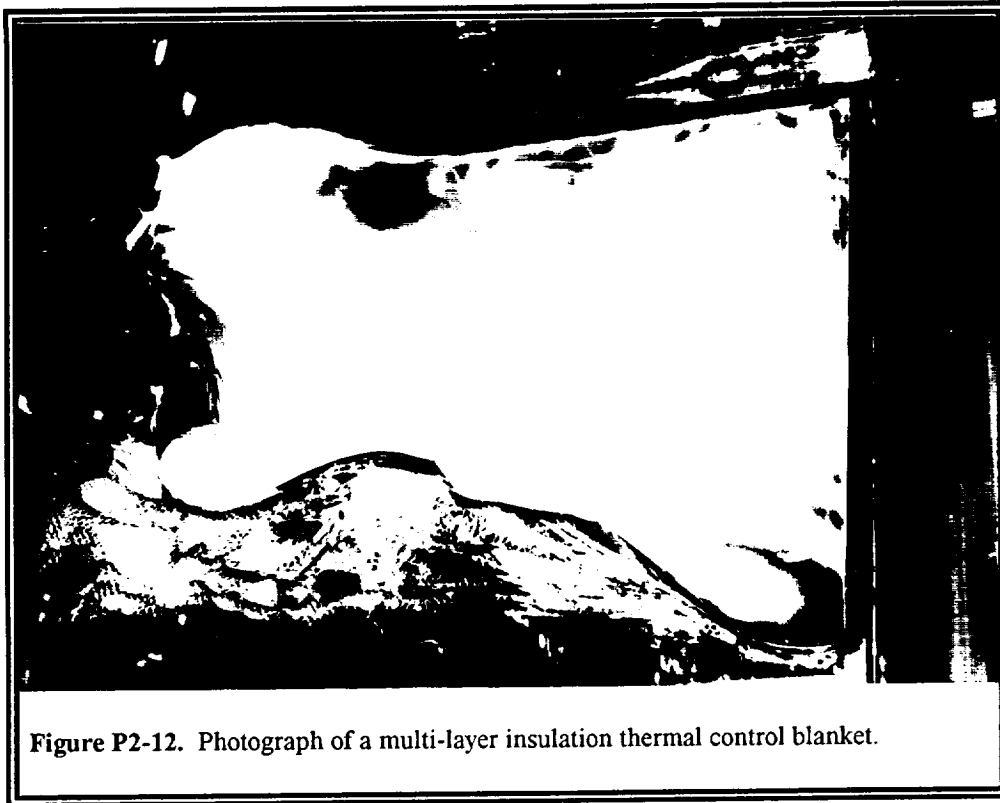


Figure P2-12. Photograph of a multi-layer insulation thermal control blanket.

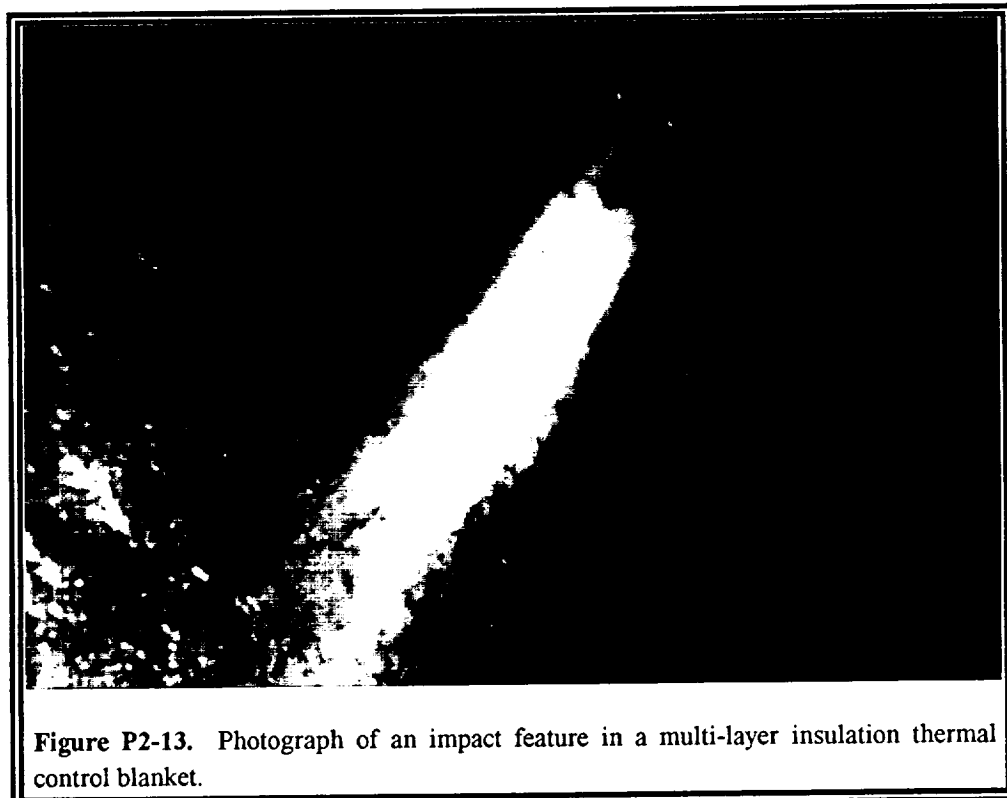


Figure P2-13. Photograph of an impact feature in a multi-layer insulation thermal control blanket.



UV and AO exposure, followed by a penetration through the top surface. This penetration caused typical tearing in the thin metal substrate as well as spallation of the paint surface and subsequent degradation from the particle ejecta. This impact was most likely a highly-oblique impact with much of the surrounding paint pigment and surface material being blown off by the impact ejecta.

**Figure P2-14 (S90-44934)** is another typical impact into these types of MLI. The "splotchy" area around the impact penetration is the thermal control paint with alternating patches of pigment particles and discolored binder. The impact penetration shows well defined lips in the metalized Mylar with spallation of paint from the surrounding material. The subsequent layers are not shown here, but the pressure pulse, combined with the spray of ejecta from this penetration, continued to damage multiple layers below the impact and the penetration hole size continued to expand through these subsequent layers. Depending on the impactor diameter, velocity, and material, it is possible to penetrate through all the layers of the MLI. An interesting note was that the Dacron mesh was often not penetrated itself, but rather left a protective shadow on the underlying layers.

**Figures P2-15a, P2-15b, and P2-15c (KSC-390C-2157.3, KSC-390C-2116.12, and KSC-390C-1770.4)** show the extent of damage caused by the synergisms of the space environment. Figure P2-15a is a photograph of an MLI from tray F09 on the leading edge of LDEF. The top surface of Mylar was completely eroded, exposing the interior surfaces to UV light, AO and thermal cycling. Due to exposure to these environments, the aluminum layers tended to break up into small pieces creating a shower of fine particles which went into orbit around the Earth in conjunction with LDEF. This created a type of atmosphere of fine particulates which completely surrounded LDEF and became an extreme contamination source for the entire satellite.

An even worse situation was created by the degradation of the aluminized Kapton which covered experiment A0054. Figure P2-15b shows the A0054 experiment which flew on the trailing edge at LDEF Bay B04. The aluminized Kapton was essentially unchanged from pre-flight.



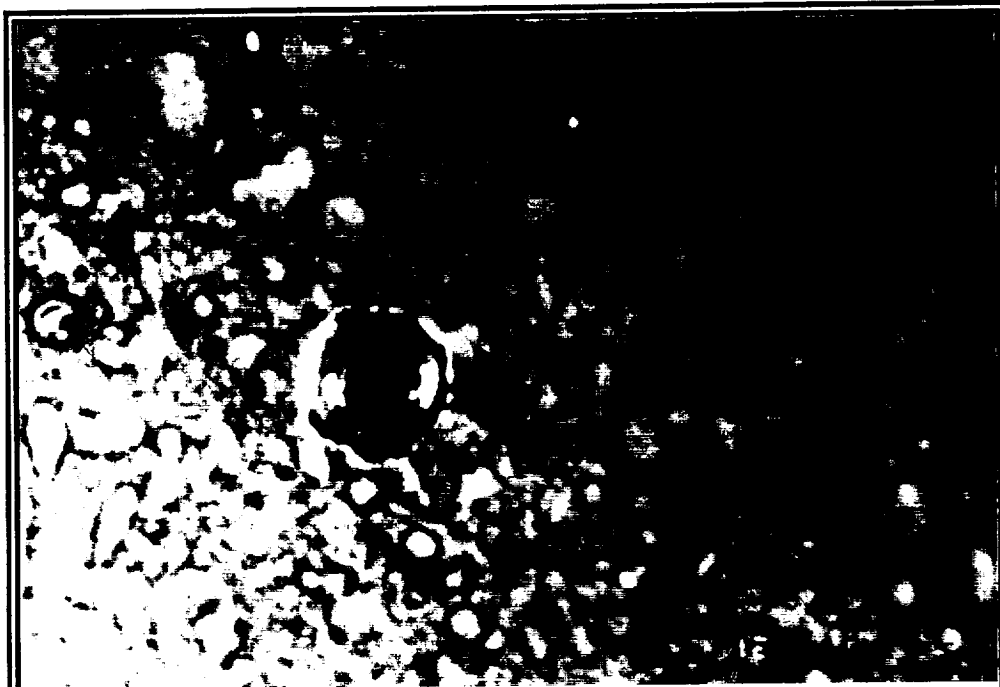
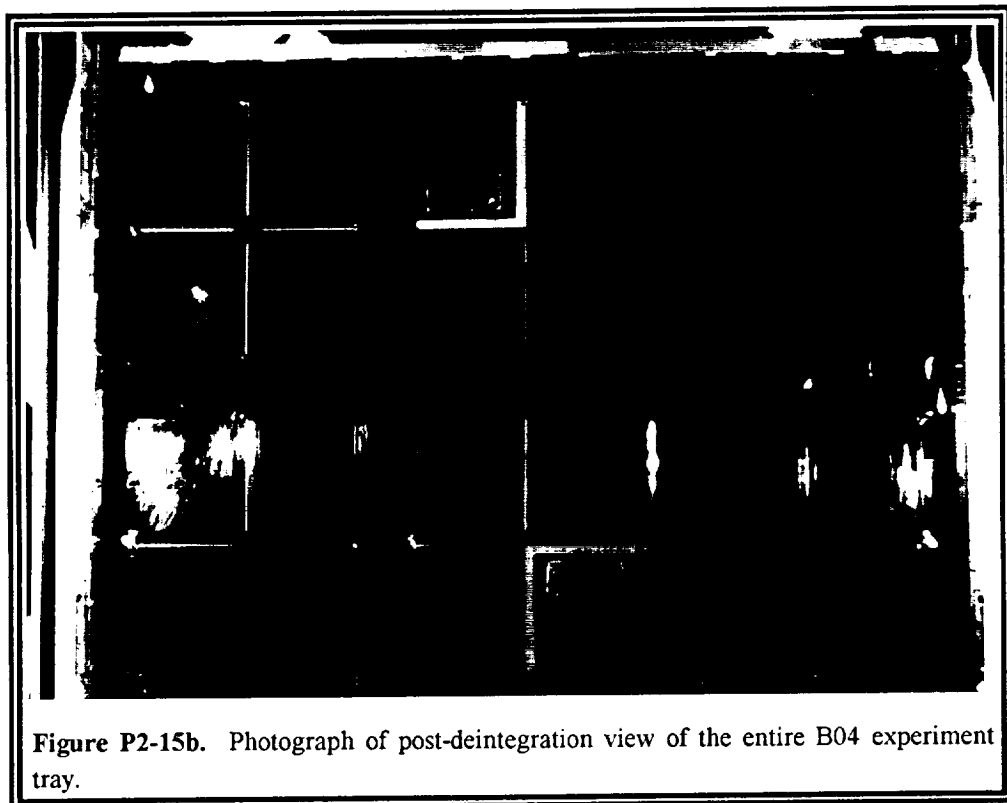


Figure P2-14. Photograph of an impact feature in a multi-layer insulation thermal control blanket.



Figure P2-15a. Photograph of a multi-layer insulation thermal control blanket.





**Figure P2-15b.** Photograph of post-deintegration view of the entire B04 experiment tray.



Conversely, Figure P2-15c shows the leading edge tray at LDEF Bay D10 with all of the Kapton eroded, leaving behind an approximately 1000 Å thick aluminum layer. This layer continued to generate particles which flaked off even after the retrieval of LDEF and became the primary source of large particle contamination for the entire satellite, even throughout LDEF's deintegration.

**Figures P2-16 and P2-17 (S90-45000 and S90-45015)** are photographs of the same penetration but from opposite sides of the material. The penetration is through an aluminized-Mylar foil. Figure P2-16 shows the front surface with the typical penetration through the Mylar leaving a large, slightly upraised area which delaminated from the lower aluminum. The penetration shows the typical large melted lips in the Mylar. Figure P2-17 shows the back surface of the aluminum. In the central area the penetration hole can be seen along with the melted lips of the Mylar and a large spallation area in the aluminum. In the delamination zone, the aluminum has cracked and petaled outwards from the spallation zone. This effect produced a large damage area ~8 times the diameter of the penetration in the Mylar.

**Figure P2-18 (KSC-390C-1038.4)** shows a very large impact in a silvered-Teflon blanket which was adhesively bonded to the aluminum heat pipe substrate at LDEF Bay B10. The central crater in the aluminum heat pipe shows well defined crater lips. The Teflon has bulged and delaminated from both the heat pipe substrate and the silver, and has large melted lips surrounding the penetration. The large delamination zone is easily identified and runs all the way to the edge of the plate. The black rings were caused by the subsequent exposure of the silver layer to AO which created a silver oxide area. This total view is ~5 cm across.

**Figure P2-19 (S90-43399)** is a picture of an entire LDEF A0178 thermal control blanket. These were silvered-Teflon blankets (Scheldahl G411500) with a back surface coating of Chemglaze Z306 black paint. The approximate thickness of the blanket was 200 microns. The picture is of the thermal blanket still attached to the experiment on LDEF. Notice the number of black dots. Each of these dots is a penetration through the Teflon, allowing access of AO to the silver layer. Instead of being reflective (as on pre-flight) the entire blanket is very milky in color. This is



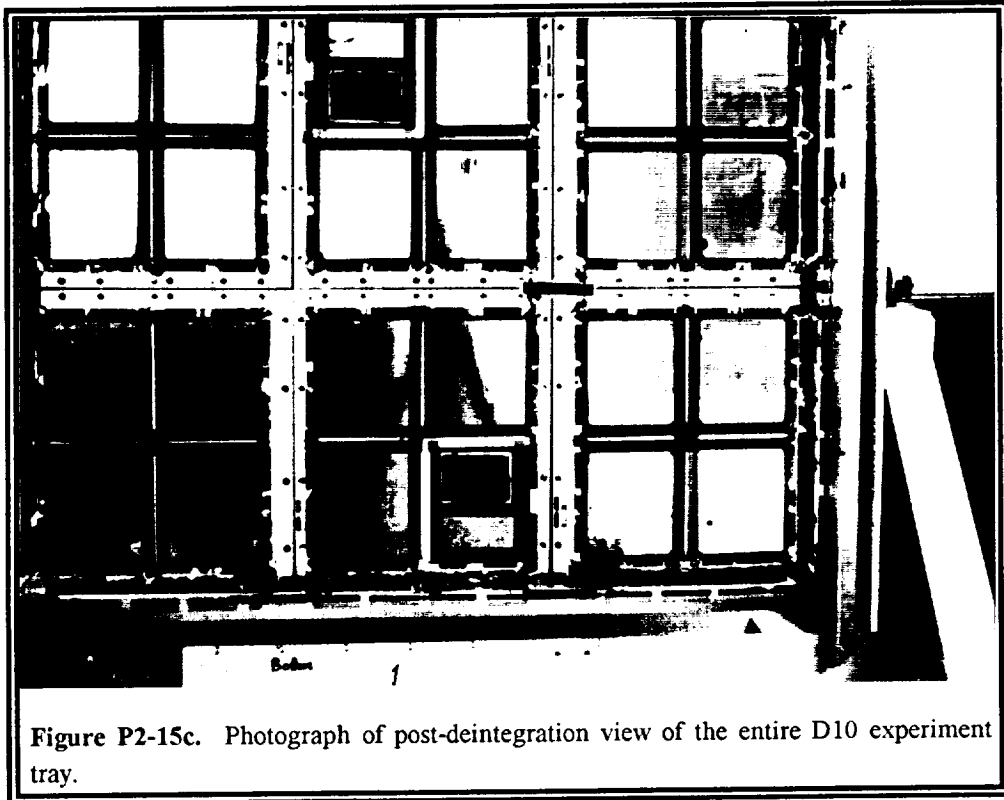


Figure P2-15c. Photograph of post-deintegration view of the entire D10 experiment tray.

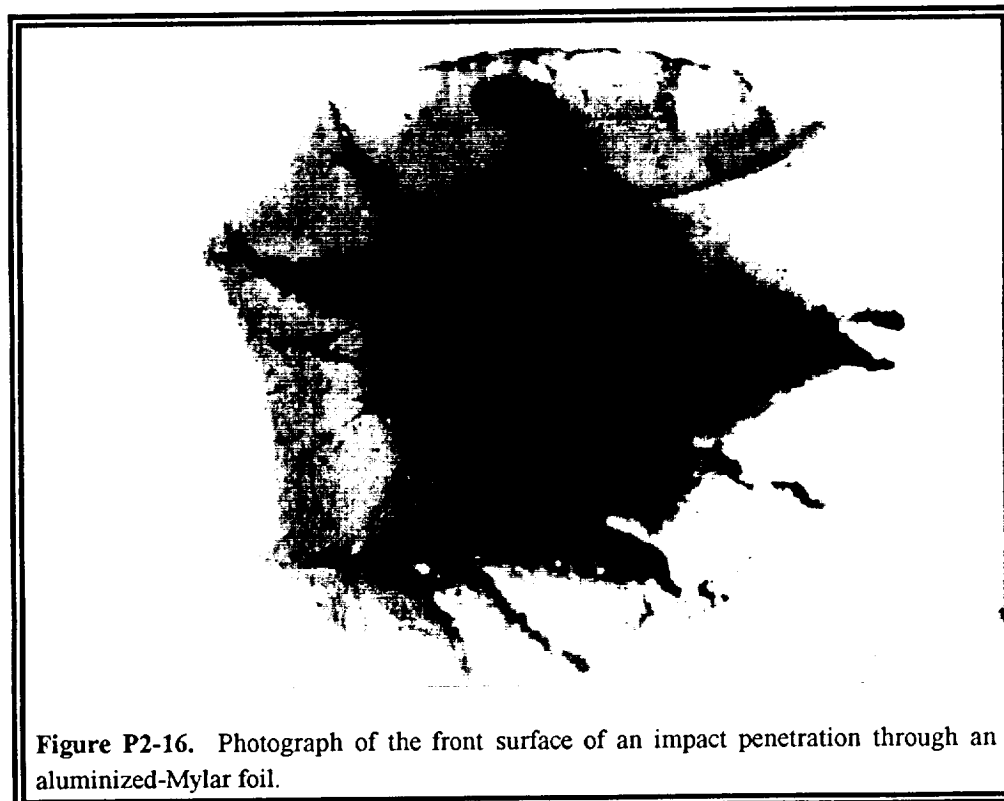
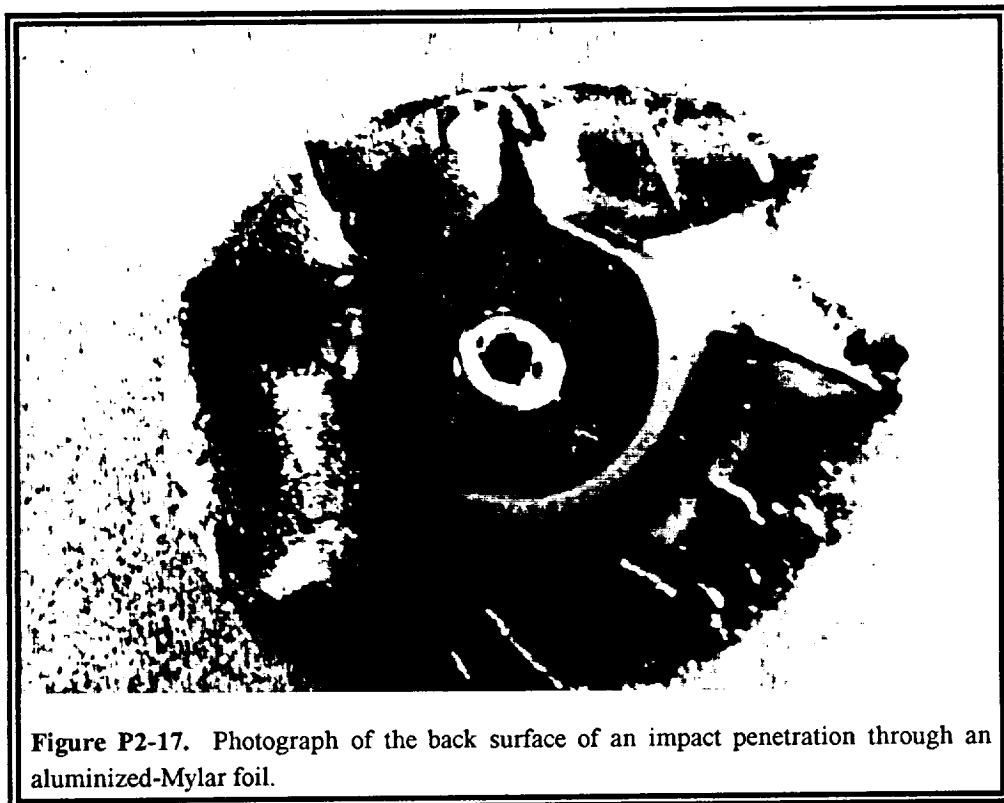
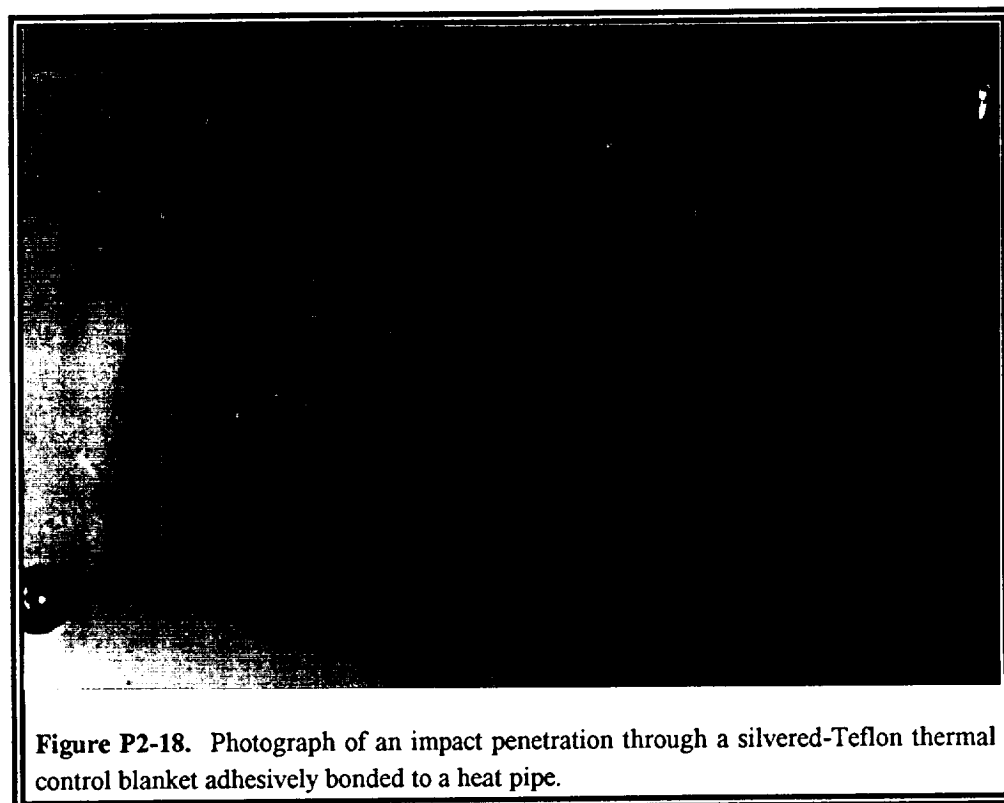


Figure P2-16. Photograph of the front surface of an impact penetration through an aluminized-Mylar foil.





**Figure P2-17.** Photograph of the back surface of an impact penetration through an aluminized-Mylar foil.



**Figure P2-18.** Photograph of an impact penetration through a silvered-Teflon thermal control blanket adhesively bonded to a heat pipe.



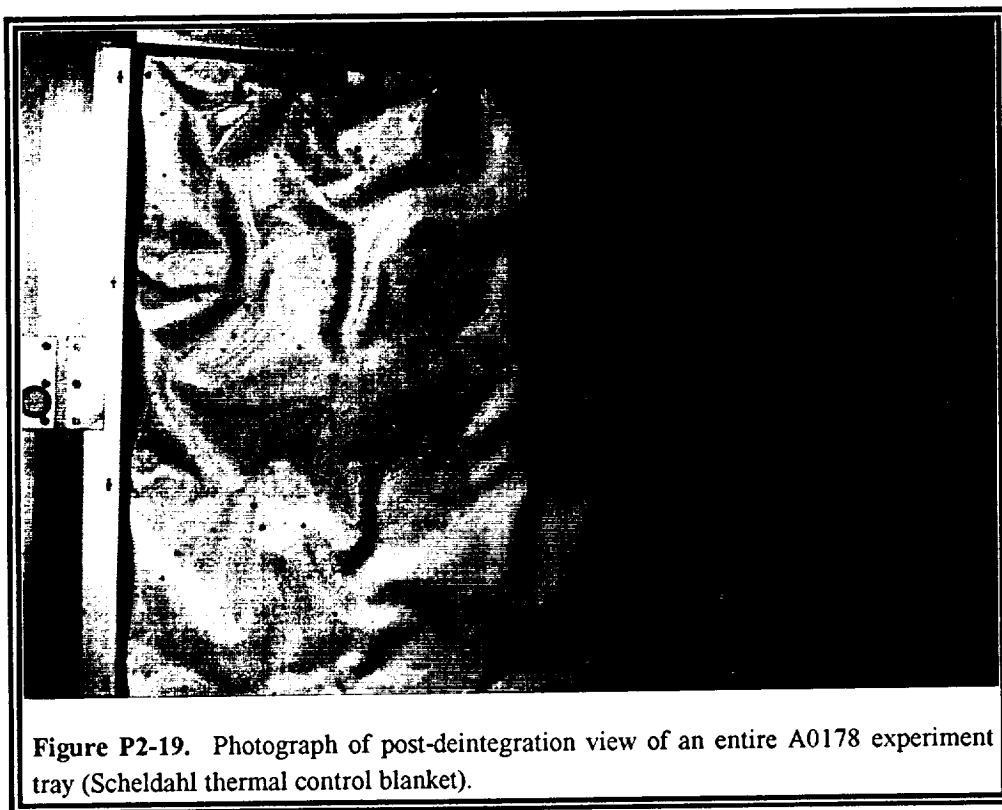


Figure P2-19. Photograph of post-deintegration view of an entire A0178 experiment tray (Scheldahl thermal control blanket).



caused by the high amount of light scattering from the newly textured surface of the Teflon. The Teflon surface was textured by AO erosion.

**Figure P2-20 (S90-43484)** shows the back surface of one-third of one of these blankets. The lighting behind it shows the large number of penetrations which allowed access of the environments into the interior of the experiment. Each of these penetrations is surrounded by an associated delamination zone, a discoloration due to AO exposure of the silver layer, and delamination of the black thermal control paint on the back surface. These blankets were attached to the trays by Velcro (examples of which can still be seen on the back of the blanket), which worked very well. The attachment lasted throughout the entire mission and, in fact, could still be used for attachment of the blankets into their respective carrying cases.

**Figure P2-21 (KSC-390C-2208.12)** is an example of a large penetration through the A0178 thermal control blanket from LDEF Bay A10. Five smaller impacts surround the large penetration. Notice that the large penetration occurred over a piece of Velcro, so that the impactor penetrated through the silvered-Teflon blanket and ended up in the Velcro attachment. This delamination zone is connected to delaminations surrounding three other impacts in the image. This combined delamination area led to very large discoloration areas for the silver. Note that each of the penetrations has very well defined melted lips from the Teflon. The total view in this picture is ~10 cm across.

**Figure P2-22 (KSC-390C-2112.3)** shows two penetrations through an A0178 blanket from LDEF Bay C11. The delamination zone connects the two penetrations. These two events were separated in time but the larger penetration (on the right) probably occurred after the smaller penetration. This disrupted the ring structure which was growing around the smaller penetration due to AO degradation of the silver, leaving the deformed pattern. This also shows the size of the delamination and shock wave caused by the larger impact. This total view measures ~9 cm across.



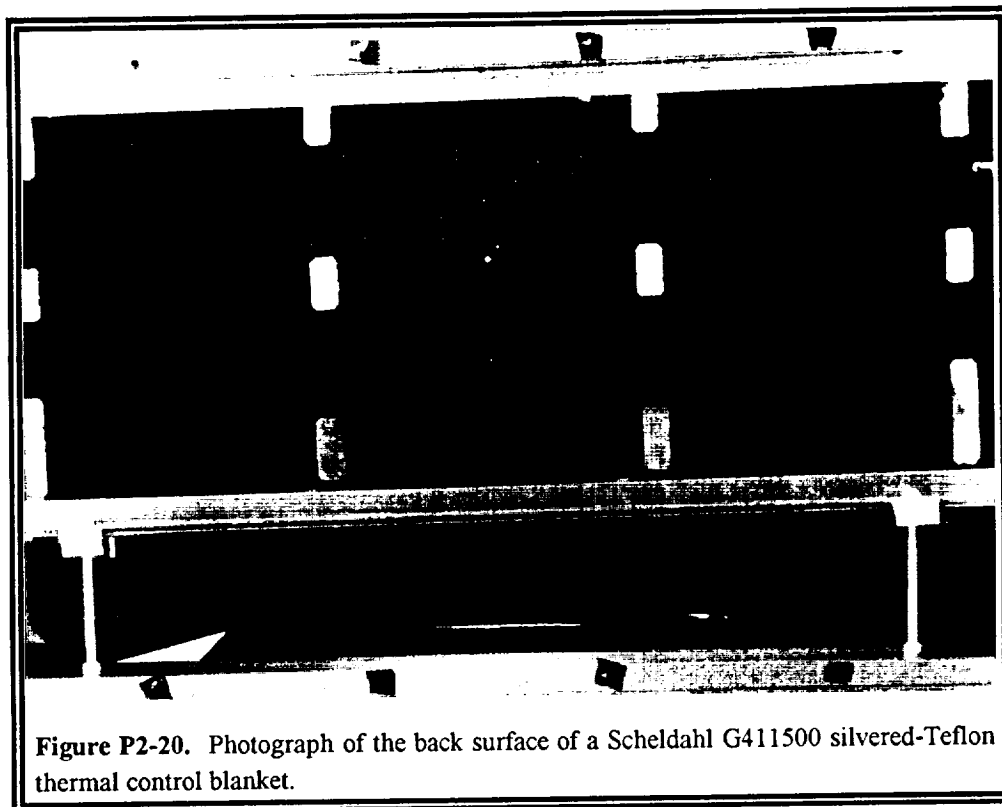


**Figure P2-20.** Photograph of the back surface of a Scheldahl G411500 silvered-Teflon thermal control blanket.

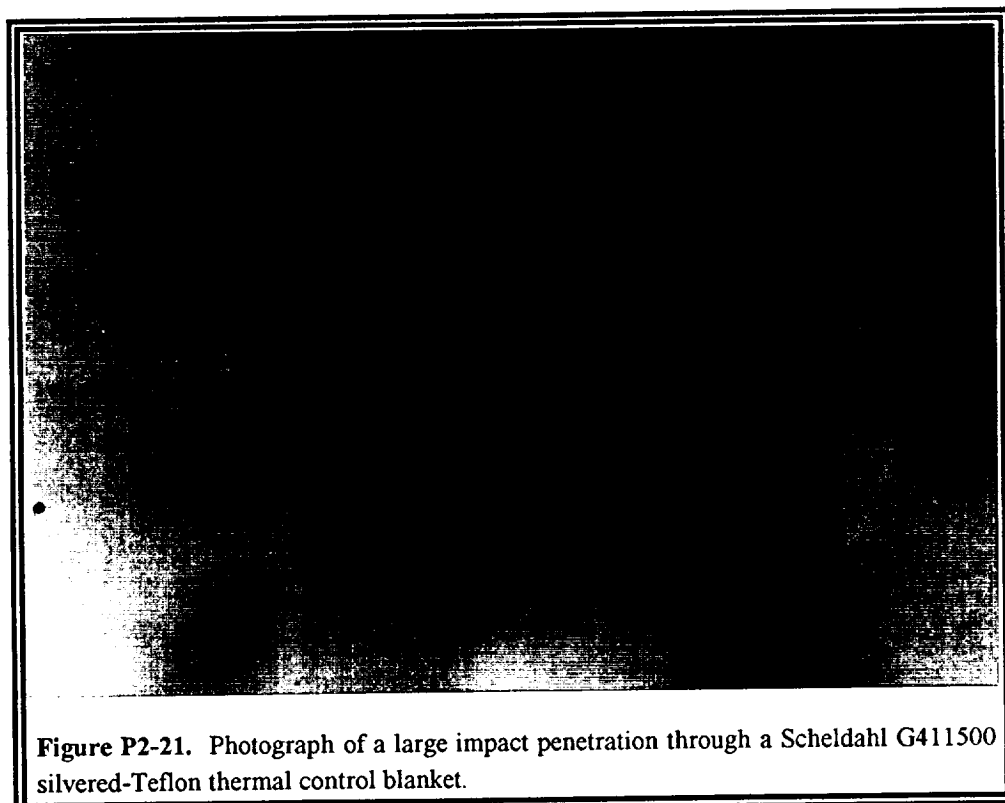


**Figure P2-21.** Photograph of a large impact penetration through a Scheldahl G411500 silvered-Teflon thermal control blanket.





**Figure P2-22.** Photograph of two impact penetrations through a Scheldahl G411500 silvered-Teflon thermal control blanket.



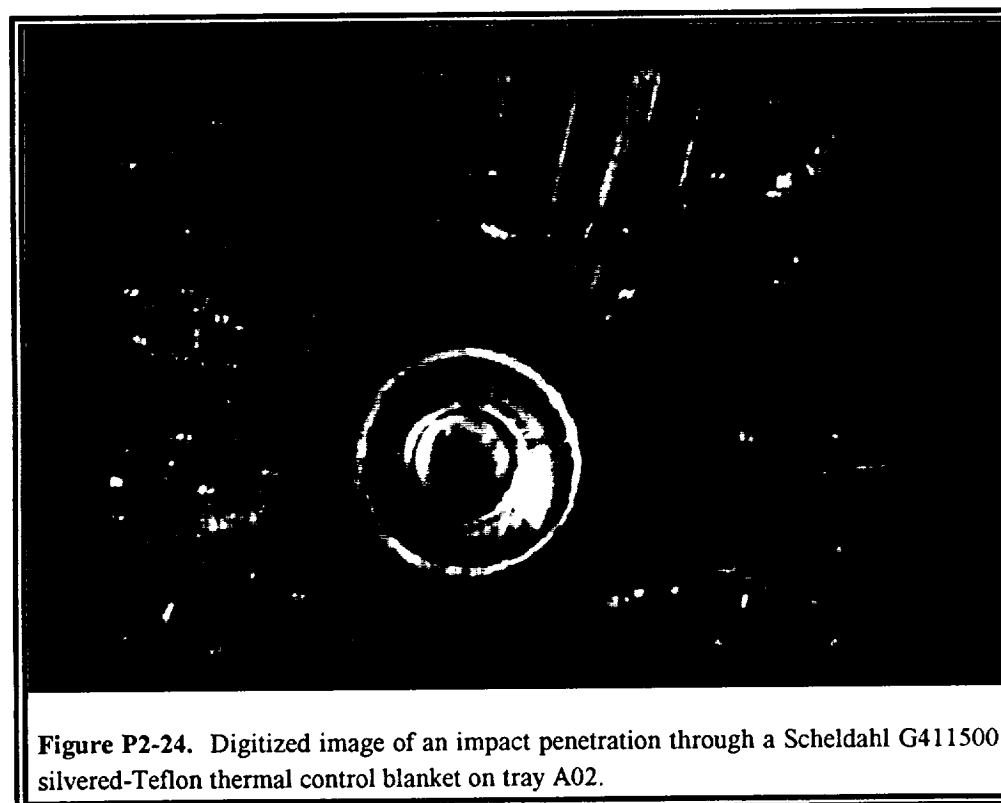
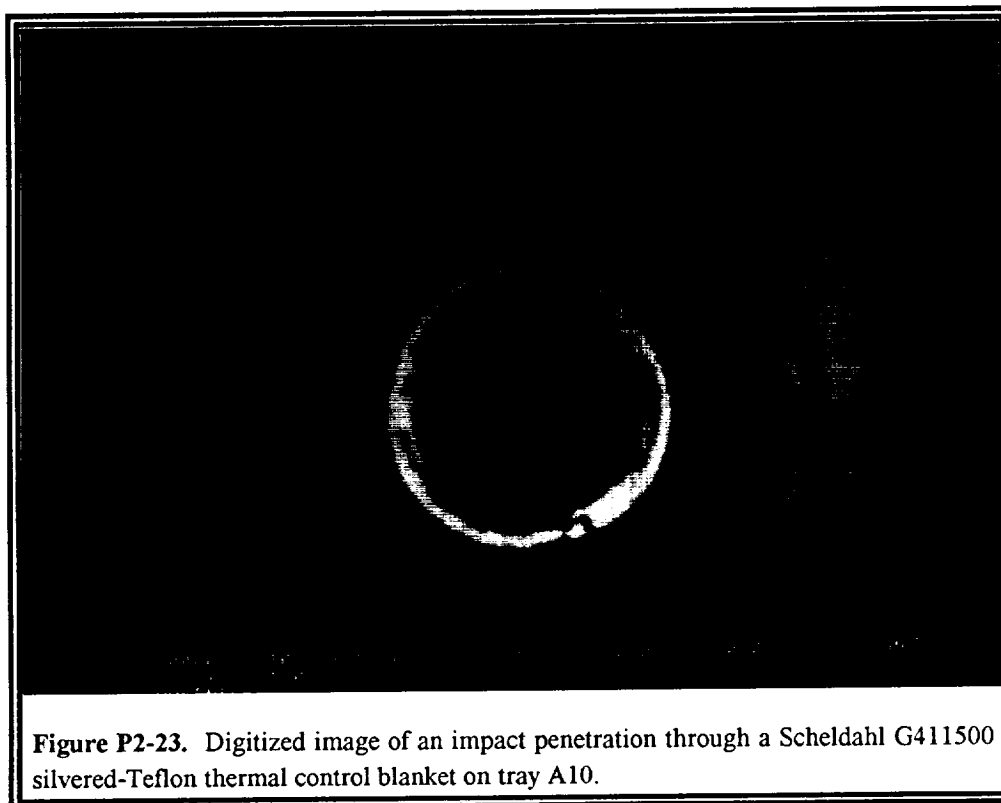
**Figure P2-23 (POD-9201-001)** is a digitized image of a penetration through the leading edge A0178 blanket from LDEF Bay A10. This penetration hole has a diameter of  $\sim 1.02$  mm. This penetration has the typical well defined melted lips, a large delamination area, and rings created by the AO effects on the underlying silver. This image is not a true color image of the rings.

By contrast, **Figure P2-24 (POD-9201-002)** is a digitized image of a penetration through the A0178 thermal control blanket on the trailing edge at LDEF Bay A02. Note the large difference in response. Thermal blankets on the trailing edge were not subjected to AO, but rather were subjected to UV light which embrittled the Teflon. Without the mitigating effects of the AO erosion, the Teflon became very brittle. While the penetration has the typical raised melted lips and an underlying (but smaller) delamination from the silver and black paint layers, it does not have AO-created rings in the silver. Instead, there are multiple cracks running out from the central penetration hole. These cracks are located in the Teflon, not in the silver or black-painted back surface.

**Figure P2-25 (S90-44988)** shows an impact, probably at a highly-oblique angle, into the A0178 Teflon blankets. This impact did not penetrate all the way through the blankets but instead cratered the surface. This caused a delamination between the Teflon and the silver and a large amount of ejecta (in the upper left corner) sprayed across the surface of the Teflon. The underlying silver had very little AO erosion.

**Figure P2-26 (KSC-390C-1544.6)** is a combined picture of several impacts on the leading edge A0178 thermal control blanket from LDEF Bay C08. This picture shows several typical penetrations with their surrounding delamination areas and ring structures due to AO. In addition, there is a large spray feature which emanates from the lower central impact and goes towards the top of the picture. This spray passes right next to a delamination zone. This delamination zone was caused by a crater which did not penetrate the Teflon, but created a large enough shock wave to cause a huge delamination between the Teflon, the silver, and the underlying black paint. This one image shows several different types of features and measures  $\sim 21$  cm across the total view.







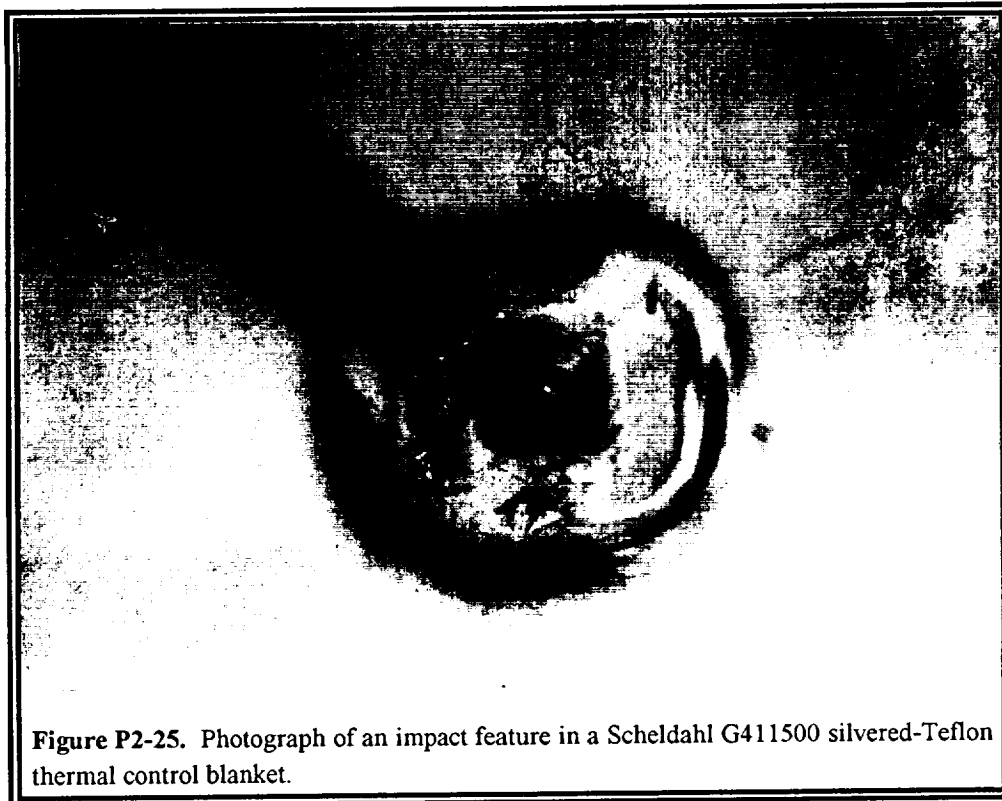


**Figure P2-25.** Photograph of an impact feature in a Scheldahl G411500 silvered-Teflon thermal control blanket.

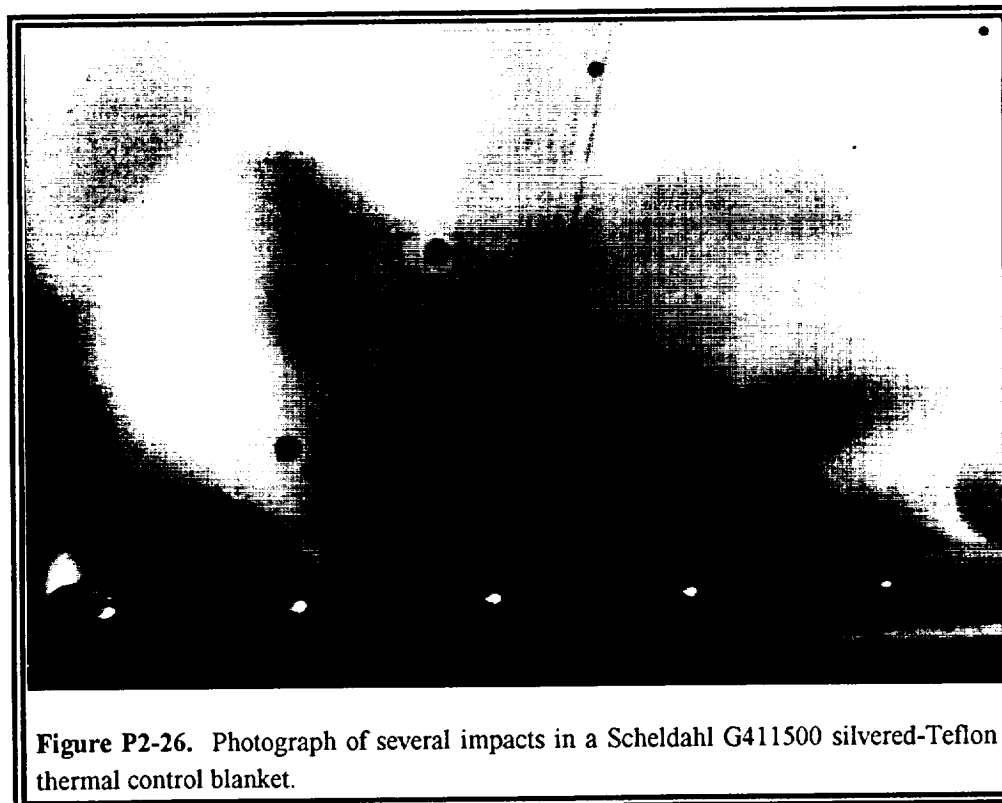


**Figure P2-26.** Photograph of several impacts in a Scheldahl G411500 silvered-Teflon thermal control blanket.



Of greatest importance for the thermal control blankets is the fact that the total damage areas are always much greater than those due to simple cratering. These impact features and their large damage areas are of concern due to the changes in reflectivity caused by the synergisms with the other space environments, particularly AO. In addition, the large delaminations from the substrates will affect thermal conductivity. This is particularly important for radiators and heat pipes.

### **2.2.2 Impact Effects on Thermal Control Painted Materials**

**Figure P2-27 (S90-43421)** is a picture of the overall M0004 experiment tray (Bay F08). This picture was taken with an oblique view to show the extent of the damaged areas on the white thermal control paint (Chemglaze A276). This paint has been exposed to AO thus removing the upper layer of binder and leaving behind a thin layer of loosely attached pigment particles. LDEF's thermal control paints showed several very interesting types of impact-related phenomena and provided the first examples of the ring phenomena. The ring phenomena occurs in many different varieties. **Figure P2-28 (KSC-390C-1937.6)** shows one type of ring morphology which was rarer than the others. This figure shows multiple craters (on the same surface shown in **Figure P2-27**) where the rings appear to be caused by the very top layer of paint being wrinkled and rolled back. This total view measures ~8cm across. **Figure P2-29 (KSC-390C-1937.7)** is a closer look at one of these craters. This figure shows a central crater surrounded by a spallation area and a cleared smooth area, which is then surrounded by the upraised rings. The rings look as though the top layer of paint has been rolled or folded back over the surface by a surface shock wave.

**Figure P2-30 (KSC-390C-1938.1)** shows the more dominant type of ring features seen in the thermal control paints. In these features, craters were typically surrounded by an area of paint spalled from the front surface. This spallation area is surrounded by a smooth area, with little or no visible damage, which is surrounded by a series of rings. These rings are upraised areas of dislodged paint or pigment powder on the surface of the paint substrate.



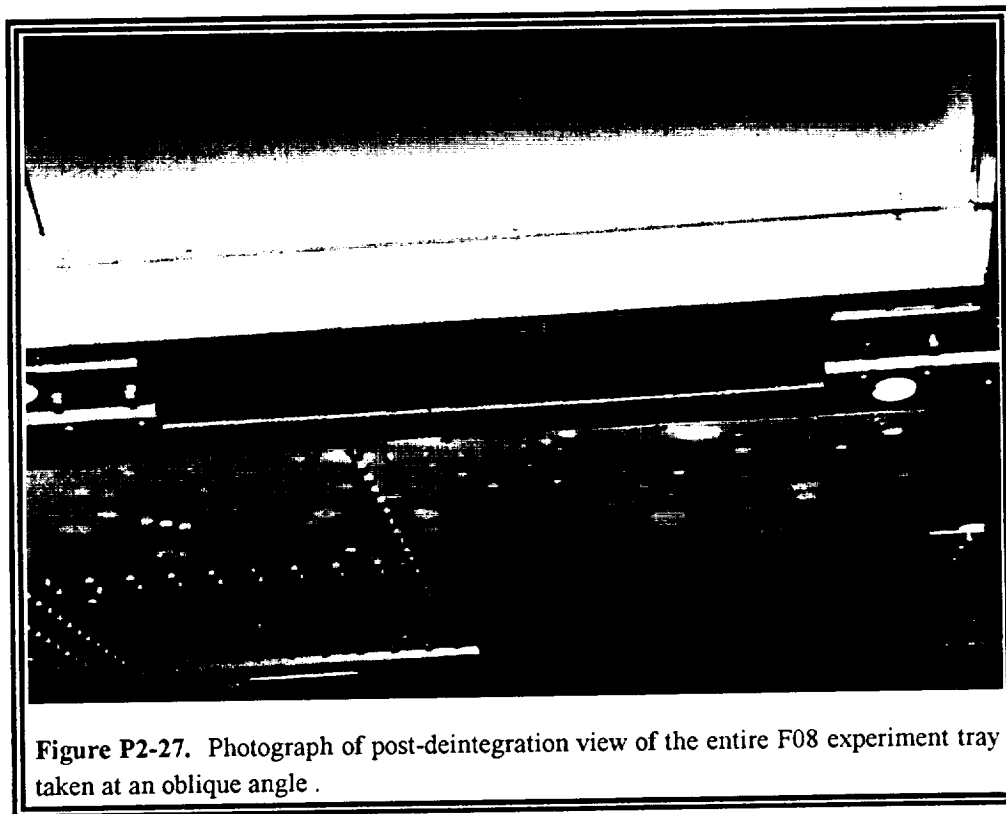


**Figure P2-27.** Photograph of post-deintegration view of the entire F08 experiment tray taken at an oblique angle .

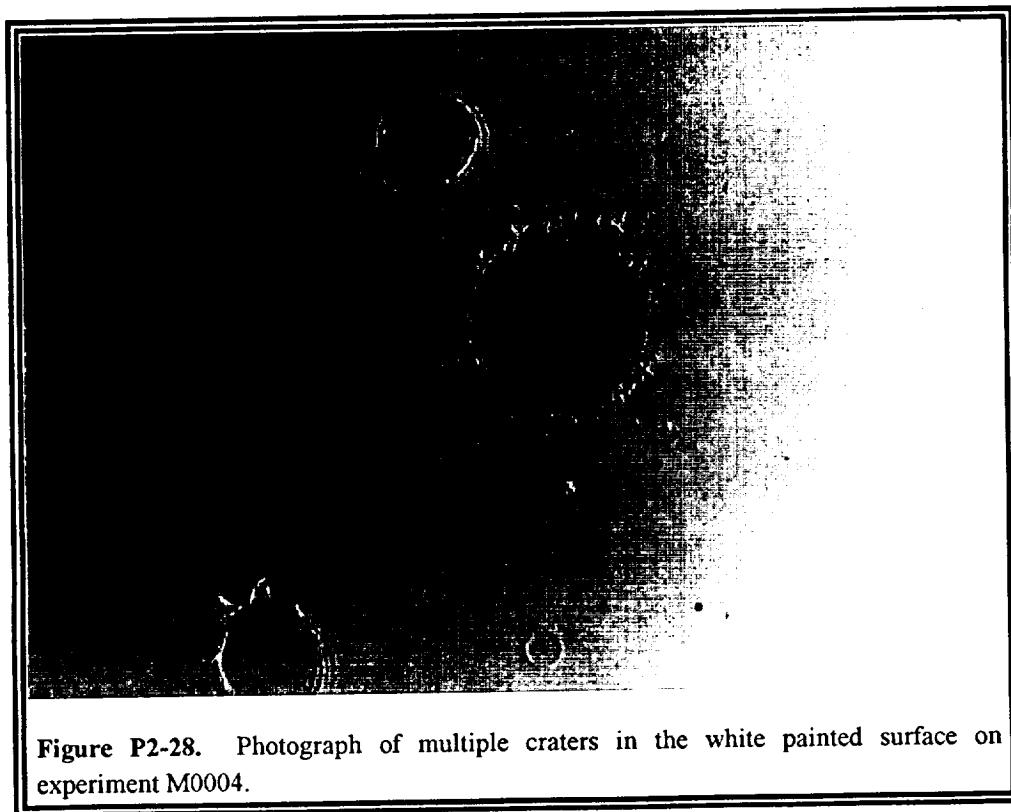


**Figure P2-28.** Photograph of multiple craters in the white painted surface on experiment M0004.



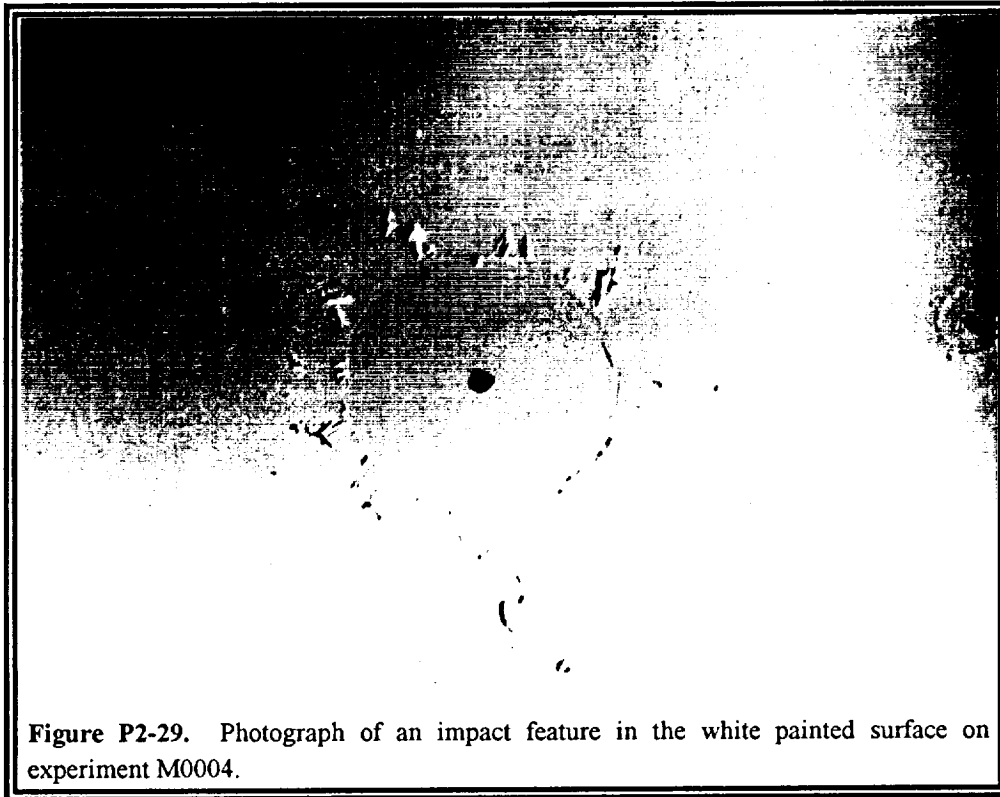


**Figure P2-29.** Photograph of an impact feature in the white painted surface on experiment M0004.

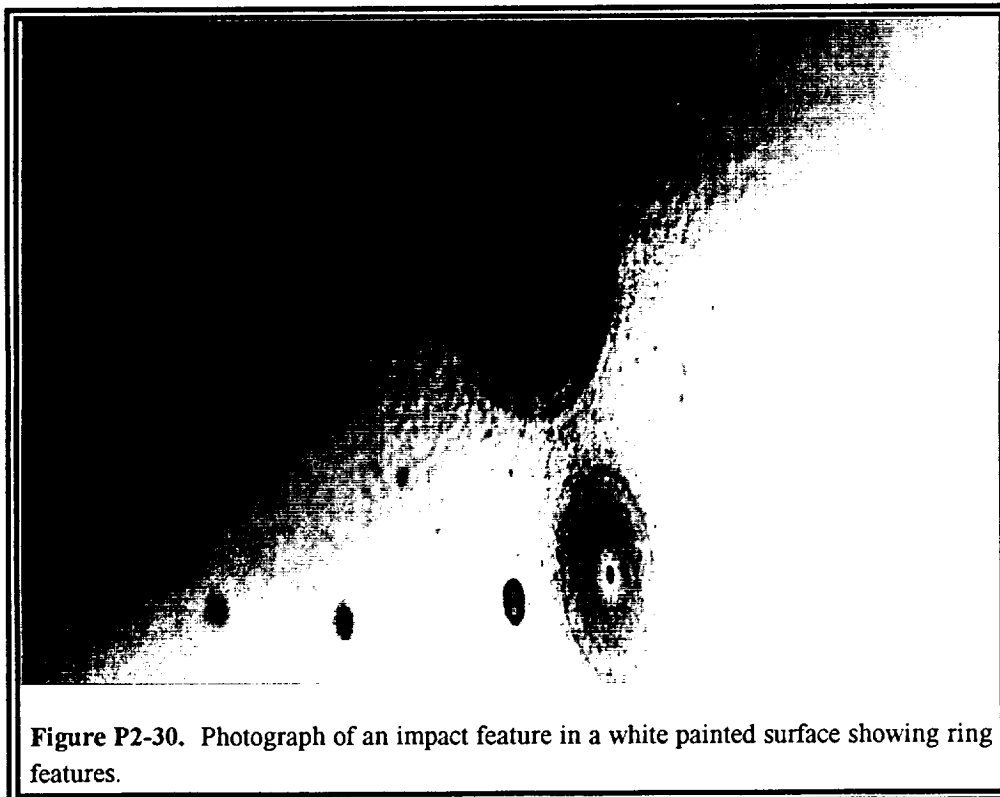


**Figure P2-30.** Photograph of an impact feature in a white painted surface showing ring features.



**Figure P2-31a (POD-9014-001)** is a picture of one of these ring features showing the central crater with its upraised lips in the aluminum substrate, and a surrounding area of spallation with a small area of uplifted paint which did not have enough energy to spall. This area is then surrounded by an area of no damage or particulates, followed by an extensive ring structure. On the left some of these rings look like merely raises in the powder, whereas on the upper right side the rings look as if the upper surface of paint folded back. **Figure P2-31b (POD-9014-002)** is a higher magnification view of this same ring structure and shows a close up of the folds described above. These folds appear to be a thin layer of rolled up or peeled back paint.

**Figure P2-32 (POD-9014-003)** appears to be a similar type of structure. However, this impactor did not go all the way through the paint and all that is seen are raised lips in the area of the crater in the paint. There is also an area of a small dome of uplifted paint where it has begun to delaminate from the aluminum substrate. Then there is the typical cleared out area followed by the outer rings. In this case the outer rings begin to look as if they were broken down by the AO and are beginning to erode. **Figure P2-33 (POD-9014-004)** shows another impact into the white painted surface with similar morphological characteristics. Note the central crater in the aluminum surrounded by a spallation area of paint, and by an area of uplifted paint which did not quite spall. In this photograph the spall energy appears to have been very low as, on the paint surface surrounding the spall where there is usually no material (*i.e.*, the smooth area), there is an area of deposited material in the lower right hand corner. The shape of this material is very similar to the shape of the piece which spalled from the paint. The ring structure here is very eroded indicating either that the rings were aged by AO exposure, or that the paint was very AO-eroded at the time of the impact and the layer of loosely attached paint pigment particles was deformed by the surface shock waves.

**Figure P2-34 (POD-9014-005)** shows the last crater in this sequence. Again the morphology is similar in that there is a central crater in the aluminum substrate, a large spallation area where the paint was removed, an area where most of the paint pigment has been removed, and then an outer area of rings. These rings have been almost totally eroded by AO, or alternately, the outer rings may be surface shock phenomena in very aged paints where there is very little binder left and



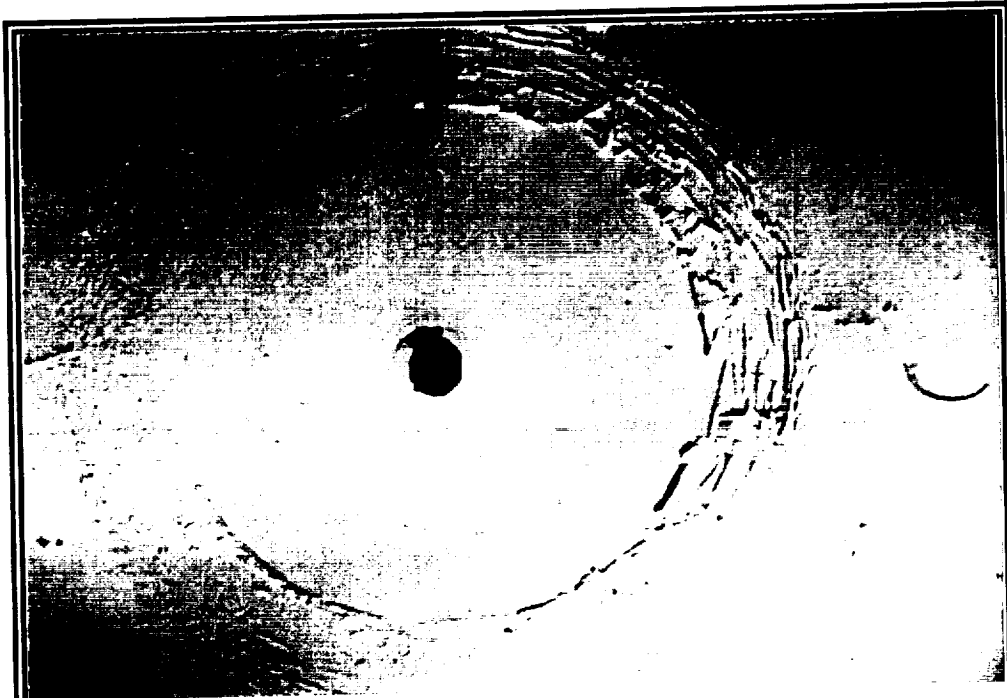


**Figure P2-31a.** Photograph of an impact feature in a white painted surface showing ring features.



**Figure P2-31b.** Photograph of the same impact as Figure P2-31a at a higher magnification showing ring features.



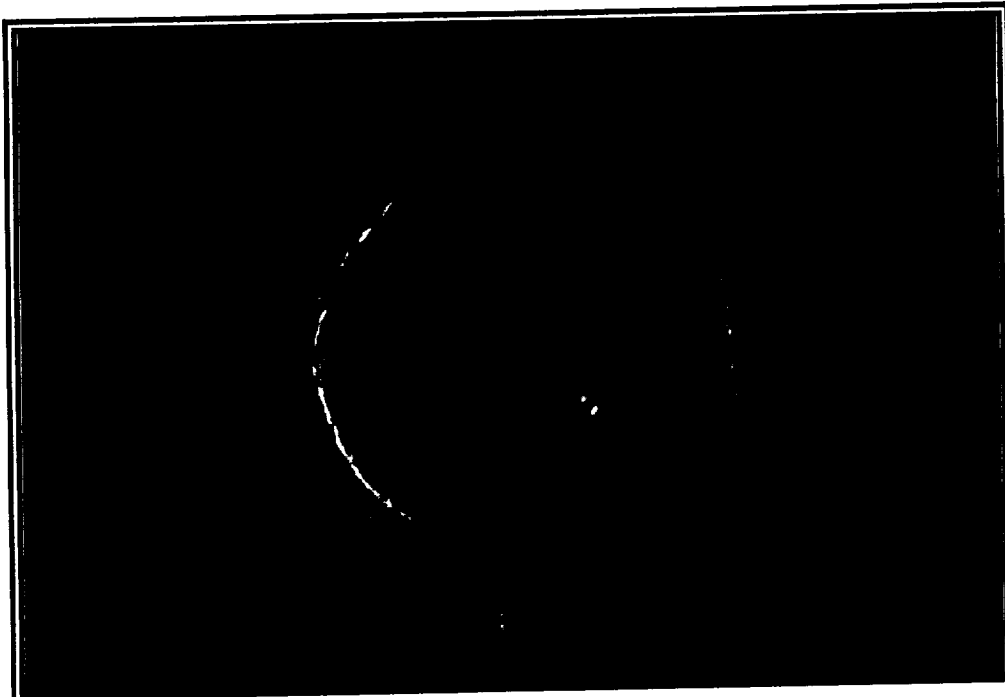


**Figure P2-32.** Photograph of an impact feature in a white painted surface showing ring features.

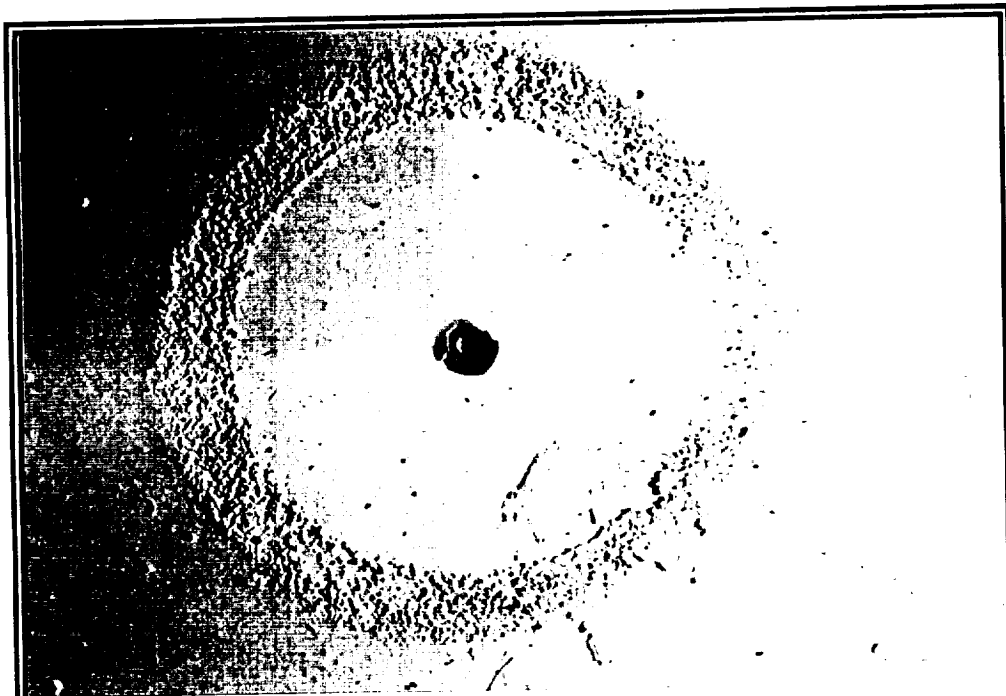


**Figure P2-33.** Photograph of an impact feature in a white painted surface showing ring features.



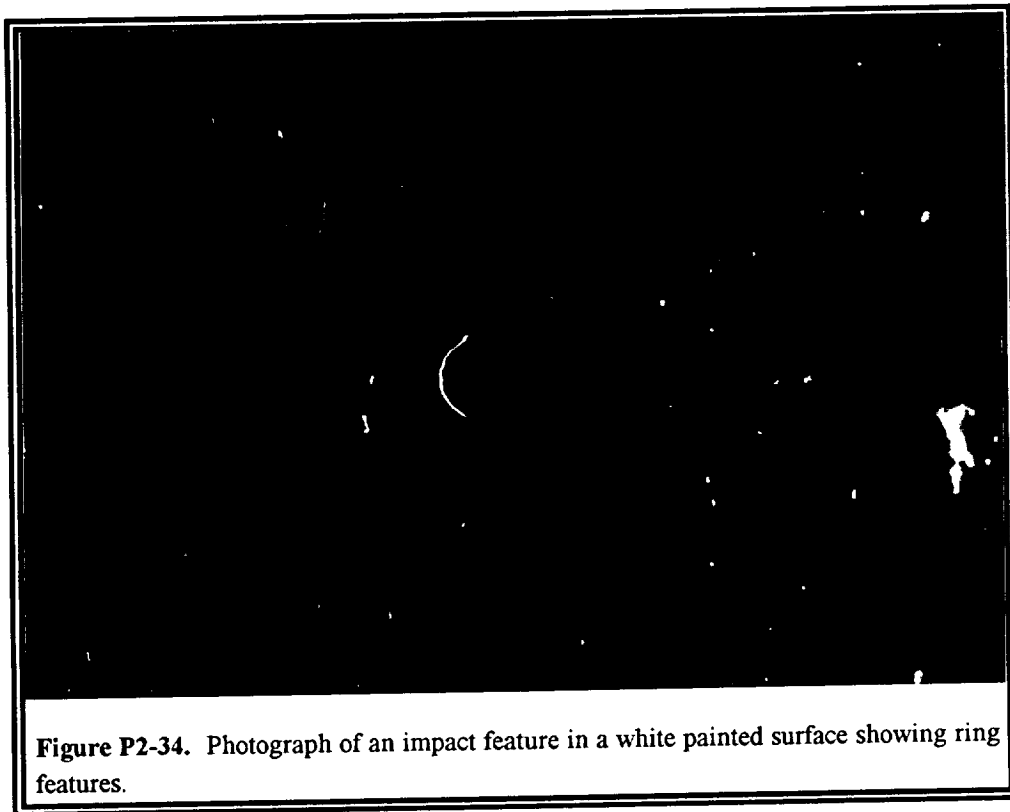


**Figure P2-34.** Photograph of an impact feature in a white painted surface showing ring features.



almost nothing but pigment particles left to be affected by the shock. Thus, this sequence of photos offers an opportunity to determine an aging or time-associated phenomena associated with the rings. Either the rings are eroded by the AO after their formation, thus creating these structures and enabling us to determine the relative time of impact, or the rings are created in different forms based on the amount of aging which the paint underwent prior to the impact, again allowing us to determine the relative time of impact. It is important to note that the total affected area of the paint is many times (sometimes 10 to 20 times) the diameter of the impact crater in the substrate. This type of phenomena was found in many of the paints on LDEF. In particular, thin paint layers (*e.g.*, with only two coatings of paint) and paints which were highly susceptible to AO were most affected by the ring phenomena.

**Figure P2-35 (S90-43597)** is a picture of a crater in the gray thermal control paint on the active grapple fixture from LDEF Bay C10. This picture shows several different impacts with surrounding ring structures in the paint. **Figure P2-36 (KSC-390C-1937.2)** is an excellent example of the rings in this grapple plate. This picture shows a central crater in the underlying aluminum substrate surrounded by a spallation zone, an outer spallation zone where only the upper layer of paint was removed, and upraised rings on the outer surface.

**Figure P2-37 (POD-9014-006)** shows an impact into the same type of grapple fixture paint but on the trailing edge at LDEF Bay C01. This grapple was not exposed to AO at any time, but UV partially embrittled this paint. The impactor formed a crater in the underlying substrate, a spallation zone around the crater and an outer spallation layer began to form and separate, as shown by the semicircular crack around the outer edge of the paint. The underlying yellow material is the remnant of the primer paint layer which was spalled. Impact features found on the trailing edge of LDEF show no rings of any form. This is to be expected since there was no AO exposure and since the paint binder has a brittle response due to UV exposure.

**Figure P2-38 (S90-44961)** shows a penetration through a white painted aluminum surface from the trailing edge. The penetration hole is typical of hypervelocity penetrations through aluminum. The penetration has large well-formed lips on the front surface in the aluminum and a large



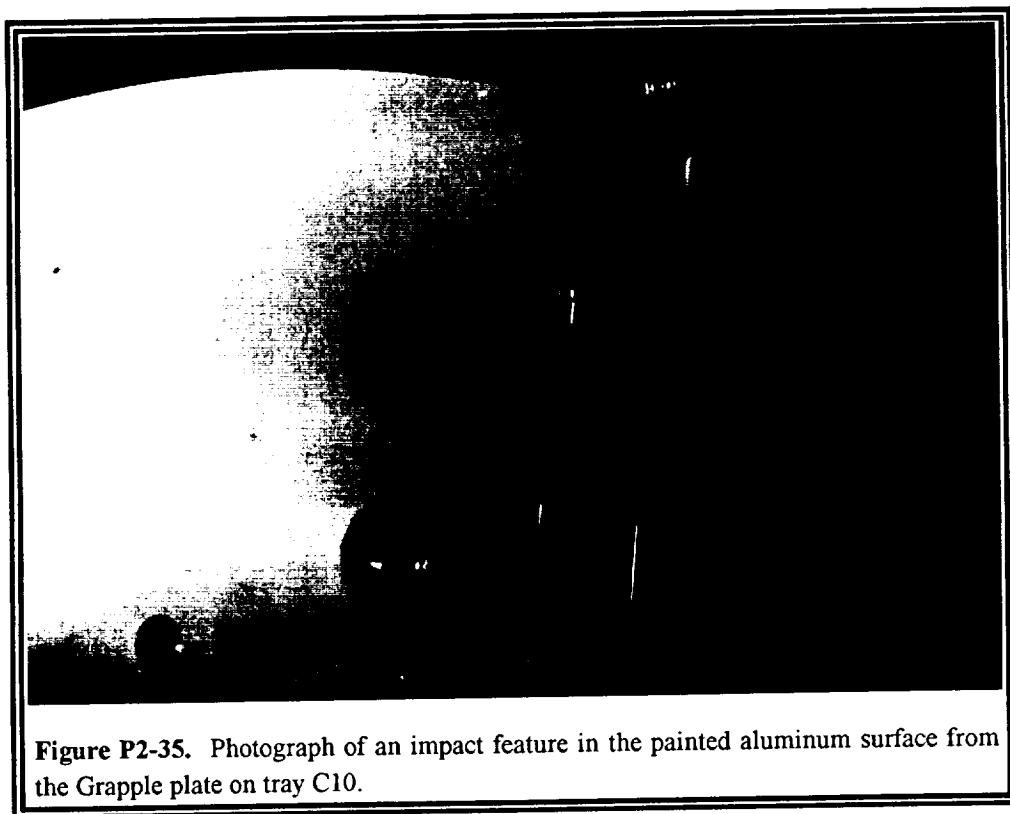


**Figure P2-35.** Photograph of an impact feature in the painted aluminum surface from the Grapple plate on tray C10.

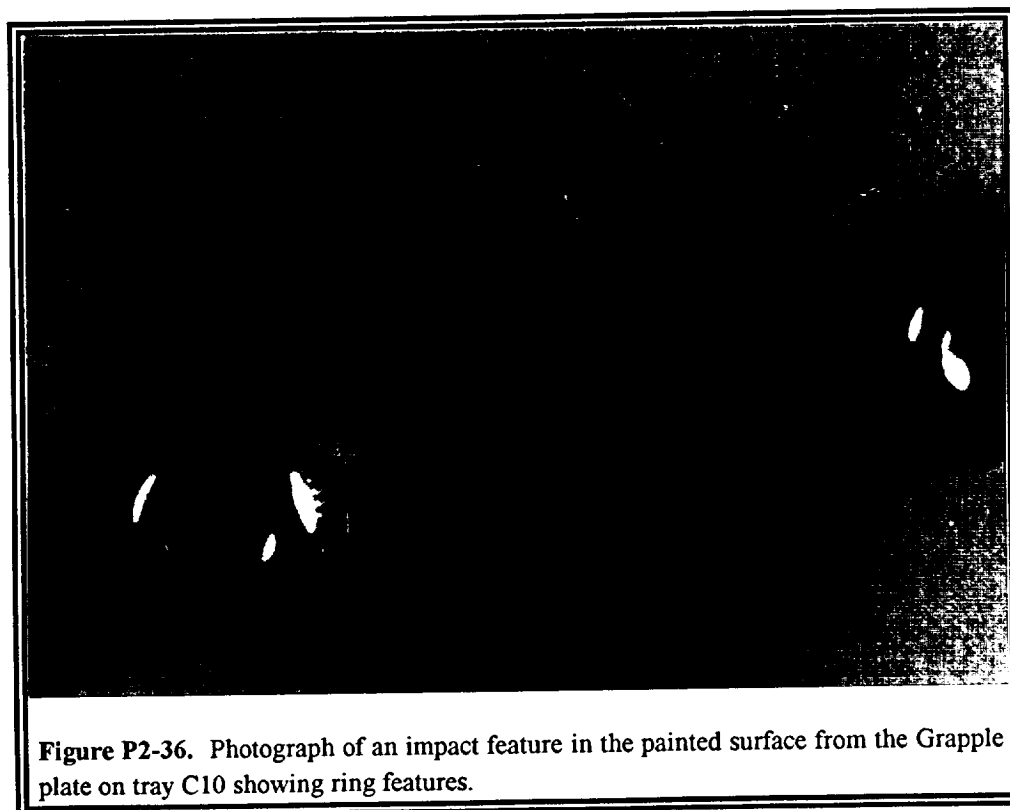


**Figure P2-36.** Photograph of an impact feature in the painted surface from the Grapple plate on tray C10 showing ring features.



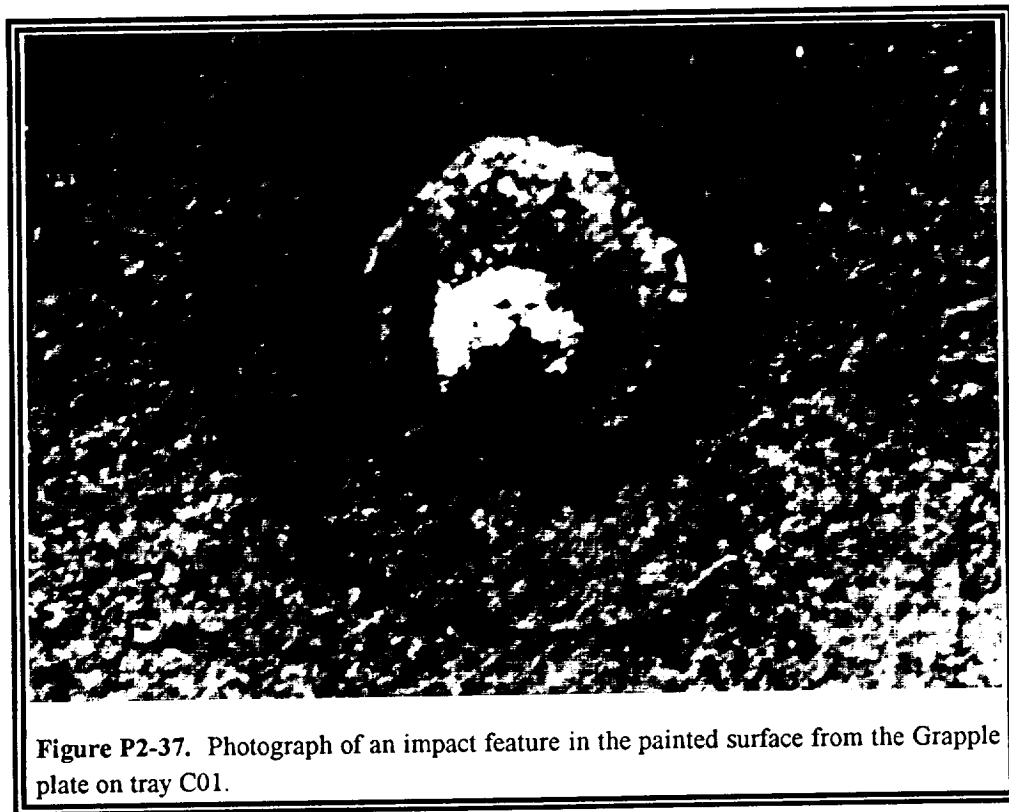


**Figure P2-37.** Photograph of an impact feature in the painted surface from the Grapple plate on tray C01.

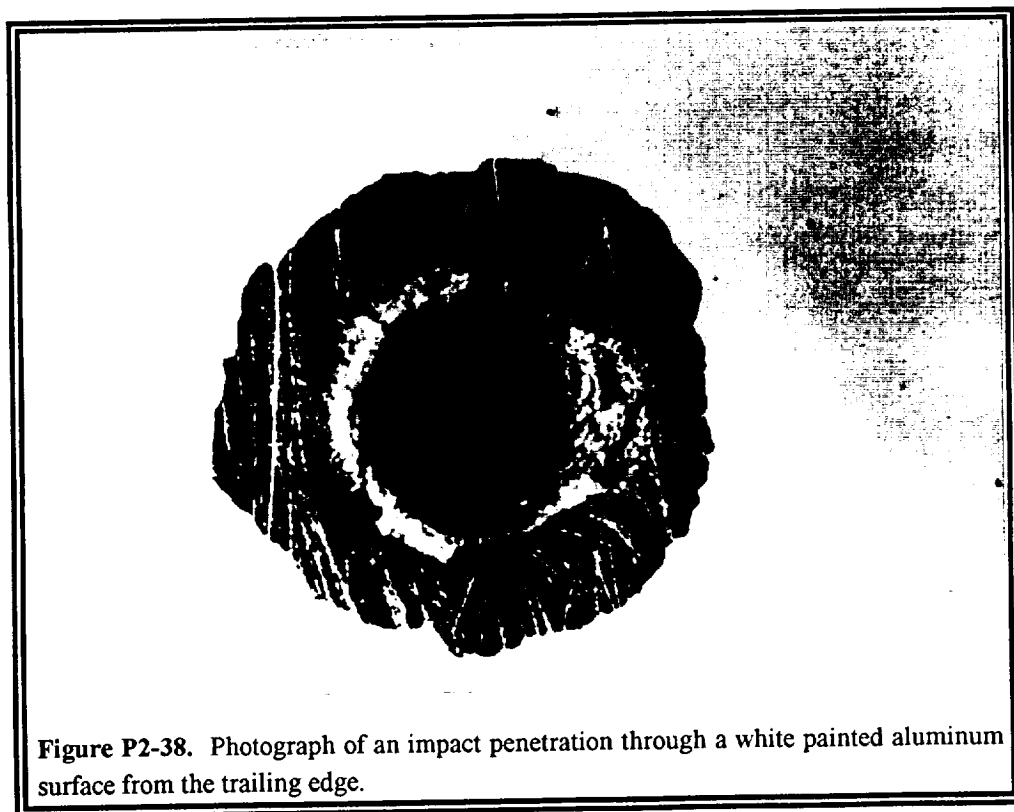


**Figure P2-38.** Photograph of an impact penetration through a white painted aluminum surface from the trailing edge.



spallation area around this surface. Note again that no ring structures were formed. The back surface of this penetration was shown in Section 2.1 as Figure P2-2.

**Figures P2-39a, 2-39b, and 2-39c (S90-45007, S90-45012, and S90-45020)** are all photos of impacts into the painted aluminum scuff plate from the trailing edge. The scuff plates had multiple, thick layers of yellow thermal control paint over a yellow primer. This series of photos shows a series of progressively more energetic impactors into the yellow painted scuff plate. Figure P2-39a shows a penetration through the paint into the underlying aluminum substrate where the impactor created a very typical hypervelocity crater in the aluminum. An area of paint was lifted and delaminated from the substrate but without sufficient energy to completely spall. Figure P2-39b shows a higher energy impact producing a larger crater, and a larger area of total spallation with only a small amount of the outer spallation area still attached. This picture is of interest in that it shows multiple layers of paint (especially in the upper right hand corner) and that, after the primary impact, a subsequent impact occurred into the now exposed substrate. This small crater is of interest because its impactor had sufficient energy to spall the primer coating in the immediate area around the crater, but not enough energy to affect the size of the paint spall zone. Figure P2-39c shows a complete spallation. Here, the crater is large enough that the primer coating was debonded and removed from the surface. This impactor must have been very energetic to cause all of these phenomena.

The rings on these painted surfaces were typically circular and indicated a shock wave phenomena. It is now theorized that the rings are caused by a Rayleigh wave propagation through the surface. If so, the sizes of the rings are dependent on both the thickness of the paint and the amount of erosion which had occurred in the paint prior to the time of the impact event.

As in the thermal control blankets, the total damage areas in the painted surfaces were always much greater than the damage areas due to simple cratering. This is of concern since the affected areas, which on LDEF approached 3% of the total painted surface areas, may have significant changes in absorptivity and emissivity, thus changing the radiative properties of the paints. In addition, the spallation and delamination areas reduce the thermal conduction effectiveness of the



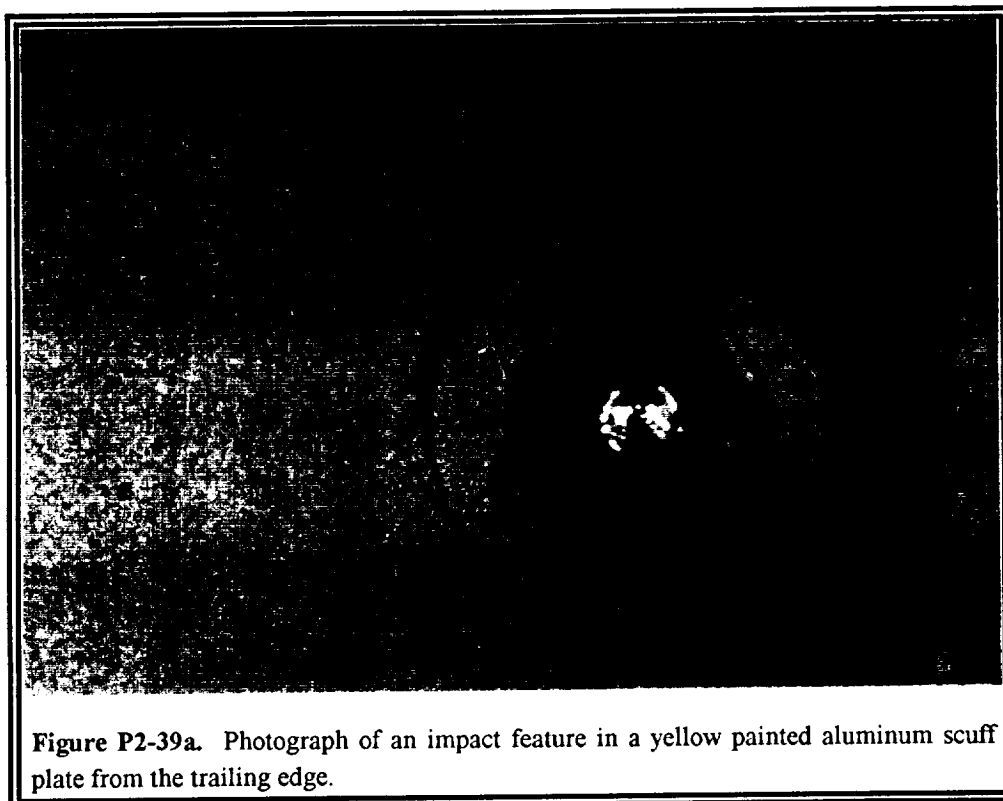


**Figure P2-39a.** Photograph of an impact feature in a yellow painted aluminum scuff plate from the trailing edge.

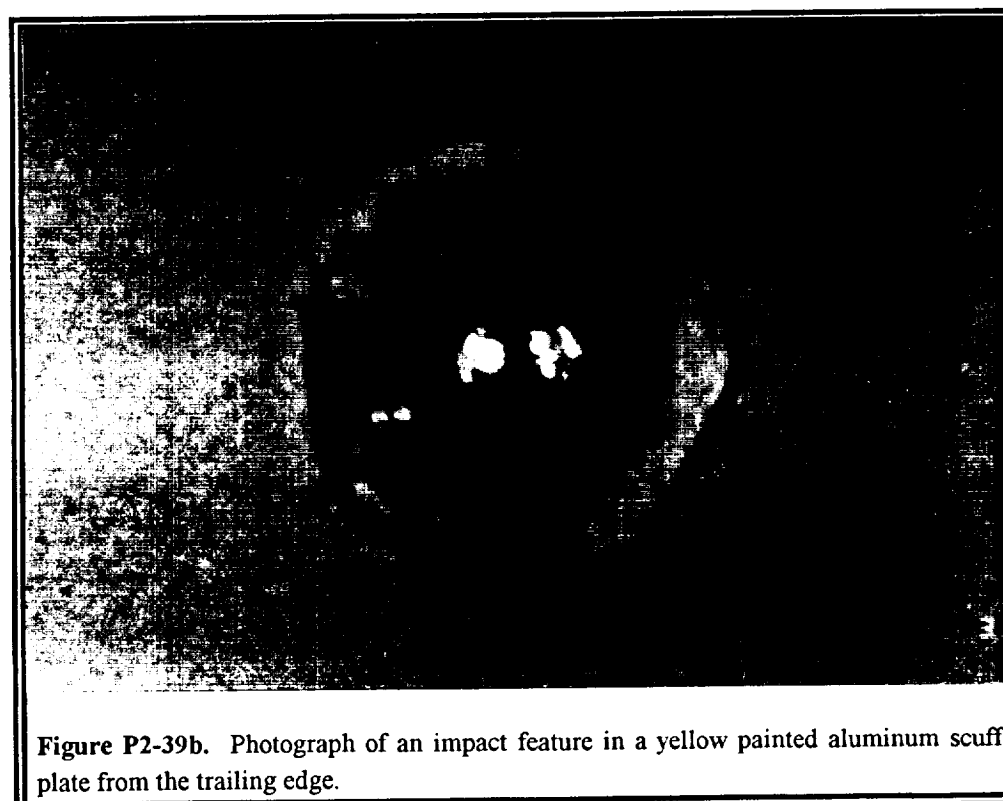


**Figure P2-39b.** Photograph of an impact feature in a yellow painted aluminum scuff plate from the trailing edge.



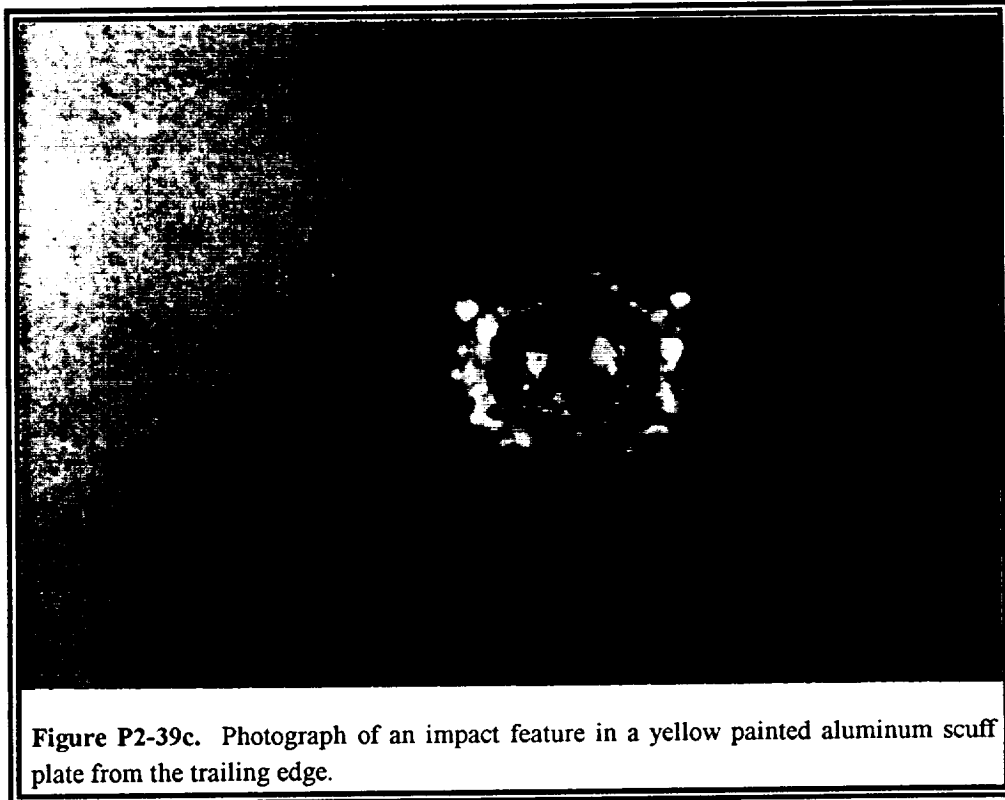


**Figure P2-39c.** Photograph of an impact feature in a yellow painted aluminum scuff plate from the trailing edge.



materials. Since these types of impact phenomena are expected in any coated materials, especially those susceptible to AO and UV, understanding these effects is particularly important for heat pipe and radiator systems.

### **2.3 Impact Effects on Optics and Power System Components**

Optics and solar power system components are typically brittle materials. Under impact, brittle materials show a different type of damage than metals and ductile materials. Brittle materials often show a central crater, usually filled with finely crushed material, and exhibit little or no crater lips. These craters are usually surrounded by conchoidal fracture areas, which act as spallation zones. Finally, there are typically 2 to 4 (occasionally more) cracks which run outward from the impact site for 10 or more crater diameters.

Impacts into windows (optical substrates) and reflective metallic mirrors have been studied for many years. Basically, it has been found that the transmissivity and reflectivity are unaffected by the impacts. However, scatter dramatically increases. Unfortunately, impact-caused scatter has not been studied significantly since most imaging optics in the past have looked directly toward the Earth and thus had little threat of being impacted. In addition, impacts into reflective optics with dielectric coatings have not been studied. The reflectivity of these latter optics may be affected since the coatings which provide the reflectivity are removed in the vicinity of the impacts. Additionally, the amount of coating material removed by an impact may be much larger than in ductile materials due to delamination of the coatings from the substrate and from each other. This section presents examples of impact features from LDEF which are typical of the damage experienced by the brittle optics and power system components.

**Figures P2-40a, 2-40b, and 2-40c (KSC-390C-1739.09, S90-44908, and S90-44909)** are a series of photographs which show an impact feature into a metal-oxide silica (MOS) sample from experiment A0201 located at LDEF Bay B12. The sample consisted of a thick silicon substrate, with a 1.0  $\mu\text{m}$  thick  $\text{SiO}_2$  layer, topped by a thin (less than 1000 Å thick) aluminum coating. The impact feature shown in Figure P2-40a is ~2.2 mm across the crater (the depression in the glass)



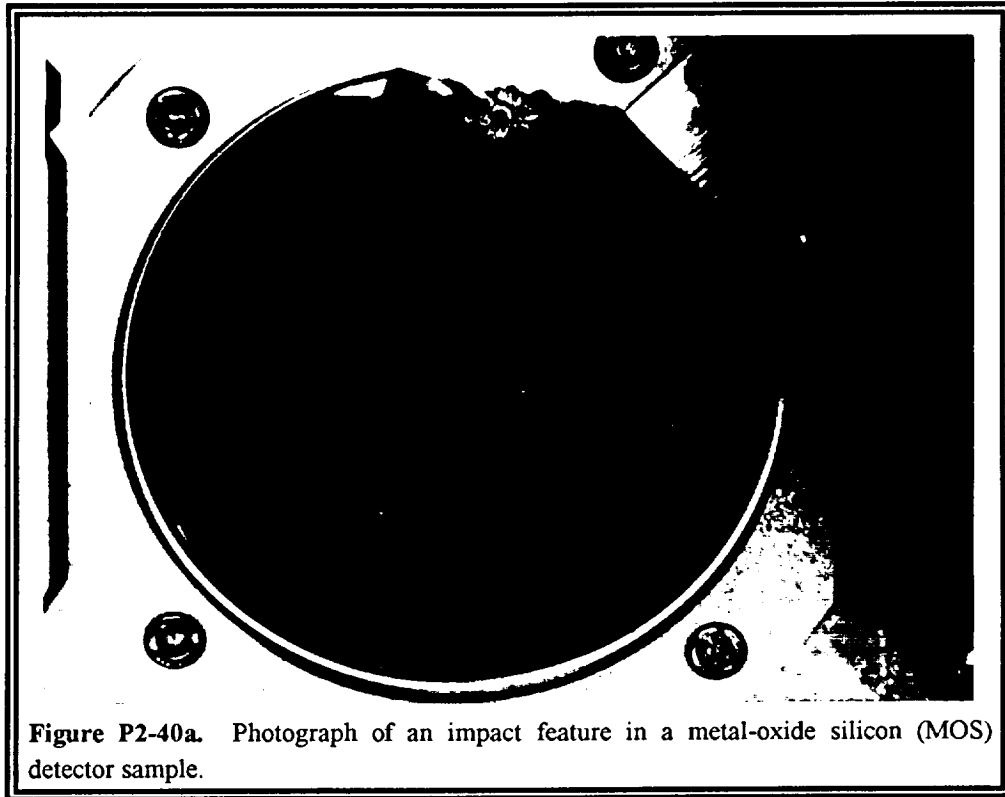


**Figure P2-40a.** Photograph of an impact feature in a metal-oxide silicon (MOS) detector sample.



with the total damage area extending to several centimeters. The total view in this photo is ~11 cm across. Notice that a piece of the MOS has been broken out of the holder as a result of the impact. Figure P2-40b is a close up of some of the damage and shows the left edge of the sample holder and the sample support structure. This structure was composed of an RTV silicone on top of an aluminum substructure. Here, the MOS silicon has completely fractured. A penetration is shown through the silicon, with surrounding spallation of the silicon and the SiO<sub>2</sub> coating. The spallation and cracking extends through the reflective aluminum layer, while the penetration goes through the silicon substrate, through the RTV silicone support structure, and into the aluminum substructure. The total MOS silicon spallation area is ~4 mm in diameter. Figure P2-40c provides a close-up view of the damage and shows the amount of cracking in the silicon and SiO<sub>2</sub> surface and the removal and cracking of the aluminum coating layer. This view also shows the crater in the underlying aluminum and the penetration through the RTV silicone. This large amount of fracturing (*i.e.*, the cracking in the surface as well as the conchoidal fractures and spallation of the substrate) is typical of impacts into brittle materials. This is further illustrated in Figure P2-41.

**Figure P2-41 (S90-44992)** is an impact into an infrared (IR) multi-layer filter material on top of a germanium substrate. As is typical, there is a small central crater and depression in the substrate surrounded by a large area, ~6 to 8 times larger than the crater diameter, where the surface has been conchoidally fractured and spalled and the entire surface coating has been removed.

**Figure P2-42 (S90-44898)** shows an impact into a germanium substrate. Note the large amount of surface cracking associated with the crater, and the surrounding conchoidal fracture and spallation damage. **Figure P2-43 (S90-44900)** is a close-up of an impact into the germanium substrate. In this picture note the 4 to 6 cracks emanating from the central crater and spallation region. This is typical of impacts in these types of brittle materials, as exemplified in the aluminum coated MOS detectors where the cracks extended all the way through the surface reflective coating. In **Figure P2-44 (S90-44897)** the impact into the germanium substrate is accompanied by a large amount of in-depth and surface cracking. This fracture structure is



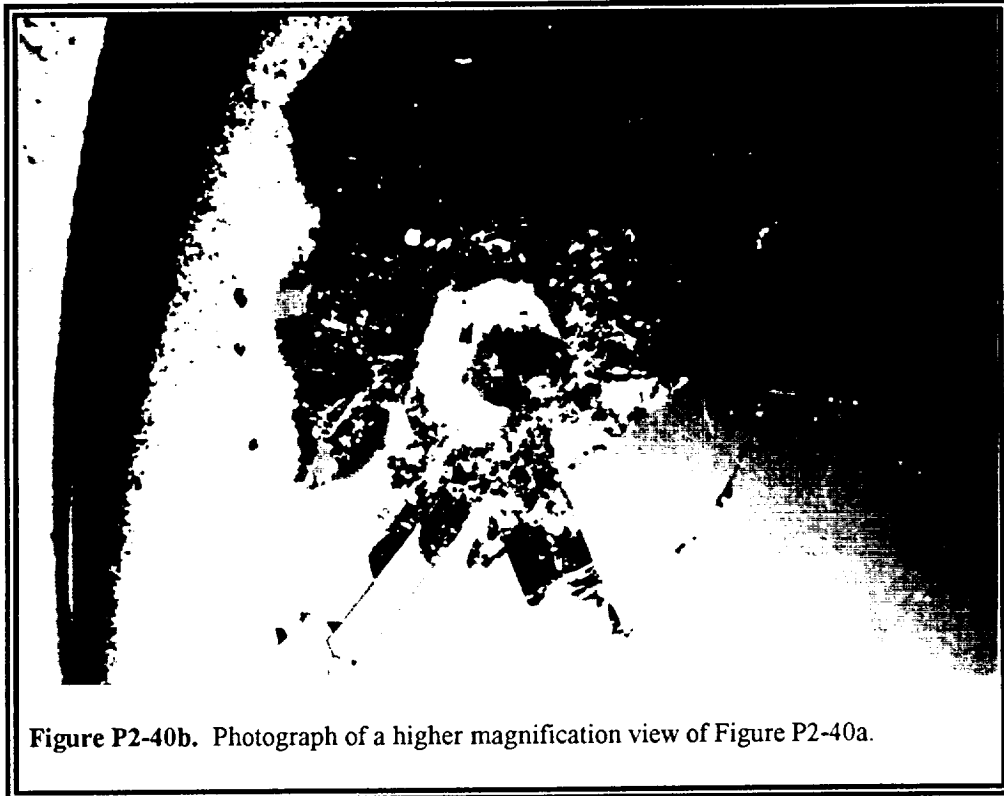


**Figure P2-40b.** Photograph of a higher magnification view of Figure P2-40a.

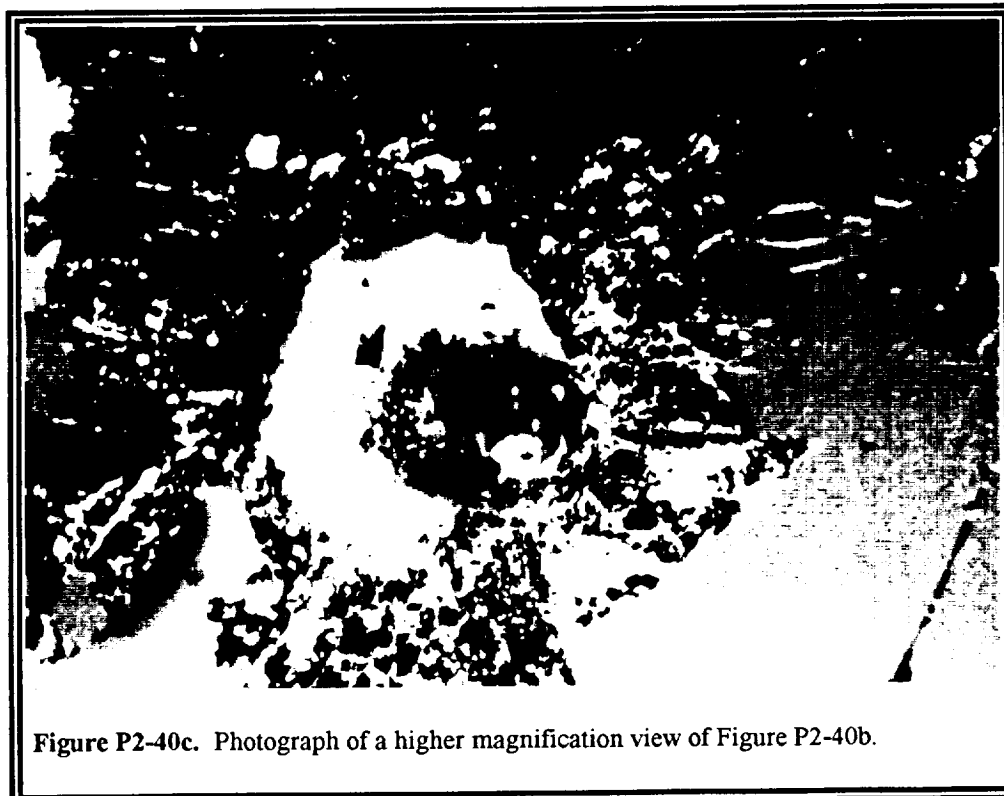


**Figure P2-40c.** Photograph of a higher magnification view of Figure P2-40b.





**Figure P2-41.** Photograph of an impact feature in an infrared (IR) multi-layer filter material on top of a germanium substrate.

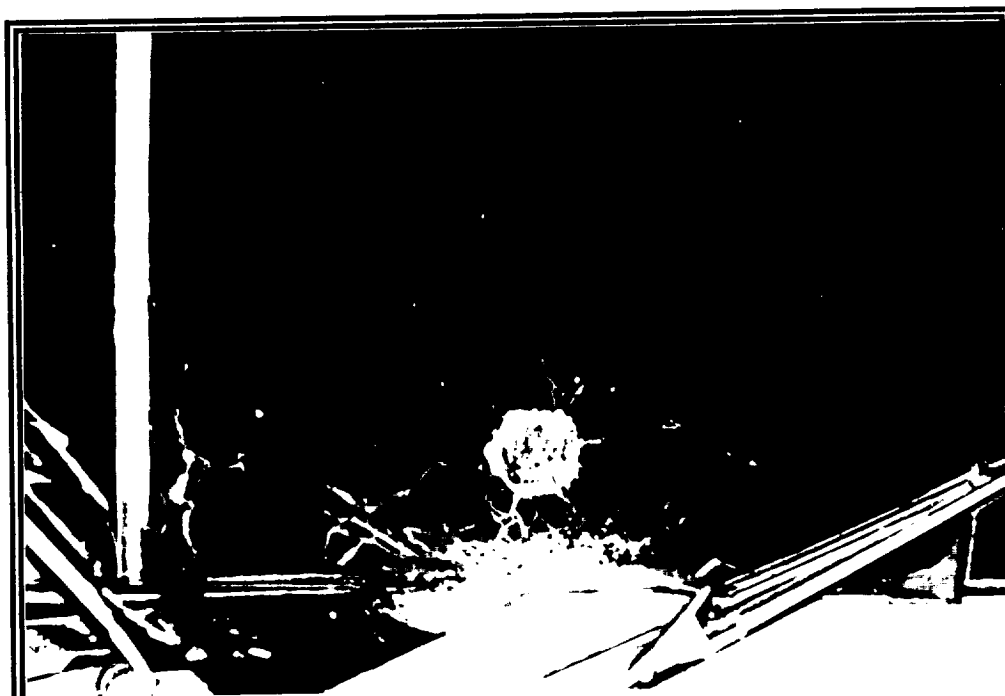


**Figure P2-42.** Photograph of an impact feature in a germanium substrate from experiment A0187-2.



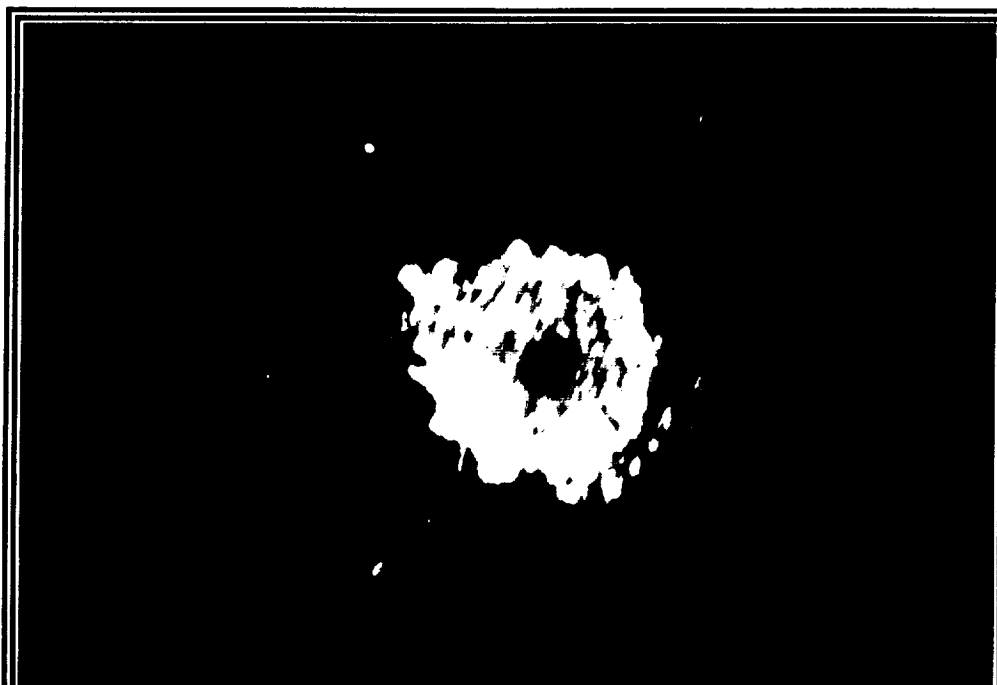


Figure P2-43. Photograph of an impact feature in a germanium substrate from experiment A0187-2.



Figure P2-44. Photograph of an impact feature in a germanium substrate from experiment A0187-2.



connected to another smaller impact feature to the left causing additional damage from these two events.

**Figure P2-45 (R-9-15)** is the best example of an impact into a brittle substrate (*e.g.*, glass) from LDEF. This glass was located at LDEF Bay B08. The picture shows an ~1 mm crater surrounded by an ~5 mm diameter spallation and associated conchoidal fracture zone. The entire sample is cracked with two large wide cracks going all the way through the substrate. These cracks effectively broke the substrate into three pieces. The glass sample size was initially ~3.8 cm (~1.5 inches) in diameter. The spalled and crushed region is composed of very finely shattered glass.

This type of damage also occurs in solar cells and their associated cover glasses. **Figure P2-46 (S90-43409)** is a picture of a solar cell panel off of the A0171 experiment. This panel dislodged from LDEF during its flight home and was retrieved from the Space Shuttle bay. The experimenters had initially placed this panel on the surface of LDEF with the cover glasses hidden and the contacts exposed to the environment to see how the contacts would react to the space environment. As the Kapton tape, which held this panel on, was slowly eroded by the AO, the panel began to float free exposing both the cover glasses and the panel backside to the environment. Thus, this piece of hardware received impacts into both the substrate side of the panel, with associated shock coupling and fracture of the cover glass, as well as impacts into the cover glass with associated damage in the solar cells and substrate. **Figure P2-47 (4-1)** shows an impact into the cover glass side of this panel. As is typical of the other glasses, there is a central crater filled with very finely shattered material, and surrounded by some spall material and a large conchoidal fracture which extends through the cover glass to the underlying solar cell. In addition, 4 large cracks radiate out from the feature. The total view is ~3 cm across.

**Figure P2-48 (KSC-390C-1412.07)** shows a broken interconnect on a solar array panel. This panel was also from the A0171 experiment and was located at LDEF Bay A08. Here, the interconnect was blown apart from its connection with the solar cell, possibly by an impact or by an electrical discharge. In either case, it created a large spray pattern which covers approximately



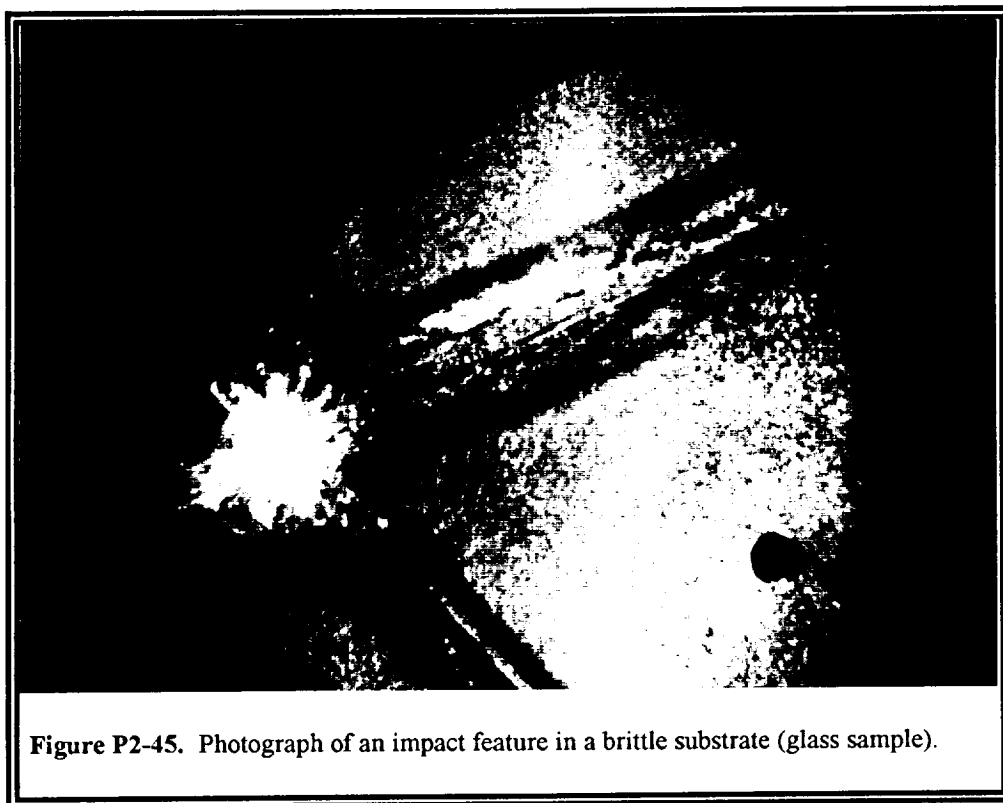


**Figure P2-45.** Photograph of an impact feature in a brittle substrate (glass sample).

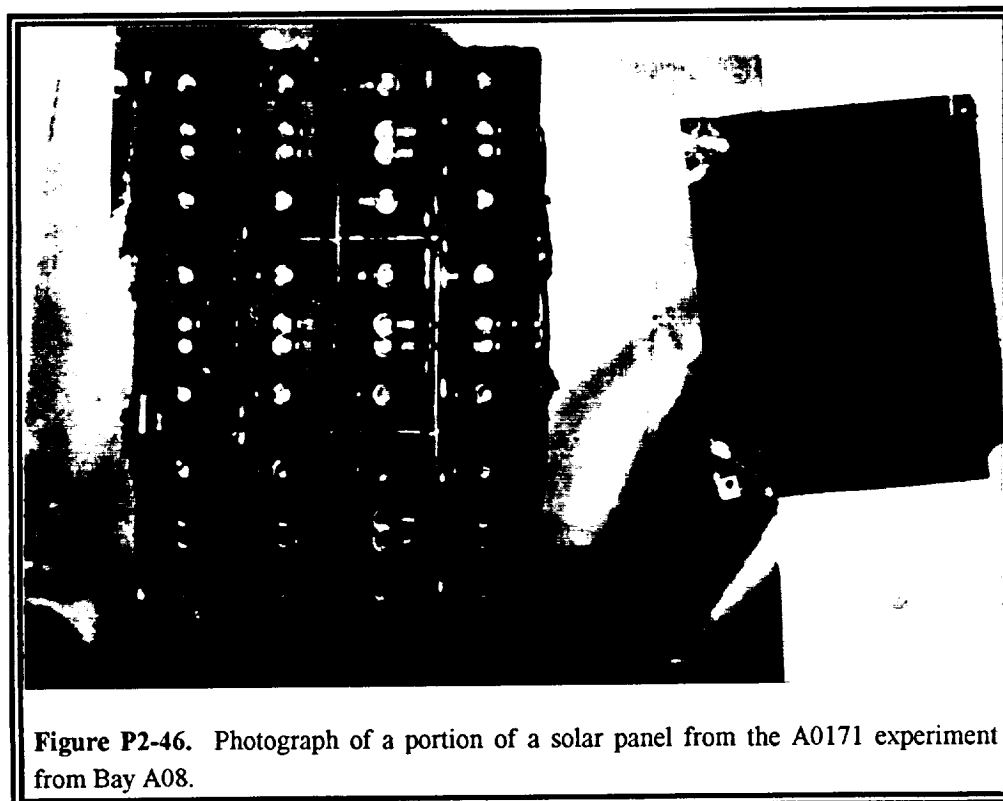


**Figure P2-46.** Photograph of a portion of a solar panel from the A0171 experiment from Bay A08.



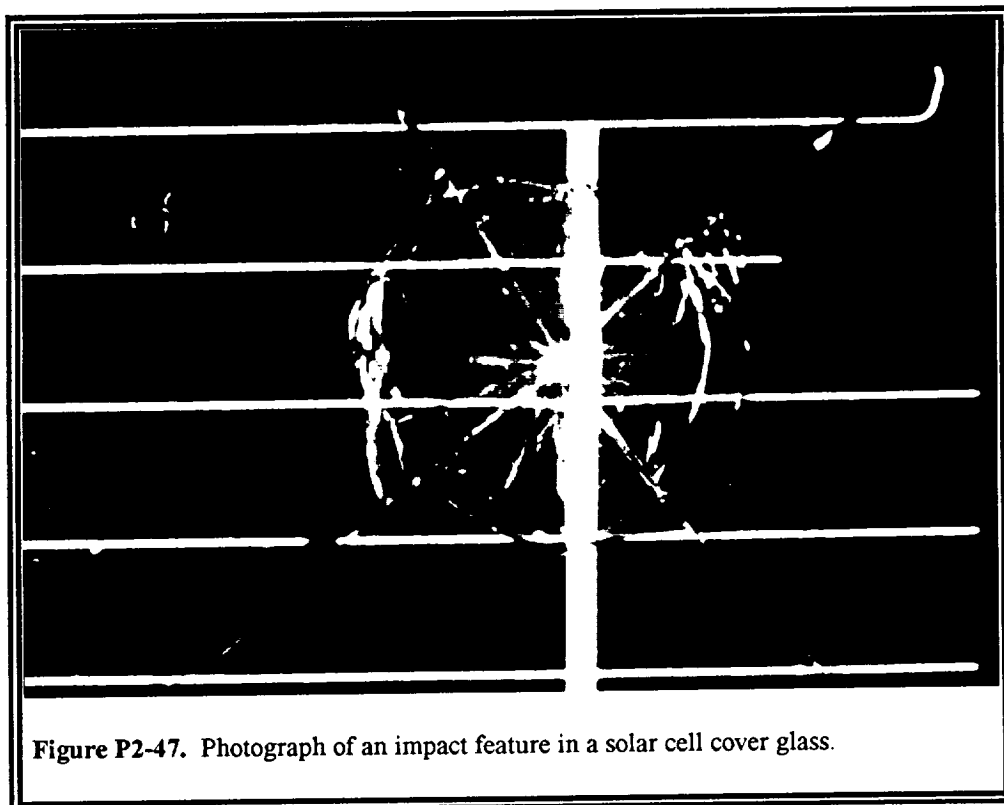


**Figure P2-47.** Photograph of an impact feature in a solar cell cover glass.

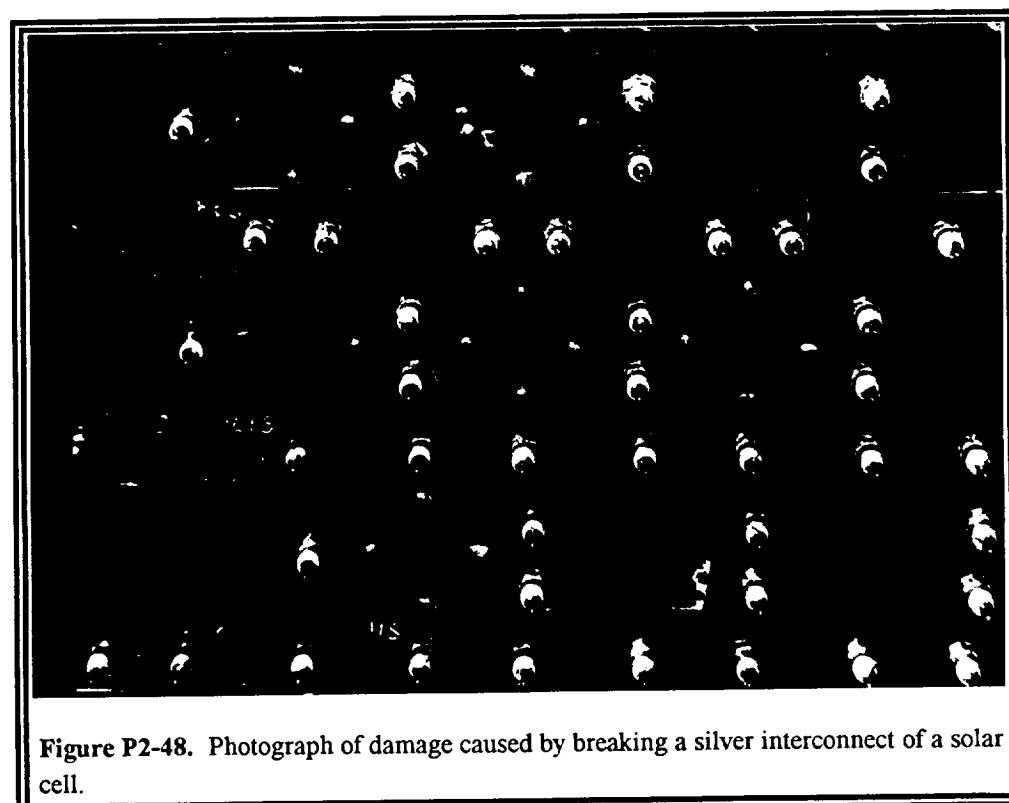


**Figure P2-48.** Photograph of damage caused by breaking a silver interconnect of a solar cell.



one quarter of the underlying solar cell area. This ejecta is primarily composed of silver solder. The total view measures ~13 cm across.

Clearly, a significant factor for impacts into these very brittle materials is the propensity to readily propagate cracks, sometimes causing complete penetration and breakup into separate pieces. Of particular concern for optics is the increased scatter caused by these impact damage areas. While scatter has a very small effect on solar power systems, the solar power system designers should note the cracks, which allow space environments, particularly electrons and protons, to have access to the underlying solar cells.

## **2.4 Impact Effects on Other Types of Materials**

LDEF had over 10,000 samples of various materials exposed to the space environment. Some examples of impact damage in materials which do not readily fit into the previous categories are shown below.

**Figure P2-49 (KSC-390C-1935.7)** is a photograph of an impact into fiber optics materials. These fiber optics bundles were sheathed in a plastic material and the majority of the impacts did not penetrate this outer plastic coating. Inside the outer plastic coating, an inner fibrous insulating material surrounded the fiber optic cables. Some of the impacts into the fiber optic bundles penetrated the plastic, causing cratering and breakage of the insulating material. The impact depicted in this photograph was from the M0004 experiment located at LDEF Bay F08. This impact penetrated through the outer coating of plastic as well as the underlying fiber insulation material to expose the fiber optic cable. The holes formed by these impactors are typically non-circular, while the underlying insulation material looks like broken fibers.

**Figure P2-50 (KSC-390C-1916.7)** is a picture of impacts into some of the samples on the upper right side of experiment A0134 from LDEF Bay B09. The sample on the left is a composite material clearly showing the fibers. The crater is largely circular with a spallation area surrounding it. Here, the crater penetrates through multiple fibers and breaks them. The material



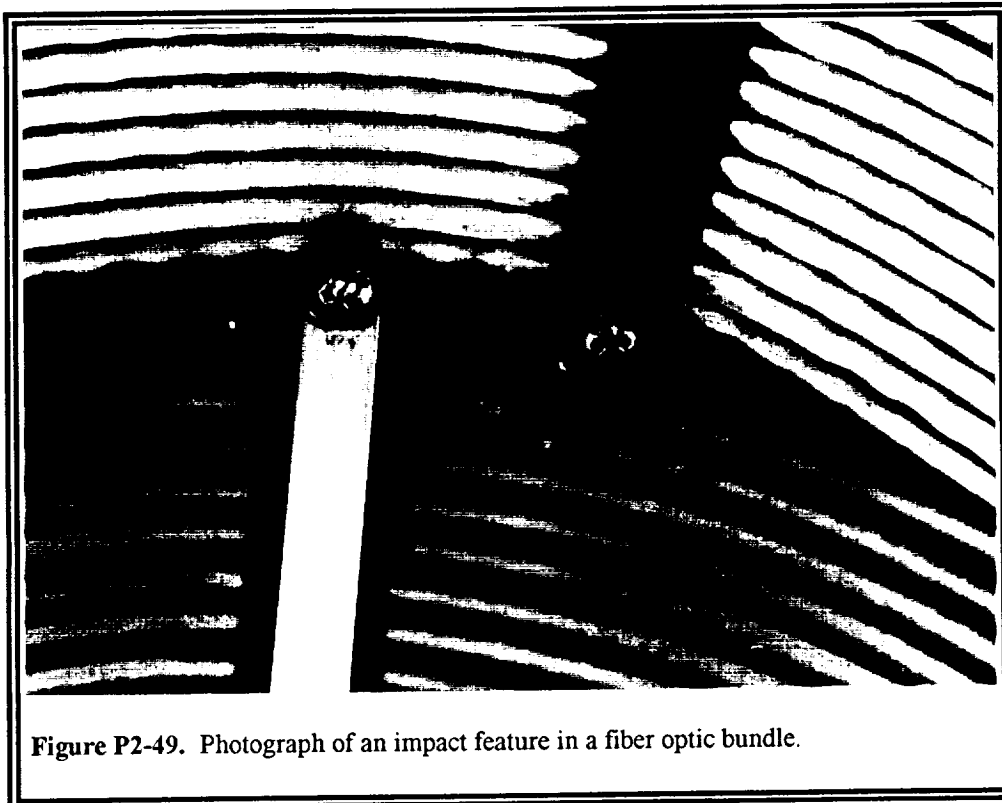


**Figure P2-49.** Photograph of an impact feature in a fiber optic bundle.

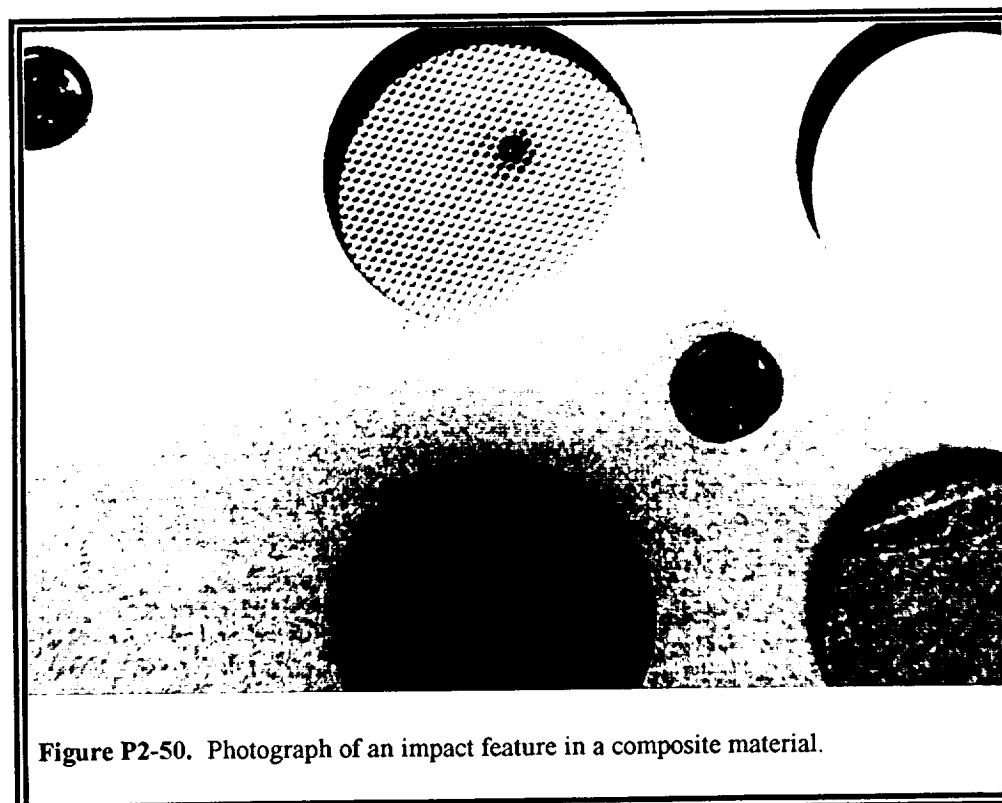


**Figure P2-50.** Photograph of an impact feature in a composite material.



on the right is a thin metallic material with very small penetrations and craters over the entire surface. The total view measures ~4 cm across.

**Figure P2-51 (KSC-390C-1916.6)** is a beta glass cloth material with an impact in the lower left hand corner. The penetration is non-circular with many broken fibers giving the impact its irregular shape.

**Figure P2-52 (S90-44927)** is a penetration through a fiberglass material. This material appears to have been embrittled by UV light and the impact, which may have been at a highly-oblique angle, tore the surface, breaking many of the fibers and creating this irregular penetration hole.

Although fiber optic bundles present a relatively small cross-sectional area for impacts, it should be noted that severe damage is not required in order to cause a significant upset in performance. Simple localized ruptures in the cladding can cause the fiber to become "leaky". Impacts into fiberglass materials as well as beta glass and other ceramic cloths are not well understood. Impacts into these materials are of concern because they break the fibers and may alter the material strength and other material properties.

## **2.5 Impact-Caused Contamination Via Ejecta Blow-off**

LDEF returned the first evidence of extensive damage to a spacecraft caused by secondary ejecta. This type of damage had been known to exist for over fifty years and had been seen on a small scale in the SMM materials. However, LDEF's large surface area and large number of material samples showed the true extent of this type of damage.

Surface contamination caused by impacts is most threatening to optics, solar cells and thermal control materials. For optics, this contamination could be caused by impacts into baffles, telescope shrouds, and optical structures, or by penetrations through telescope shrouds. Optical surface contamination causes increased scatter and may reduce reflectivity and transmissivity. For



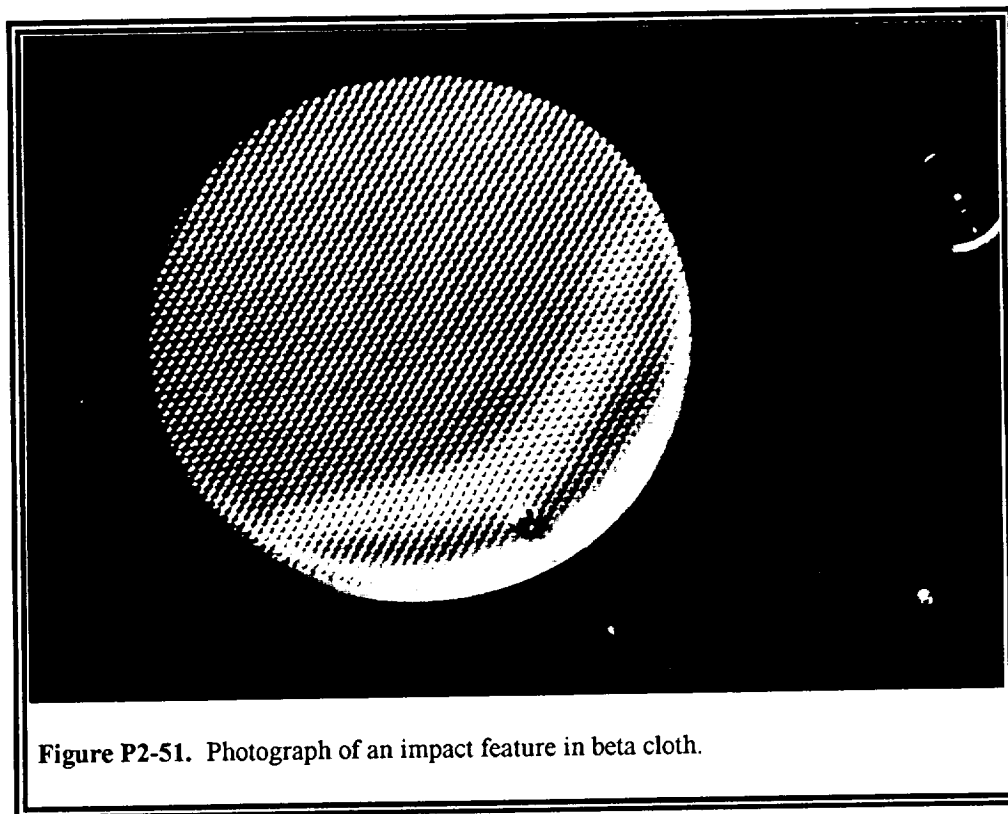


**Figure P2-51.** Photograph of an impact feature in beta cloth.

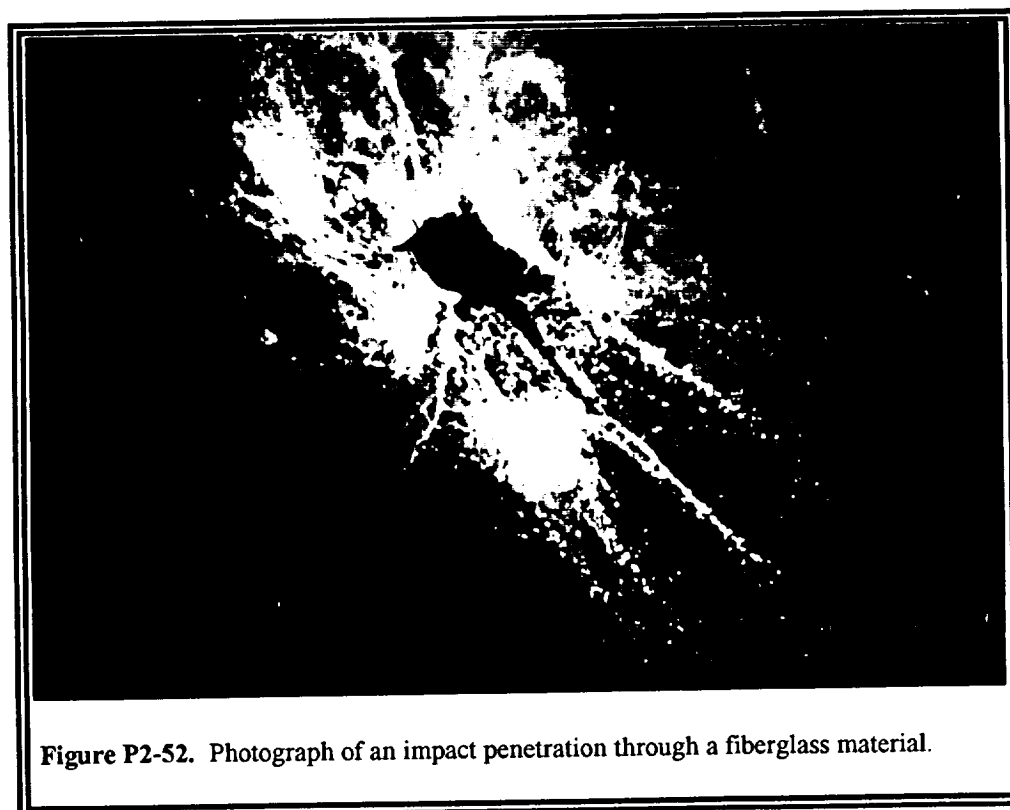


**Figure P2-52.** Photograph of an impact penetration through a fiberglass material.



thermal control materials and solar cells, impact-caused contamination originates primarily from impacts into nearby structures.

Another source of impact contamination comes from impacts by urine. The urine originates from Space Shuttle and space station holding tank dumps and remains in orbit as ice crystals. Upon impact these ices melt and form contaminating splashes. **Figure P2-53 (POD-9201-003)** is an example of a urine spot. These were found on every surface of LDEF. They have been seen on all space-returned materials, particularly since the advent of the Space Shuttle.

**Figure P2-54 (S90-44919)** is an example of the more typical ejecta contamination seen on LDEF. This figure shows the ejecta spray surrounding a crater in a germanium substrate. This ejecta spray resulted from a penetration through an overlaying foil of metal-coated plastic which is now gone. The impactor penetrated the foil and caused a crater with surrounding spallation and cracks in the germanium. The ejecta from this crater impacted the back surface of the foil, which caused further ejecta to spray across the surface of the germanium, as shown. Notice that the ejecta spray pattern is over 10 times the diameter of the inner crater on the germanium surface.

**Figure P2-55 (S90-44896)** shows an impact into the side of an aluminum structure which then sprayed material for over 40 impact crater diameters across the germanium surface adjacent to it. This is the type of contamination which would be expected from an impact on the inside of an optical telescope shroud.

**Figure P2-56 (KSC-390C-1726.4)** shows an ejecta pattern caused by an impact into the edge of an experiment tray holder located at LDEF Bay H09. The crater can be seen at the bottom of the photograph with the impact ejecta at the top. This view measures ~12 cm across.

**Figure P2-57 (S90-44976)** is an impact into the edge of an optic sample holder. This extremely small impact threw ejecta across the surface of the optic to almost 100 times the size of the crater. This particular optic was a multi-layer IR filter from experiment A0056 located at LDEF Bay B08.



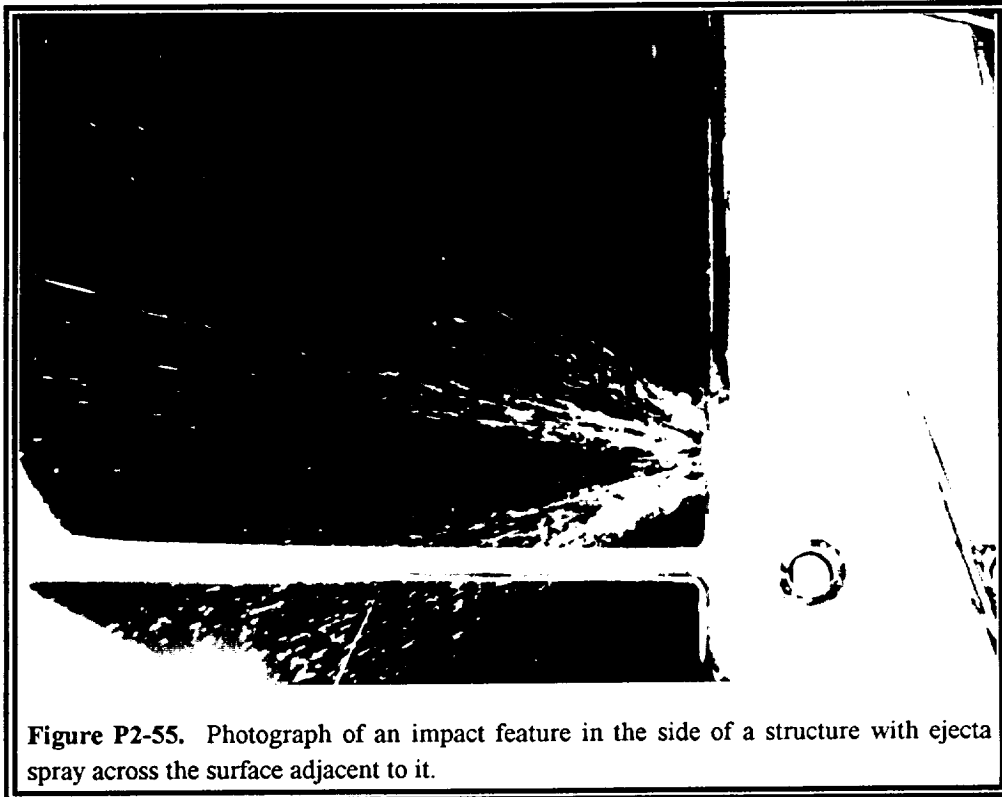


Figure P2-53. Photograph of a urine spot contamination feature.

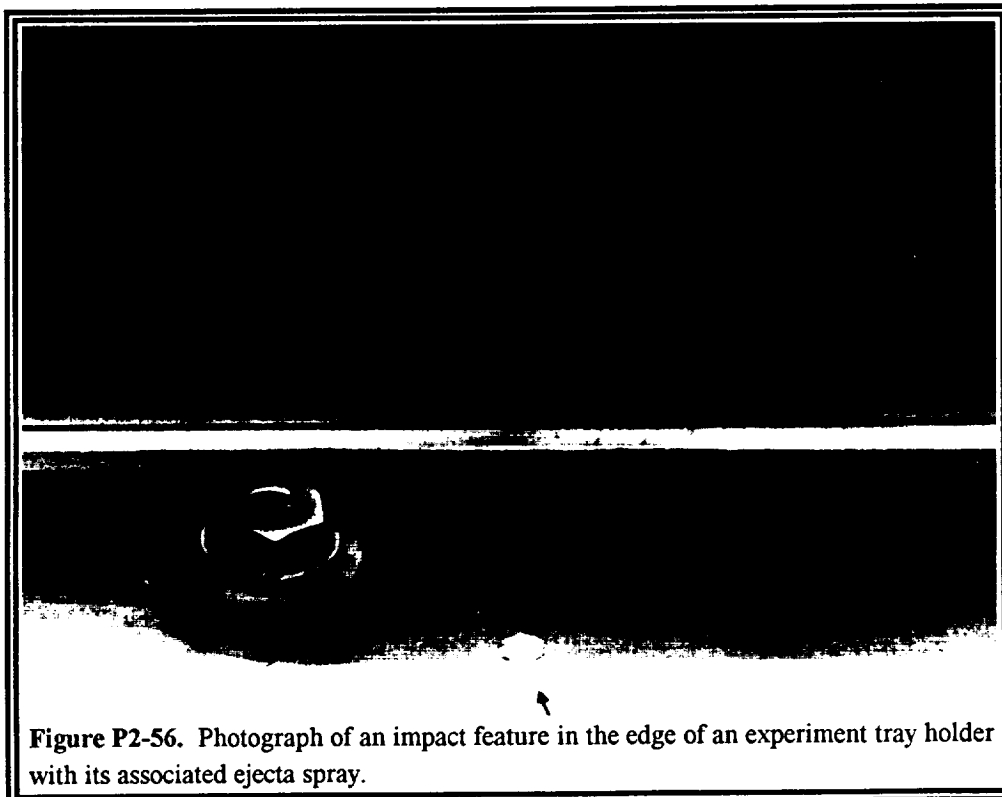


Figure P2-54. Photograph of ejecta spray onto a germanium substrate on experiment A0187-2.





**Figure P2-55.** Photograph of an impact feature in the side of a structure with ejecta spray across the surface adjacent to it.



**Figure P2-56.** Photograph of an impact feature in the edge of an experiment tray holder with its associated ejecta spray.



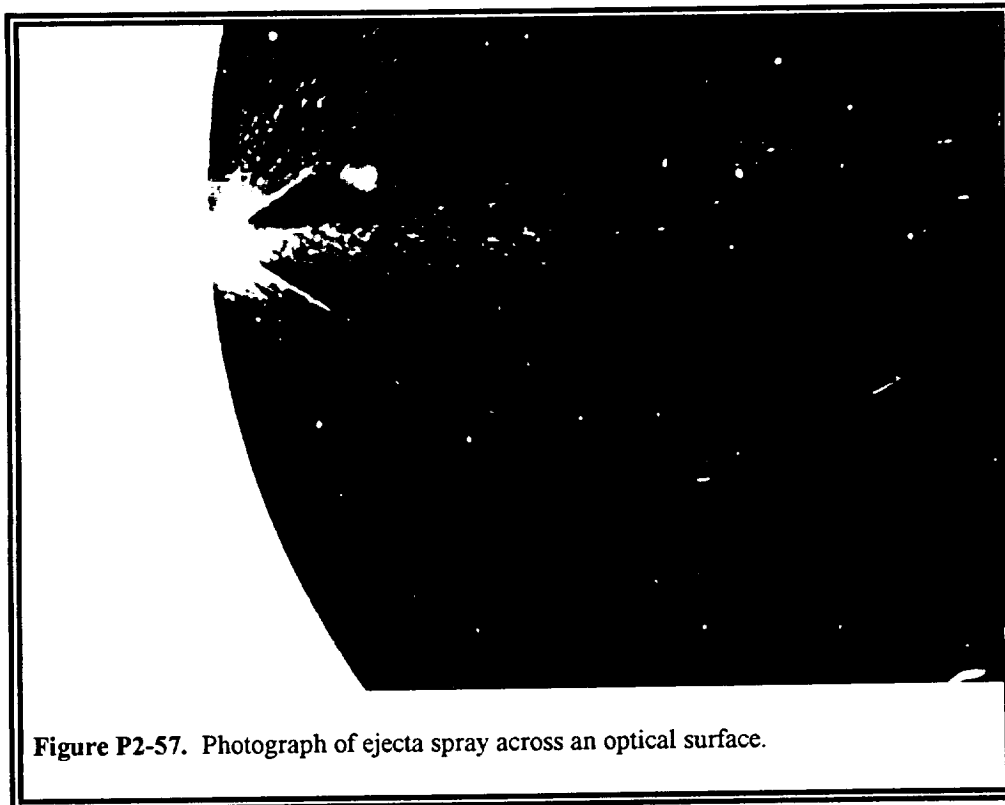




**Figure P2-58 (S90-43435)** shows an impact into an aluminum tray lip with an impact spray onto the associated aluminum structural member. **Figure P2-59 (KSC-390C-2067.12)** shows an impact into a structural support and holder for solar cells and the subsequent spray across the adjacent surface.

**Figure P2-60 (KSC-390C-2033.08)** shows the largest impact on LDEF and the associated spray pattern from the crater. This crater, which had penetrated through the Teflon tape, sent a spray of molten Teflon, silver and aluminum across all of the adjacent surfaces out to distances of many crater diameters. This spray went up over the adjacent Z-frame (on the right) and onto the thermal blanket surface which was attached to it. The bulge in the Teflon measures ~1 cm from lip to lip.

Contamination on satellites also occurs due to outgassing of many organic materials. Impact-related contamination is more localized, but can be generated from impactors and targets which are non-volatile and normally considered "safe". These spray patterns and their sizes are directly related to the separation distance from the crater and the geometrical orientation of the material surfaces with respect to the crater. The localized, heavy contamination is of particular concern to imaging optics due to the increased scatter. For solar power systems and thermal control materials, the concern is for reduced reflectivity and transmissivity and altered absorptivity and emissivity.



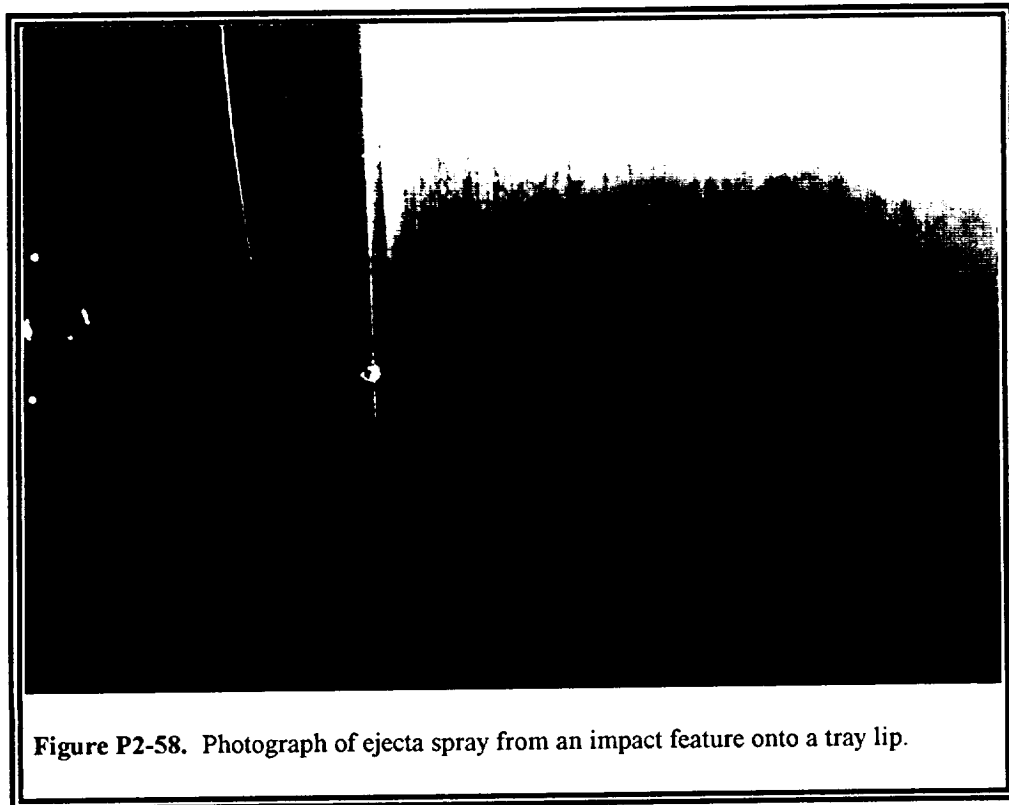


**Figure P2-58.** Photograph of ejecta spray from an impact feature onto a tray lip.

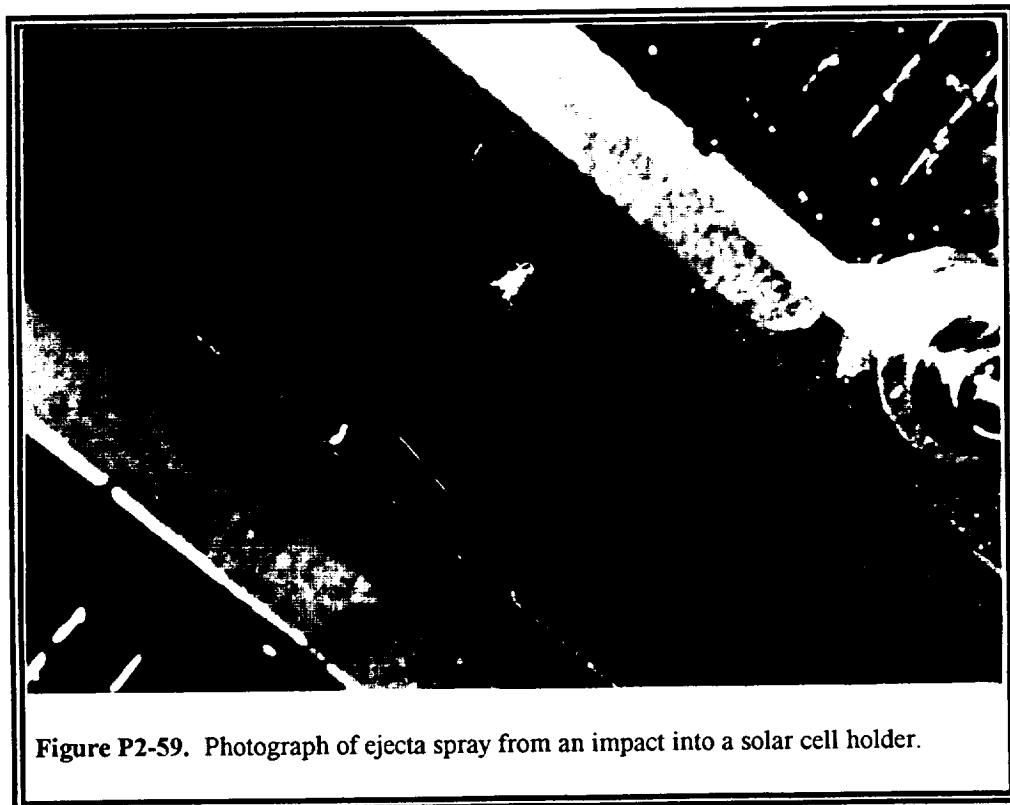


**Figure P2-59.** Photograph of ejecta spray from an impact into a solar cell holder.



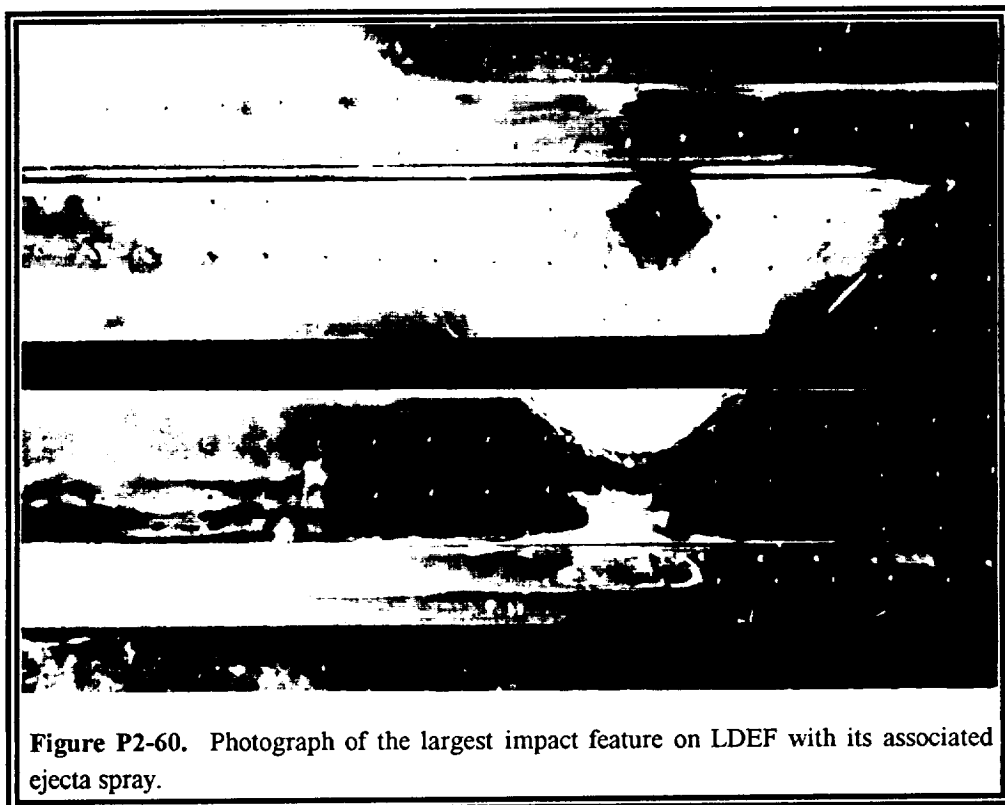


**Figure P2-60.** Photograph of the largest impact feature on LDEF with its associated ejecta spray.



### 3.0 CONCLUSIONS AND RECOMMENDATIONS

This report has hopefully demonstrated that impact damage is not comprised of just a crater or a hole. In fact, the crater or penetration may be only a small percentage ( $<10\%$ ) of a given impact's damage area. Therefore, any assessment must include the entire damage area and its varying effects on system survivability, reliability and performance. For example, pure cratering on LDEF amounted to a total surface area damage of only  $\sim 0.1\%$ . However, when the "extended" damage areas due to spallation, delamination, and cracking are included, the total surface damage area was  $\sim 3\%$ .

In order to determine or predict the performance capability of space systems during their operational lifetimes, assessments must be made of the combined environment effects. This includes impacts which occur throughout the satellites' lifetime. Some of these damage responses can be modeled. The appendix illustrates a few examples of computer results using the CTH hydrodynamics code (Ref. 17). Such effects as cratering and perforation in metals are easily computed. Effects such as localized delamination and dome formation in simple layered structures can also be computed. However, the cracking and ring formations for brittle materials and paints are far more difficult to model. Lastly, modeling of composite structures and fiber optics is extremely difficult.

Since no models currently exist which can predict impact effects in these latter materials, tests must be performed. These tests should include the materials in various states of simulated space environment exposure. In addition, since such tests can be very expensive, additional efforts should focus on data collection and the development of new physical models for these effects. In order to support this model development, many aspects of impact response require further experimental testing and analysis. For example, the responses to impacts of painted thermal control surfaces need characterization with regard to changes in absorptivity and emissivity. Likewise, changes in impact response caused by UV-induced color changes and embrittlement need evaluation, as do AO erosion effects on impact response. Damage to solar cell coverglasses needs evaluation. Although pits and cracks cause forward scattering of light (a non-problem for a

solar cell), cracks which completely penetrate the coverglass can leave the solar cell vulnerable to AO, electron and proton attacks. Impact damage in the solar cells proper is also poorly understood. The same holds true for the near-Earth space impact environment. As this environment is not fully understood, additional efforts should focus on data collection, data analysis, and new model development in order to improve our comprehension of this environment's dynamics and threat potential.

Of particular importance for evaluating system performance are the interactions and synergisms of the various space environments (*e.g.*, UV and AO) with the impact environments. Space environment exposure alters material properties, thereby changing the responses and defects created by impacts. This is exemplified by the impact effects on LDEF's thermal control paints and composites. The impacts themselves can further alter material states and expose underlying materials, allowing the space environments to further increase the damage area and to begin damaging previously unexposed areas. This is epitomized by the impact effects on LDEF's thermal control blankets. In addition, the other space environments (*i.e.*, AO and UV) combine with impact ejecta to cause extensive contamination. This is illustrated by the impact-caused contamination on LDEF's optics, solar cells and thermal control materials.

Impact damage will be of increasing importance in the future since many satellites are being designed for ever-longer mission times (*e.g.*, 5 to 10 years), and the debris environment is steadily worsening. This report has shown the extent of damage which can be caused by impacts into different types of spacecraft materials. Hopefully, this report has brought system designers and engineers a new awareness of the magnitude of this damage. In addition, program managers should now have a better understanding of the need to thoroughly assess this damage. With increased awareness and improved understanding, spacecraft can be designed which will have improved reliability, survivability, and performance, even during long missions.

## REFERENCES

1. The Long Duration Exposure Facility (LDEF) Mission 1 Experiments. NASA SP-473, 1984.
2. 69 Months in Space: A History of the First LDEF (Long Duration Exposure Facility). NASA NP-149, 1991.
3. Peters, P. and Gregory, J. "Pinhole Cameras as Sensors for Atomic Oxygen in Orbit; Application to Attitude Determination of the LDEF." LDEF - 69 Months in Space - First Post-Retrieval Symposium Proceedings, NASA Conference Publication 3134, June 1991.
4. Mulholland, J.D., et al. "IDE Spatio-Temporal Impact Fluxes and High Time-Resolution Studies of Multi-Impact Events and Long-Lived Debris Clouds." LDEF - 69 Months in Space - First Post-Retrieval Symposium Proceedings, NASA Conference Publication 3134, June 1991.
5. Cour-Palais, B.G., et al. "Meteoroid Environment Model - 1969 (Near Earth to Lunar Surface)." NASA SP-8013, March 1969.
6. Grün, E., et al. "Collision Balance of the Meteoritic Complex." *Icarus*, Vol. 62, 1985.
7. Zook, H.A. "Asteroidal Versus Cometary Meteoroid Impacts on the Long Duration Exposure Facility." Second LDEF Post-Retrieval Symposium Abstracts, NASA Conference Publication 10097, June 1992.
8. Watts, A., et al. "LDEF Penetration Assessment final Report." Final Report, Contract F33615-90-C-5903, Task 0008, June 1992.
9. Kessler, D.J. "Orbital Debris Issues." *Advances in Space Research*, Vol. 5, No. 2, 1985.
10. Kessler, D.J. and Reynolds, R.C. "Orbital Debris Environment for Spacecraft Designed to Operate in Low-Earth Orbit." NASA TM-100471, September 1988.
11. Kessler, D. J. "Origin of Orbital Debris Impacts on Long Duration Exposure Facility's (LDEF) Trailing Surfaces." Second LDEF Post-Retrieval Symposium Abstracts, NASA Conference Publication 10097, June 1992.
12. Divine, N. and Agüero, R.C. "New Meteoroid Model Predictions for Directional Impacts on LDEF." Second LDEF Post-Retrieval Symposium Abstracts, NASA Conference Publication 10097, June 1992.
13. See, T.H., et al. "Meteoroid and Debris Impact Features Documented on the Long Duration Exposure Facility - A Preliminary Report." NASA JSC #24608, August 1990.

14. Watts, A.J., et al. "Optical Scatter Due To Impact Effects." SPIE's 1992 International Symposium on Optical Applied Science and Engineering Proceedings, Vol. 1761, July 1992.
15. Coombs, C.R., et al. "Damage Areas Due to Impact Craters on LDEF Aluminum Panels." Second LDEF Post-Retrieval Symposium Abstracts, NASA Conference Publication 10097, June 1992.
16. Zukas, J.A., et al. "Impact Dynamics: Chapter 6 - Hypervelocity Impact Mechanics." A Wiley-Interscience Publication, John Wiley & Sons, 1982.
17. Bell, R.L., et al. "The CTH Code (Version 1.024)." Structural and Solid Mechanics Department, Sandia National Laboratory, Albuquerque, NM, October 1991.

## APPENDIX

### A.1 CTH Code Validation

The first task with the CTH code was to perform a validation between experimental results and reproducible computer simulations. The data from a series of gas gun experiments were provided by Dr. Fred Hörz of NASA Johnson Space Center.

The data provided by Dr. Hörz contained many combinations of materials which were used for the impactor and the projectile. In order to get reasonably accurate results with the CTH code the materials chosen had to have material properties which were readily available and well characterized. Complex compound materials were ruled out, leading to a choice of an aluminum target and an impactor made of soda-lime glass. Results from the validation comparisons are illustrated below in Table A-1.

Table A-1: Data Comparison from CTH Run and Hörz Laboratory Data

Shot Number	Projectile Diameter (mm)	Aluminum Thickness (mm)	Velocity km/sec	Hole Diameter (mm) HÖRZ TEST	Hole Diameter (mm) CTH
785	3.175	9.525	5.91	2.24	9.8
786	3.175	9.02	5.8	3.62	10
787	3.175	8.64	5.81	7.31	12.5
788	3.175	7.62	5.79	10.19	12.5
789	3.175	1.6	5.87	8.766	10
791	3.175	19.94	5.84	13.73*	11.000*

\*These values are for crater diameters, they were not penetrations.

Several models were available in the CTH code, however, the one chosen was the Mie-Grüneisen. The variables used in the CTH computer simulations are shown below in Table A-2.

Table A-2: Variables used in CTH Calculations

Material	Density (g/cm <sup>3</sup> )	Sound Speed (cm/sec)	Grüneisen	Heat Capacity (erg/cm <sup>3</sup> /eV)	Constant in Linear Hugoniot
Aluminum	2.7	$5.31 \times 10^5$	2.25	$1.049 \times 10^{11}$	1.34
Soda-Lime	2.2	$5.91 \times 10^5$	0.4	$8.744 \times 10^{10}$	1.5

The aluminum alloy which was used in the experiments was an Al-1100 variety, but the temper was not known. The temper of the metal can result in large changes in the tensile strength and the yield strength. In order to match the experimental results, it was necessary to run several calculations which used a range of yield and tensile strengths. The final values that were arrived at are listed in the following Table A-3:

Table A-3: Yield and Tensile Strengths Used in CTH Calculations

Material	Yield Strength (kbar)	Poisson Ratio	Fracture Stress (kbar)
Aluminum	1.3	0.345	1.6
Soda-Lime Glass	10	0.16	1.2

The primary goal of this series of runs was to replicate the wall penetration limit that was seen in the experimental results. The final values listed above successfully simulated this experimental limit. Exact replication of the hole diameters for penetration was not expected, since only small changes in velocity or material properties produce rapid changes in the perforation. The aluminum alloy that best matched the NASA-JSC data was identified as Al-1100-H16.

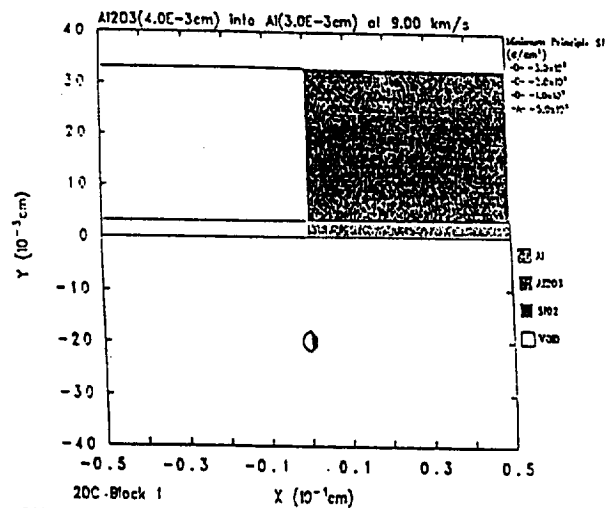
## A.2 Illustration of CTH Results

Figures A-1 and A-2 show some typical CTH results. These example problems include an aluminum coating on a silica substrate (Figure A-1) and a two-layer alumina/aluminum coating on silica (Figure A-2). In both cases the impactors have been alumina or aluminum. Parameter options investigated include impact speed and interlayer adhesion strength. In each figure, the

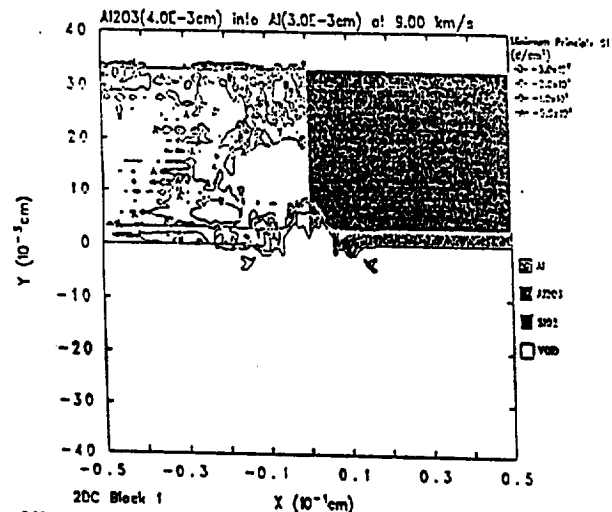
sequence progresses from the top to bottom, with the top image at 0 time. Projectile velocity was 9.0 km/s for both examples, and the time is given in seconds.

The effect of interlayer bond strength is interesting. For zero strength, the layer locally "peels back" by a small amount around the impact hole in the layer and the layer debonds rapidly in a radial manner away from the hole, such that the entire layer essentially jumps off the substrate. The silica substrate develops a typical crater. As the bond strength is increased, the debonding becomes limited to a region around the impact site, but at the expense of greater localized peel back at the hole edge. Depending on details, the local peel back can resemble the standard lips for a metal target impact, or can spall off and cause secondary ejecta. If the coating is a brittle one (e.g., alumina) with high compressive yield strength but low fracture strength, the tendency is to crack off the lips. Conversely, for a soft metal coating the tendency is to develop considerable plastic/molten flow, and droplets peel off.

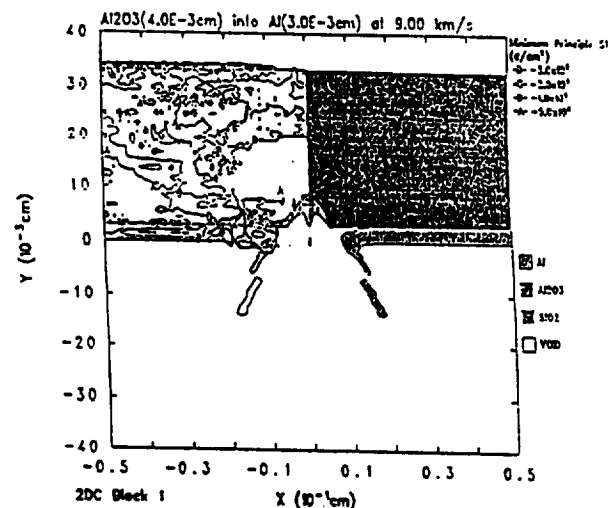
In all high speed ( $>9$  km/s) impacts modelled to date, the impacting particle, whether brittle alumina or soft aluminum, has always been forged into a self-forming jet structure which expels itself back out of the hole. This occurs because the impact pressures are sufficiently high to cause gross plastic flow at elevated, shock-induced temperatures, and the geometry causes convergence effects, thus giving the jet. The result is that only small portions of the impactor remain within the crater. This behavior is consistent with many LDEF observations, where frequently the impactor is either difficult or impossible to identify due to limited or zero remnants. For the two-layer coating problem, both layers peel back and delaminate from each other and the substrate. Figure A-2 shows such a case and indicates the complicated morphology around the impact site.



POD Penetration Test to duplicate delamination of thin layers.  
 FRQAXJ C 6/18/92 16:10:07 CTH 0 Time=0.



POD Penetration Test to duplicate delamination of thin layers.  
 FRQBAN 6/19/92 10:35:34 CTH 1326 Time=3.0065x10<sup>-7</sup>



POD Penetration Test to duplicate delamination of thin layers.  
 FRQBAN 6/13/92 20:22:06 CTH 440 Time=2.00142x10<sup>-7</sup>

Figure A-1: Example of an alumina projectile impacting a 2-layer target.

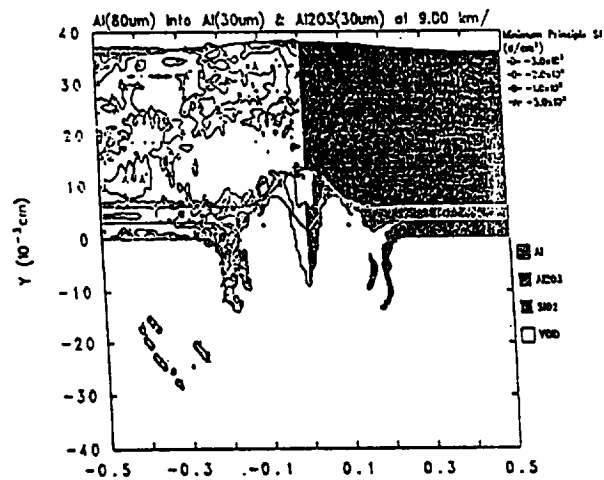
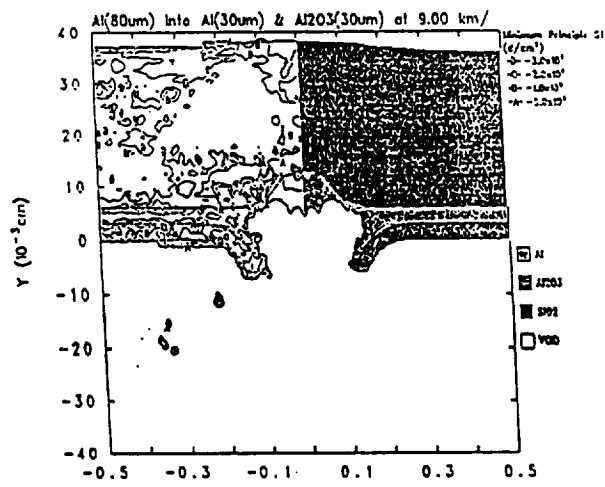
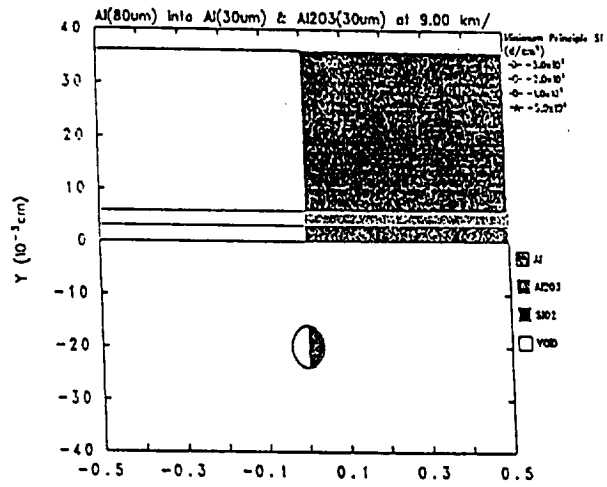


Figure A-2: Example of an aluminum projectile impacting a 3-layer target.

